GRI-03/0065 vol. 4

Seal Control of Hydrocarbon Migration and its Physical and Chemical Consequences

VOLUME IV: GAS WASHING OF OIL AND ITS IMPLICATIONS

FINAL TECHNICAL REPORT
(6/19/1997-12/31/2001)

Prepared by:
S. Losh and L. M. Cathles

Cornell University
Department of Earth & Atmospheric Sciences
Snee Hall
Ithaca, NY 14853

OSP #32006

Prepared for:

GAS TECHNOLOGY INSTITUTE
5097-260-3787

December 2002

REPORT DOCUMENTATION PAGE

Form Approved
OMB No. 0704-0188

1. REPORT DATE *(DD-MM-YYYY)*	2. REPORT DATE	3. DATES COVERED *(From - To)*
12/16/2002	Final Technical Report	06/19/1997-12/31/2001

4. TITLE AND SUBTITLE
Seal Control of Hydrocarbon Migration and Its Physical and Chemical Consequences

Volume IV: Gas Washing of Oil and Its Implications

5a. CONTRACT NUMBER

5b. GRANT NUMBER
5097-260-3787

5c. PROGRAM ELEMENT NUMBER

6. AUTHOR(S)
Cathles, Lawrence, M., III
Losh, Steven

5d. PROJECT NUMBER

5e. TASK NUMBER

5f. WORK UNIT NUMBER

7. PERFORMING ORGANIZATION NAME(S) AND ADDRESS(ES)
Cornell University
Office of Sponsored Programs
115 Day Hall
Ithaca, NY 14853

8. PERFORMING ORGANIZATION REPORT NUMBER
OSP #32006

9. SPONSORING/MONITORING AGENCY NAME(S) AND ADDRESS(ES)
Gas Research Institute
1700 South Mount Prospect Road
Des Plaines, IL 60018-1804

10. SPONSOR/MONITOR'S ACRONYM(S)
GTI, GRI

11. SPONSORING/MONITORING AGENCY REPORT NUMBER
GRI-03/0065 vol. 4

12. DISTRIBUTION AVAILABILITY STATEMENT

13. SUPPLEMENTARY NOTES

14. ABSTRACT

The process termed 'gas washing' (Meulbroek, 1997), whereby a stream of gas mixes with oil, removes relatively low-molecular weight compounds from it, and then separates, is here documented for a suite of samples from a 200-km long transect from the Louisiana coastline to the Gulf of Mexico deepwater. Oils nearest the shore are the most intensely affected by this process, having lost over 90% of their n-alkanes, and 84% of their total mass, to a vapor phase. The extent of gas washing, in terms of both mass fractionation and the molecular weight of compounds involved, decreases regularly with distance from the shoreline, and shows no dependence on tectonostratigraphic province. The deepwater oils, from the Jolliet field, are not gas washed at all. Similarly, the maximum pressure (and depth) at which oils were gas washed decreases with distance from the shoreline. Equation of state modeling combined with geologic reconstructions demonstrates that gas washing takes place at the depth of the first aerially extensive sand that is encountered by the ascending fluids. Gas washing analysis can illuminate subsurface fluid migration pathways and processes.

15. SUBJECT TERMS

16. SECURITY CLASSIFICATION OF:			17. LIMITATION OF ABSTRACT	18. NUMBER OF PAGES	19a. NAME OF RESPONSIBLE PERSON
a. REPORT	b. ABSTRACT	c. THIS PAGE			Prof. Lawrence M. Cathles III
U	U	U	SAR	74	19b. TELEPONE NUMBER (*Include area code)* 607-255-7135

GRI Disclaimer

LEGAL NOTICE

This report was prepared by Cornell University as an account of contracted work sponsored by the Gas Research Institute (GRI). Neither Cornell University, GRI, members of these companies, nor any person acting on their behalf:

a. Make any warranty or representation, expressed or implied, with respect to the accuracy, completeness, or usefulness of the information contained in this report, or that the use of any apparatus, methods, or processes disclosed in this report may not infringe upon privately owned rights; or

b. Assumes any liability with respect to the use of, or for damages resulting from the use of, any information, apparatus, method, or process disclosed in this report.

Table of Contents

Volume IV. Gas Washing of Oil and Its Implications.

Steven Losh and Lawrence Cathles III, Dept. of Earth and Atmospheric Sciences, Cornell University, Ithaca NY 14853

I. Summary

The interaction of gas with oil in the subsurface can be a major process in sedimentary basins, in terms of both mass transfer and compositional effects. The process termed 'gas washing' (Meulbroek, 1997), whereby a stream of gas mixes with oil, removes relatively low-molecular weight compounds from it, and then separates from it, is here documented for a suite of samples from a 120-mile long transect from the Louisiana coastline to the Gulf of Mexico deepwater. Oils nearest the shore are the most intensely affected by this process, having lost over 90% of their n-alkanes, and 84% of their total mass, to a vapor phase. The extent of gas washing, in terms of both mass fractionation and the molecular weight of compounds involved, decreases regularly with distance from the shoreline, and shows no differentiation by tectonostratigraphic province. The deepwater oils, from the Jolliet field, are not gas washed at all. Similarly, the maximum pressure, and by extension the maximum depth, at which oils were gas washed decreases with distance from the shoreline. The covariation of extent of gas washing with pressure of gas washing indicates that this phenomenon is more efficient at greater depth. The greater maximum depth of gas washing near the shoreline, diminishing in the offshore direction, is consistent with the distribution of sand in the Gulf of Mexico sedimentary section. Gas washing is related to the distribution of permeable sediment: combined equation of state modeling and geologic reconstructions demonstrate that gas washing takes place in or near the first sheet sand that is encountered by the ascending fluids. Thus, the maximum depth of gas washing of oil in a particular area can be a guide to the location of sand that may be charged with hydrocarbons.

II. Introduction

This report is one in a series of reports that describe our efforts to understand physical and chemical processes in the GRI Corridor. The report series is "Quantifying Gas, Oil, and Brine Migration in a 125- by 200 – km Area of the Offshore Louisiana Gulf of Mexico." The six volumes that comprise this series are:

- Volume I: Executive summary
- Volume II: Geology, Geophysics, Geochemistry and GoCAD Database
- Volume III: Chemistry of 137 Oils and Gases
- Volume IV: Gas Washing of Oil and Its Implications
- Volume V: A Modeling Analysis of Hydrocarbon Chemistry and Gas Washing, Hydrocarbon Fluxes, and Reservoir Filling
- Volume VI: A Theoretical Analysis of Inorganic Alteration By the Flow of Brines Through Seals.

The objective of this report is to describe the effects of 'gas washing' of oil in a 120 – mile transect offshore Louisiana, in both chemical and geological terms. Insights gained from this investigation lead

to conclusions regarding the role of gas in creation of capillary seals in the subsurface, the geological factors that control subsurface gas-oil interactions, and the possible existence of gas-washed oil below known reserves. Inasmuch as these lines of inquiry lead to better understanding of the petroleum system of which natural gas is a part, exploration for natural gas is advanced by the work described herein.

Oil and gas interact with one another in the subsurface, in many instances altering one another's compositions and physical properties. Over time, the extent over which these interactions are known to operate has broadened. Silverman (1965) proposed that oil composition is modified by the exsolution of gas due to pressure decrease during ascent, a process known as 'migration fractionation'. This type of process can include effects due to gas cap separation during production. Under most circumstances, the extent of potential compositional modification to oil resulting from such a process is quite small, being limited by the amount of gas that can be dissolved in oil and by the amount of oil compounds that partition into that volume of vapor. Thompson (1987) broadened the scope of compositional effects of gas separating from oil by means of an 'evaporative fractionation' mechanism, whereby variably-sized, but possibly large, batches of gas mix with oil and subsequently separate from it, removing n-alkanes preferentially to naphthenes and aromatics. His mechanism further involved sequential steps of vapor – liquid mixing and separation that eventually produced a condensate that was enriched in aromatics relative to the oil from which it was originally derived. Meulbroek (1997) and Meulbroek et al. (1998) expanded on Thompson's concept of fractionation per se (without implying any compositional endpoint) to incorporate the effects of a continuous gas stream flowing past oil, removing compounds in order of their relative fugacity in the vapor phase, a process they referred to as 'gas washing' (n.b., this term has existed for some time in the oil industry (R. Sassen, pers. comm.)), but has not appeared in peer-reviewed literature until Meulbroek et al. (1998)). Depending on the pressure and liquid composition, the vapor stream theoretically has the potential to ultimately take into solution nearly the entire liquid phase.

The importance of processes that involve large amounts of gas relative to oil will depend on the 'oil-proneness' of a basin and on the 'plumbing system' of that basin with respect to oil and gas migration. In the Gulf of Mexico, gas and oil are both abundant, providing a good setting for evaluating the nature and extent of gas-oil interactions. This study focuses on documenting the nature and amount of gas washing of oils collected along a 120 – mile transect from just offshore Louisiana to the continental slope (Figures 1 and 2). We demonstrate that the oils are indeed variably gas-washed, to the exclusion of other processes that could produce similar signals, and that the extent of washing is highly variable and in some cases extreme, removing up to 91% of an oil's n-alkanes by mass. The extent of gas washing decreases offshore, owing to differences in sediment thermal maturity and/or variations in plumbing system of oil versus gas.

III. Methods, Assumptions, and Procedures

III. a. General.

This report describes the geology and petroleum geochemical setting of four study areas within the transect, with the primary focus being that of understanding

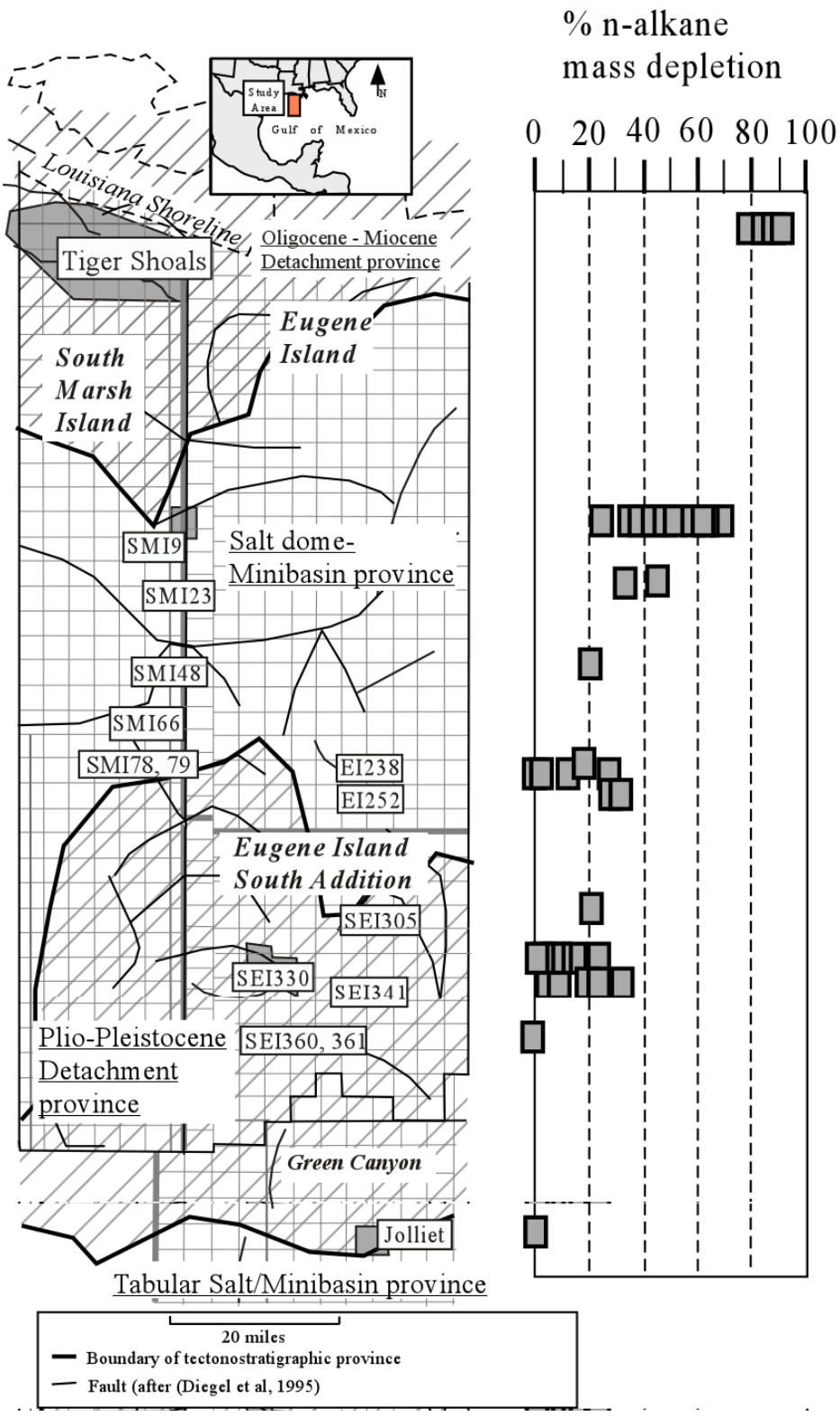

Figure 1. Location map for sample transect, offshore Louisiana. Tectonostratigraphic provinces (from Diegel et al., 1995) and the four main study areas are shown. Panel on right shows n-alkane mass depletion for sampled oils, projected onto north-south section along transect axis.

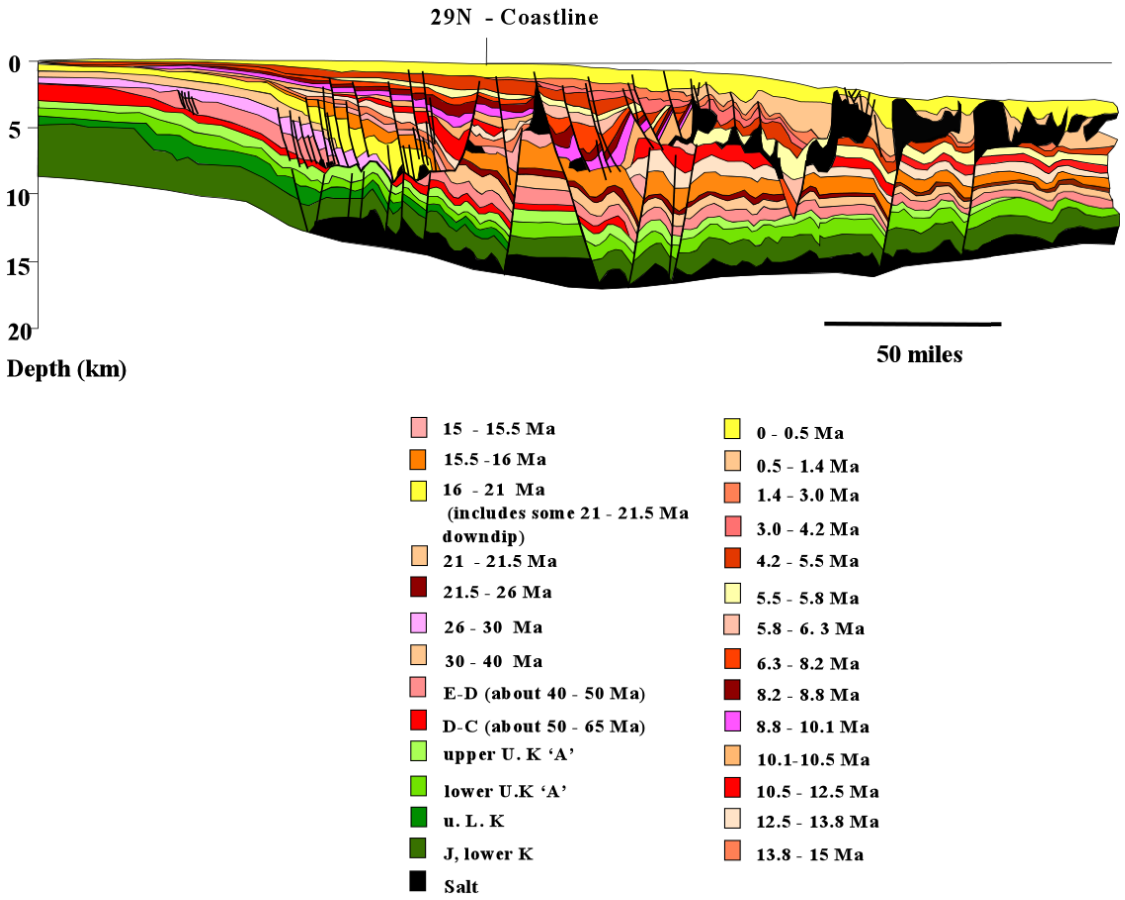

Figure 2. North (left) to south (right) cross section parallel to sample transect, approximately 60 miles to east (from McBride, 1998). Locations of study areas are approximately projected about 60 miles east onto plane of section, attempting to show the samples in terms of both distance from shore and geologic/water depth environment. Numbers correspond to (1) shoreline, (2) Tiger Shoals, (3) SMI9, (4) SEI330, and (5) Jolliet.

the nature of, and controls on, gas washing. Of particular interest is determination of the depth at which gas washing took place, as the phenomenon can then be related to geological features to elucidate controls on gas washing. Several lines of indirect evidence must be tapped in order to arrive at an estimate of the depth of gas washing. First, thermodynamic modeling of the composition of the vapor-liquid system as a function of pressure and temperature (e.g. Meulbroek et al., 1998) allows the computation of actual pressures at which gas washing took place. Second, since the degree of gas washing is in large part a function of fluid pressure (Meulbroek et al., 1998), the evolution of fluid pressure in a given study area over time must be known. This is carried out by evaluating the relationship between porosity and effective stress. If sediment porosity is a function of effective stress, as determined by examination of porosity-related logs and initial reservoir pressure data, then the compaction history of the sediment can be inverted to provide a history of fluid pressure in the study area. Such a relationship can be determined for sediments that have undergone neither cementation nor secondary porosity development, which is the case for the relatively shallow (<4 km) Neogene and Quaternary siliciclastics that comprise the sampled section. Conversely, if the porosity of these uncemented sediments is not a function of effective stress,

then the timing of overpressure development is necessarily relatively recent in the compaction history. Third, the timing of gas washing is estimated by evaluating the timing of reservoir filling. The assumption that gas washing took place at roughly the same time as reservoir filling is likely sound in cases where gas washing took place not far below the reservoirs, and becomes less sound with increasing vertical separation between the site of gas washing and the present location of the oil or condensate. As it turns out, gas washing probably took place not far below current reservoir depths in all of the studied fields.

Timing of reservoir filling is addressed by evaluating the distribution of biodegraded oils in the reservoir section by means of the oil's pristane/n-C_{17} ratio. If temperature is the primary or sole control on the distribution of biodegraded oils in the transect, which is probably the case, then biodegradation takes place at depths shallower than the 'sterilization isotherm' corresponding to the maximum temperature at which bacteria that degrade oil are viable in that particular setting. Thus, the presence of unbiodegraded oils deeper than this isotherm reflects filling after the reservoir sediments had been buried to at least the depth of that isotherm. This method does not take into account the possibility of filling at temperatures below the sterilization isotherm, followed by biodegradation of all the n-alkanes, followed by burial and later charging at temperatures above the sterilization isotherm. Only the migration time of the gas-washed oil, particularly the n-alkanes, is of concern in this investigation; the timing of older oils that were biodegraded before the gas-washed oils charged the reservoirs is not important in the context of evaluating the conditions of, and factors controlling, gas washing. When the burial history is taken into account, the maximum age of migration of gas-washed oil into the reservoir, hence the timing of gas washing itself, can be computed (Figure 3). When combined with the evolution of the fluid pressure profile, and augmented with the burial history since gas washing, the present–day depth of sediments in which gas washing of reservoired oils took place in the past can be determined. Applications of this methodology are given in this report for the Tiger Shoals and SEI330 fields.

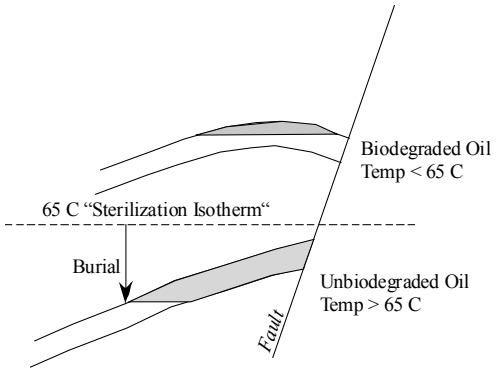

Figure 3. Model for use of distribution of biodegraded vs unbiodegraded oils to evaluate time of reservoir filling. Oldest migration time for deeper oil is determined by dividing the depth below the "sterilization isotherm" by the sedimentation rate. This assumes the geothermal gradient has remained unchanged during burial below the 65 C isotherm.

Do the oils and the gases that wash them travel together throughout the petroleum system, or were they generated separately and interact in relatively shallow parts of the basin? Isotopic data allow evaluation of the sources of reservoir gases, which are then compared to oil carbon isotopic data to determine consanguinity. As documented in the report, isotopic and chemical data indicate that oils and condensates share the same source, but that the reservoir gases, which are shown to have been involved in washing of the oils, have different sources than the liquids. A by-product of this investigation is a determination of the fraction of bacteriogenic methane present in the reservoir gas. This methane presumably is residual from bacterially mediated processes in the first kilometer or so of sediment below the seafloor.

From north to south, the study areas are the Tiger Shoals complex, the SMI9 field, the SEI330 area (including SEI341 and SEI361), and the Jolliet field (Figures 1, 2). In addition, geochemical data are presented

from several fields within the transect, and a study was begun in the SEI341 and SEI361 fields after preliminary evaluation of the initial transect data showed that oils from these fields appeared to be anomalous in terms of their Pressure-Temperature-Composition (PTX) conditions of gas washing. One hundred sixteen oil samples and 17 gas samples were collected and analyzed in support of this investigation, and an additional 103 oil analyses and 28 gas analyses are incorporated into this study (Tables A1 and A2; all data tables are in Appendix A).

III. b. Method for determination of n-alkane mass depletion due to gas washing

Thompson (1987) noted that separation of hydrocarbon vapor from a hydrocarbon liquid depletes the liquid in relatively high-fugacity compounds. Meulbroek (1997) and Meulbroek et al. (1998) modeled the phase behavior of the n-alkanes as part of equation of state modeling of whole-oil fractionation. Low molecular weight n-alkanes are fractionated from liquid into a coexisting vapor phase preferentially to higher molecular weight n-alkanes. In this paper, we calculate the mass depletion of oil in n-alkanes, relative to an unfractionated oil, by gas washing in a 190 km long N-S transect offshore Louisiana. The calculation merely quantifies the mass depletion relative to an unaltered oil, and is independent of the actual cause of such depletion.

Mature unfractionated oils are typically characterized by exponential distribution of compounds, particularly n-alkanes, in homologous series (Kissin, 1987). Throughout the transect, as well as in an additional study area in which extensive equation of state modeling has been done (Muelbroek et al., 1998), unfractionated oils display this exponential abundance distribution of n-alkanes. If abundance data for n-alkanes are converted to mole fractions and plotted as $\log_e$(mole fraction of n-alkane of carbon number C_i) vs the carbon number, C_i, the plot (called a 'molar fraction plot') for an unfractionated oil is characterized by a straight line having the equation

$$\ln X_{n\text{-}Ci} = mC_i + b \qquad \text{(Eqn. 1)}$$

(Kissin, op cit.), where m is the slope of the plot, and b is the intercept. For unaltered oils, the slope of this best-fit line, termed the 'n-alkane slope', is a function of oil maturity (Kissin, 1987; Meulbroek, 1997; Meulbroek et al., 1998); the more mature the oil, the steeper (more negative) the slope. The n-alkane spectrum of a gas-washed oil comprises two parts: the unfractionated portion at high carbon numbers, where data are best fit by a straight line on the molar fraction plot, and a depleted portion at lower carbon numbers, which deviates from the straight line fit in a regular fashion. The n-alkane carbon number at which the two portions of the spectrum join is called the 'break number' by Meulbroek (1997; Figure 4).

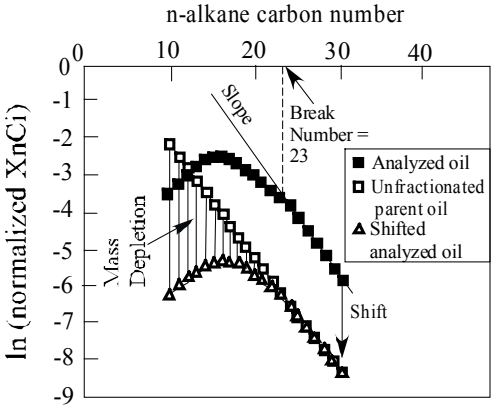

Figure 4. 'Molar Fraction Plot' for sampled oil (Tiger Shoals Amber N360), showing log-linear n-alkane distribution for equivalent unfractionated oil, and parameters incorporated in computation of mass depletion of n-alkanes from the sample.

As shown by Thompson and confirmed by Meulbroek, the 'break number' is strongly affected by the pressure at which phase separation and attendant fractionation took place.The break number is much less affected by other variables in the gas washing process, including temperature and

the mass ratio of gas to oil, and is thus useful as a proxy for the pressure at which phase separation took place. The slope of the unfractionated n-alkane spectrum beyond the break at $C_i > C_b$ (where C_b is the break number; Figure 1) is used to re-create the unfractionated n-alkane spectrum, in conjunction with the requirement that all mole fractions of n-C_i in the unfractionated oil add to unity. To avoid complications due to separator and sample handling losses, this analysis only incorporates n-alkanes having carbon numbers of 10 or higher. The n-alkane spectrum for the unfractionated oil has the same slope, but a different intercept than does the extrapolated best fit line through the data points. The intercept, b, is determined as follows.

As noted above,

$$\ln X_{nCi} = mC_i + b, \qquad \text{(Eqn. 1)}$$

where C_i = carbon number of compound *i*.

Exponentiating both sides, we have

$$X_{nCi} = e^{mCi+b} = e^{mCi}e^{b} \qquad \text{(Eqn. 2)}$$

We then impose the requirement that the sum of the mole fractions of compounds *i* is unity. We take the e^b term outside the summation, as it is a constant.

$$\Sigma X_{nCi} = \Sigma e^{mCi}e^{b} = e^{b}\Sigma e^{mCi} = 1.0. \qquad \text{(Eqn. 3)}$$

From the last equality, we rearrange to determine

$$e^{b}=1/\Sigma e^{mCi} \qquad \text{(Eqn. 4)}$$

and finally, the intercept b is determined to be

$$b = -\ln\Sigma e^{mCi} \qquad \text{(Eqn. 5)}$$

Thus, the n-alkane spectrum for the unfractionated oil is defined in terms of Equation 1, where the mole fractions sum to 1.0.

To determine the n-alkane mass depletion, the n-alkane spectrum of the analyzed oil is compared with the computed unfractionated spectrum, as shown in Figure 4. For this analysis, the mole fractions of the analyzed sample must be normalized such they sum to 1.0. If both sets of points are plotted on the same molar fraction plot, it can be seen that the analyzed points are offset from the unfractionated oil points by a constant difference, f, for $C_i > C_b$.

$$f = \ln X_{nCi} - (mC_i+b), \qquad \text{(Eqn. 6)}$$

where X_{nCi} pertains to n-alkane mole fractions in the analyzed oil, and mC_i+b is the expression that describes the unfractionated oil. This equation is valid only for $C_i > C_b$.

The molar depletions of each compound can thus be computed directly as

$$\Delta\ln(\text{moles n-}C_i) = mC_i + b - (\ln X_{nCi} - f). \qquad \text{(Eqn. 7)}$$

By subtracting f, and thereby shifting the n-alkane mole fractions in the analyzed oil to coincide with the calculated unfractionated oil n-alkane spectrum at $C_i>C_b$, the vapor is in effect being added back into the system. The shifted analyzed n-alkane data points represent the mole fractions of each n-alkane that is present within the liquid phase in the liquid + vapor mixture. The difference in molar fractions, hence moles, of each n-alkane between the fractionated sample and the calculated unfractionated parent is then readily expressed in terms of a depletion factor (D) for each n-alkane. This factor is defined in terms of the fraction of each n-alkane that has been lost into the vapor phase:

$$D_i = e^{\Delta\ln(\text{moles n-}Ci)} \qquad \text{(Eqn. 8)}$$

Introducing A as the number of moles of n-C_i in the depleted oil, relative to the unfractionated oil, we have

$$A_i = e^{(mCi + b)}/D_i \qquad \text{(Eqn. 9)}$$

Converting moles (X_{nCi}) to mass (M_{nCi}) by multiplying A_i by the appropriate molecular weight, and defining Q as the n-alkane mass depletion fraction summed over all the n-alkanes heavier than n-C_9, we have

$Q = 1 - (\Sigma M_{nCi}$ (analyzed oil)/ΣM_{nCi} (unfract oil)). (Eqn. 10)

The n-alkane mass depletions are then tied to overall mass depletion of the oil by means of condensate-oil mass balance (Appendix B). The n-alkane mass depletions themselves can be placed into their geologic context and compared with one another to discern patterns of gas washing in the transect.

III. c. Discussion of other processes.

Gas washing of oil can be distinguished from other processes that alter an oil's n-alkane distribution, notably biodegradation and water washing, as well as condensation from a vapor phase. The n-alkane pattern documented here is not a result of biodegradation for the following reasons. 1) The oils used for analysis of gas washing in this paper are unbiodegraded as determined by their having pristane/heptadecane ratios less than one (ex., Curiale and Bromley, 1996); the great majority are less than 0.8. Many of these oils have had n-alkanes as heavy as triacotane (at Tiger Shoals) and eicosane (at SMI9) removed. If biodegradation were responsible for this, the Pr/nC_{17} ratio would be accordingly high. As it is, the process that removed the n-alkanes also removed iso-alkanes, a pattern consistent with gas washing. 2) A characteristic of gas washing is the nearly exponential distribution of n-alkane mass depletions at carbon numbers less than the break number, and the removal of low - molecular weight aromatics and naphthenes as well as n-alkanes. Biodegradation affects n-alkanes in the same carbon number range as gas washing, but the depletions tend to be either uneven, and the n-alkane spectrum "ratty", or biodegradation eradicates the entire n-alkane spectrum. In either case, the significant biodegradation that is needed to produce large n-alkane depletions also typically results in an Unresolved Complex hump that is small (relative to nC_{20}) or absent in even heavily gas-washed oils. 3) The presence of mid-range n-alkanes (ie., nC_{15}) in an oil that has lost nearly all of its light aromatics and naphthenes (Figure 5) is not at all characteristic of a biodegraded oil (e.g. Peters and Moldawan, 1993). Conversely, it is possible to determine that an oil has not been gas washed, as the lack of gas washing is evident by a log-linear abundance distribution of n-alkanes. Biodegradation would disrupt this distribution; thus oils that are characterized by a log-linear n-alkane distribution are by default unbiodegraded, at least as far as their n-alkanes are concerned.

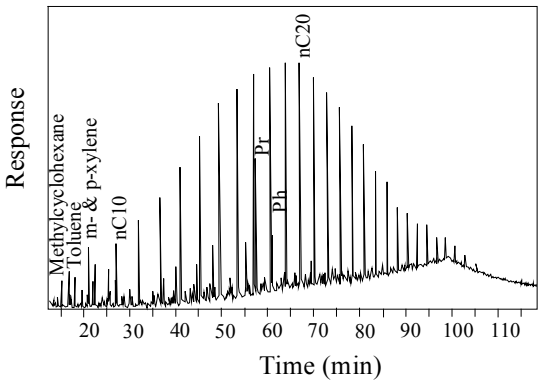

Figure 5. Gas chromatogram of a gas-washed oil (SMI9 field, sample GRI48). Note strong depletion of all light ends while mid-range n-alkanes and isoprenoids are preserved. The unresolved complex hump that peaks beneath about nC31 may be due to biodegradation of an earlier oil charge, it may be intrinsic to the unbiodegraded oil, or it may represent column bleed. The absence of a similar hump beneath about nC18, which is typical of biodegraded oil, indicates that the measured hump is probably due to the second and/or third factor.

A gas-washed oil is also compositionally distinct from commonly-observed oils that have been biodegraded and

then mixed with a young, unbiodegraded condensate. Such oils show light-end enrichments and unresolved complex showing a broad "hump" beneath the location of the nC18 peak. Both of these features are absent from gas-washed oils described in this report (Figure 5). Mixed biodegraded and unbiodegraded oil is also readily identifiable on the molar fraction plot by a steep n-alkane slope at low carbon numbers coupled with a less steep slope or scattered data points at higher carbon numbers.

Water washing shares with gas washing the capacity to fractionate low molecular weight compounds from the oil relative to heavier ones, but differs in the relative solubilities of compounds, decreasing in the order aromatics, n-alkanes, naphthenes (Lafargue and Barker, 1988). These workers found that even relatively minor water washing strongly depletes oil in toluene and naphthalenes compared to a relatively insoluble n-alkane such as nC_{20}. A number of transect oils that display substantial n-alkane depletion nonetheless contain significant toluene (2 - 5 g/l). The presence of significant concentrations of other aromatics (naphthalenes, phenanthrene, dibenzothiophene) in oils that have undergone strong n-alkane depletion also points to gas washing rather than water washing as the primary, if not sole, cause of that depletion (cp Palmer, 1984).

Condensation of liquid from a vapor phase during ascent, accompanied by fractionation of that liquid, proposed as a general process by Price et al (1983), is also not considered a likely explanation for the analyzed oil compositions. First, oils, including transect samples, contain heavy asphaltenes, which have extremely low solubility in methane. Price et al. (1983) determined a solubility of 0.014 g "F15" asphaltene, distilled from oil, per liter STP methane, at 11,200 psi and 250 C. Assuming a molecular weight of 600 g/mole for the tar fraction (see Price et al., 1983), and that the F15 fraction comprises 0.5 weight percent of the oil (a reasonable value), a molar gas:oil ratio of 2400:1, or a volume ratio of about 3100:1 at reservoir conditions, is required to take even this small concentration of asphalt into the vapor phase. Such relative volumes of gas to oil are geologically unreasonable on the scale of the petroleum systems studied in the Gulf of Mexico. Although most oil components may be soluble in methane at very high pressures and/or temperatures, the heavier of these would condense far below the depths of existing reservoirs, as well as far below the calculated depths of gas washing. The composition of liquid dissolved in vapor at ambient reservoir conditions is given by the gas condensates, not by the oils themselves.

A second line of evidence against the 'progressive condensation' model is derived from the data on which Price et al (1983) based their own model. According to them, gas generated in the source rock takes earlier-generated (but not migrated) oil into 'solution' and the two ascend as a single phase to the dewpoint, where the oil condenses. This model appeals to the substantial solubility of oil in gas at conditions that prevail in the gas generation window. Below (Figure 6) is a plot of the solubility of their Spindle oil versus depth, assuming geothermal gradient of 25C/km and hydrostatic pressure to 2 km, jumping to 0.93 times lithostatic pressure by 2.5 km, and increasing along a lithostatic gradient below that. Their solubility data were regressed to the form

$$S = 10^{0.0013P+0.0047T - 1.72} \quad \text{(Eqn. 12)}$$

where solubility (S, in g oil per liter of gas as measured at STP) is a function of pressure (P, in bars) and temperature (T, in Celsius). The logarithmic nature of the solubility versus depth curve (with a small kink in it at the jump in fluid pressure gradient) results in an apparent 'economic basement', a narrow depth interval over which oil solubility decreases by a large factor (Gatenby, 2001), but which is actually just an artifact of the scale at which the plot is made. In fact, there is no particular depth at which liquid condenses as a single batch (except at the critical point), as there is no pressure or temperature discontinuity in the subsurface

large enough to make this happen. The large majority of gas-oil fluids do not pass through their critical points on the way to the surface. However, once dewpoint is attained as the vapor ascends, it would continually condense liquid, such that the vapor composition would be continually modified by the loss of heavy compounds. Simulations of such a scenario using the n-alkanes as an example, however, show this is not the case. Given that the liquid that condenses from a vapor phase has a log-linear distribution of n-alkanes, and that

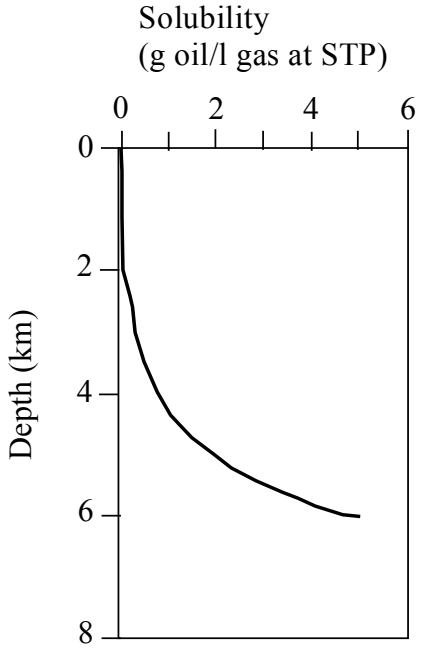

Figure 6. Solubility of Spindle oil at STP (25 C, 1 bar) versus depth, as discussed in text. Data from Price et al. (1983).

it will be preferentially enriched in heavy compounds relative to the coexisting vapor, the compositional evolution of a vapor that serially condenses liquids through a PT gradient can be shown. For the sake of example, a single phase gas-oil vapor is taken as having an n-alkane slope of –0.20. As the vapor ascends, it condenses liquid having an n-alkane slope of, for the sake of discussion, –0.19, preferentially depleting the vapor in heavy compounds relative to light ones, resulting in steepening of the n-alkane slope (concentration of lower – molecular weight compounds) in the vapor. Further ascent to lower pressure causes a liquid to condense that has an even greater relative concentration of heavy n-alkanes to light ones due to the stronger fractionation of heavier compounds into the liquid phase at lower pressures, here represented by an oil of slope –0.18. Figure 7 shows the resulting n-alkane composition of the vapor phase in terms of ln(mole fractions). To more accurately represent the compositional evolution of vapor, each compound should be considered individually, but the model used here is adequate to illustrate the compositional effect of serial condensation.

The cumulative selective depletion of heavy compounds in the vapor eventually produces a downward curvature in the n-alkane plot at high carbon numbers.

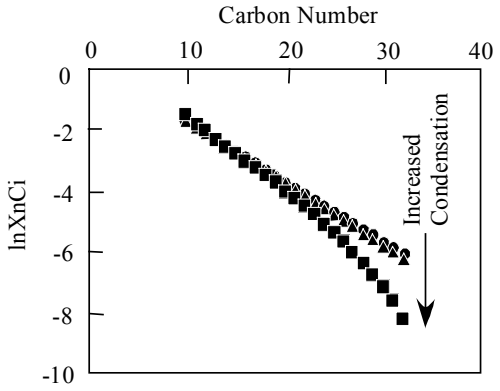

Figure 7. Molar fraction plot for vapor n-alkane composition, following model of sequential condensation of oil from vapor having initial n-alkane distribution of slope –0.20 as discussed in text.

Subsequently - condensed liquids will still be preferentially enriched in heavy compounds relative to the vapor, having oil-like n-alkane slopes, but will be relatively deficient in or entirely missing heavy n-alkanes that have been largely lost to previously condensed liquids. Furthermore, oils of a wide range of n-alkane slopes would be expected as a result of this condensation mechanism, as the vapor ascended and continually condensed liquids. However, neither of these types of effects are evidenced by available data in the transect, and they probably do not exist. Instead, oils have a narrow range of n-alkane slopes, with a full complement of heavy compounds,

including asphaltenes that would normally be expected to condense from vapor at PT conditions much higher than those attributed to gas washing.

Furthermore, in contrast to condensation, gas washing produces cumulative mass depletion at the oil's *light end*. Analysis of some of the gas-washed oils shows that the removed n-alkane fraction has a log-linear distribution of mole fraction with respect to carbon number, indicative of a single-stage fractionation into a vapor phase. Gas condensates produced at the wellhead show this same log-linear distribution of n-alkanes above nC_7 or nC_8 (ex, SEI330), consistent with their derivation from a single step of gas washing. Multiple stages of washing at different pressures would produce kinked or curved molar fraction plots for the "removed" fraction rather than the observed log-linear distribution of n-alkane abundances with respect to carbon number. These lines of evidence indicate that the oils were liquid at least throughout the portion of their history that is relevant to the compositional fractionation interpreted as gas washing; that is, they were liquid prior to, during, and subsequent to gas washing, and their compositions arose uniquely from fractionation of high-fugacity compounds from that liquid into a vapor phase.

Other processes that affect oil composition can also be ruled out as causes for the observed oil compositional patterns. 1) Paraffin precipitation, like condensation, affects n-alkanes at the high carbon-number end of the molar fraction plot, and is thus not readily confused with the effects of gas washing, which, at least in this study, only affects compounds as heavy as triacotane. 2) Sample evaporation (storage or deliberate topping losses) may produce substantial to total depletions of light ends. However, the samples were analyzed shortly after collection, and they were not topped. The GC of gas-washed oil does not show the abrupt discontinuity of compound abundances at about C15 that characterizes a topped oil. 3) Gas cap separation, fractionation in the separator, and short-term evaporation of sample after collection are shown by Meulbroek (1997) and Meulbroek et al. (1998) to affect compounds only as heavy as decane or so, depending on actual reservoir or separator pressures. As noted earlier, to avoid any complications from production-related compositional effects, the n-alkane depletion computations in this paper do not incorporate n-alkanes having carbon numbers less than 10. In addition, gas washing also involves large ratios of gas to oil. Meulbroek et al. (1998) concluded that oils at the SEI330 field interacted with up to 14 moles of gas per mole of oil, or about 18 volumes of gas per volume of oil at reservoir conditions. This volume of gas far exceeds that which can dissolve in oil at any one time, and requires the mixing of oil with, and separation from, a migrating gas stream, ruling out gas cap separation or migration fractionation at reservoir conditions as an explanation for the observed n-alkane distributions.

IV. Results and Discussion

IV. a. Gas washing of oil at the four study sites.

The sample transect includes four areas for which geology, fluid pressure measurements, and data from numerous oil and gas analyses were combined to provide a geologically-based investigation of gas washing in four tectonostratigraphic provinces in the Gulf of Mexico. From north to south, the study areas are the Tiger Shoals complex, the SMI9 field, the SEI330 field, and the Jolliet field. Respectively, they lie in the Oligocene-Miocene detachment belt, the salt dome-minibasin province, the Plio-Pleistocene detachment belt, and the salt sheet-minibasin province of Diegel et al. (1995) (Figure 1). As such, the study areas span a range of sediment ages and tectonic styles, the latter giving rise to possible differences in tectonic 'plumbing system'

which could affect the migration of oil and gas as well as their interaction with one another. The relationship between gas washing and tectonic province is addressed later.

Tiger Shoals

The Tiger Shoals and nearby fields have been owned and operated by Texaco since the 1960's. Data provided by Texaco for this study include the following: 3D seismic survey, with wells, well logs, well tops; paper maps and log sections; measured fluid pressure and reservoir temperature data; gas chromatographic and high-resolution GCMS biomarker data for oils and condensates; whole-oil compositional and isotopic data; compositional and compound-specific isotopic data for gases; and cumulative and ultimate production data for the fields that comprise the study area. Normal alkane mole fraction data were provided by P. Meulbroek.

Geologic setting. The Tiger Shoals study area is located just offshore Louisiana, within the Vermilion and South Marsh Island Outer Continental Shelf (OCS) lease areas. The study area measures about 20 miles E-W by 10 miles N-S, and contains the Starfak, Tiger Shoals, Mound Point, Lighthouse Point, Amber, Trinity Shoals, and Aquamarine fields (Figure 8). Total initial reserves are 133 MMbbl oil, 43 MMbbl condensate, and 6.4 Tcf gas.

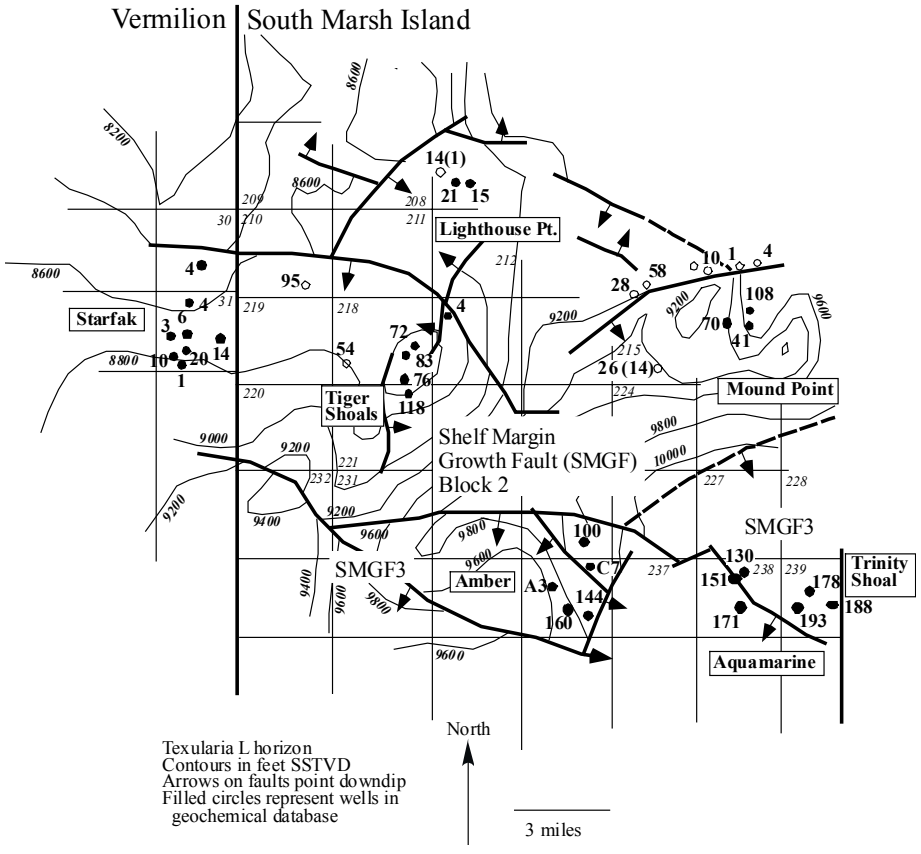

Figure 8. Structure contour map on Textularia L horizon, Tiger Shoals study area. Locations are shown for wells from which geochemical and well log data were obtained. OCS lease block numbers are also shown.

Oil, gas, and condensate production is from four-way closures and fault traps in a section of predominantly deltaic Miocene sands (Figure 9), between 6000 and 12,000 feet in most of the fields, and as deep as 14,000 feet at Starfak. The section is predominantly massive shale below the deepest (12,000 feet) producing sands at Tiger Shoals, and little exploration has been conducted in the Rob L and deeper sands except at the Starfak field. Salt domes are absent from the study area, although features that appear as salt sills and pillows are evident in the deeper reaches of the seismic data below the reservoirs.

Two main fault sets transect the area in an east-west direction, dividing it into two blocks designated Shelf Margin Growth Fault (SMGF) blocks 2 and 3 (Figure 8). The main individual faults have up to 1000 feet of down-to-the-south displacement at the level of the deepest productive sands. These faults, as well as several subsidiary faults, cut to the surface, and so appear to be presently or recently active. Many other faults do not cut significantly above the Bigenerina 'A' (6.3 Ma) marker. The greater activity of faulting during the Miocene is consistent with sedimentation rates that were somewhat higher in the Miocene (0.3 mm/yr) than they have been since 'Big A' time (0.2 mm/yr).

Hydrocarbon distribution. SMGF#2 fields (Starfak, Tiger Shoals, and Mound Point) and SMGF#3 fields (Amber, Trinity Shoals) initially contained similar total amounts of hydrocarbon liquids as measured at the wellhead (74 MMbbl in SMGF#2 vs 99 MMbbl in SMGF#3), but the SMFG#2 fields (particularly Mound Point and Tiger Shoals) contain much more gas than do SMGF#3 fields (6.3 Tcf vs 0.5 Tcf). Over half of the liquids in the SMGF#2 fields are condensates, whereas nearly all of the liquids in the SMGF#3 fields are oil. Within the Tiger Shoals field, oil, condensate, and gas are irregularly distributed. Oil is found in three sands, the '12000', the V and the N. The largest condensate accumulations are found in the sands just above the oil reservoirs, implying a genetic association between oils and condensates (Figure 9). All gas-producing reservoirs, regardless of oil content, produce gas condensate. Most gases have gas/ liquid condensate ratios between 100 and 400 Mscf/bbl, regardless of reservoir size.

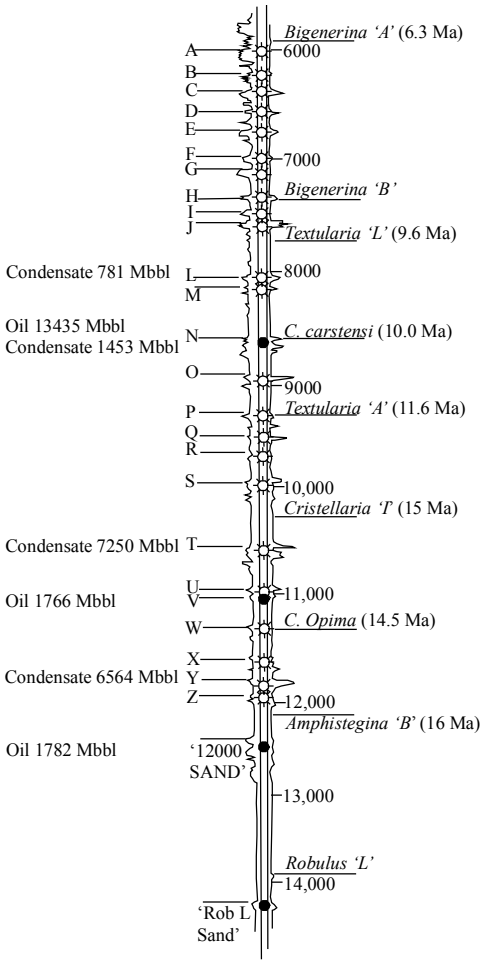

Figure 9. Type well log (SP on left, long normal resistivity on right), Tiger Shoals field, showing main oil and condensate volumes.

Fluid pressure. Although the pressure measurements shown in Figure 10 do not necessarily reflect pre-production reservoir pressures, these data are nonetheless useful in estimating the pre-production fluid pressure profile. In SMGF#2 (including the Tiger Shoals, Mound Point, Starfak, and Tiger Eye fields), fluid pressures are hydrostatic to a depth of about 10,000 feet, and 'hard' overpressures are encountered at Mound Point and Starfak at about 11,000 feet (Figure 10), compatible with the shale-rich nature of

the stratigraphic section at and below that depth (Figure 9).

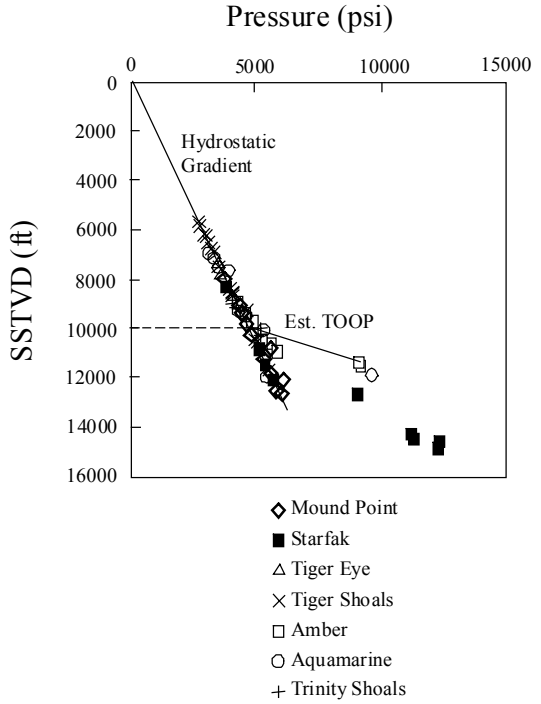

Figure 10. Static bottom hole pressure measurements, Tiger Shoals, Mound Point, Starfak, and Tiger Eye fields. Sub-hydrostatic pressures have been culled, as they are attributed to production.

Below that depth, the maximum fluid pressures appear to define a lithostatic gradient. The top of overpressure in SMGF#3 may be somewhat shallower than in SMGF#2 (Figure 10), similar to the pressure distribution documented in south Texas by McKenna (1997). Because of the paucity of data, however, fluid pressure gradients in the two fault blocks are assumed to be the same.

Sonic and density logs from six wells that penetrate to depths greater than the top of overpressure at 10,000 feet in the Starfak, Tiger Shoals, and Mound Point fields (Figure 11) show varying evidence for arrested compaction in the overpressured zone. The sonic logs show slightly elevated porosity in overpressured sediments, and a normal porosity dropoff with depth, compared to normally compacted shales (sonic $\phi = (1 - 67.07/\Delta t)^{1/2.19}$ (Issler, 1992); normal $\phi(z) = \phi_0 e^{-3.68x10\text{-}2(.0032z(ft))}$), whereas density logs show anomalously high porosities and arrested or reversed porosity profiles at depths below about 10,500 feet in three wells. These porosities are consistent with arrested compaction at depths of about 6000 to 7000 feet, indicating that overpressuring

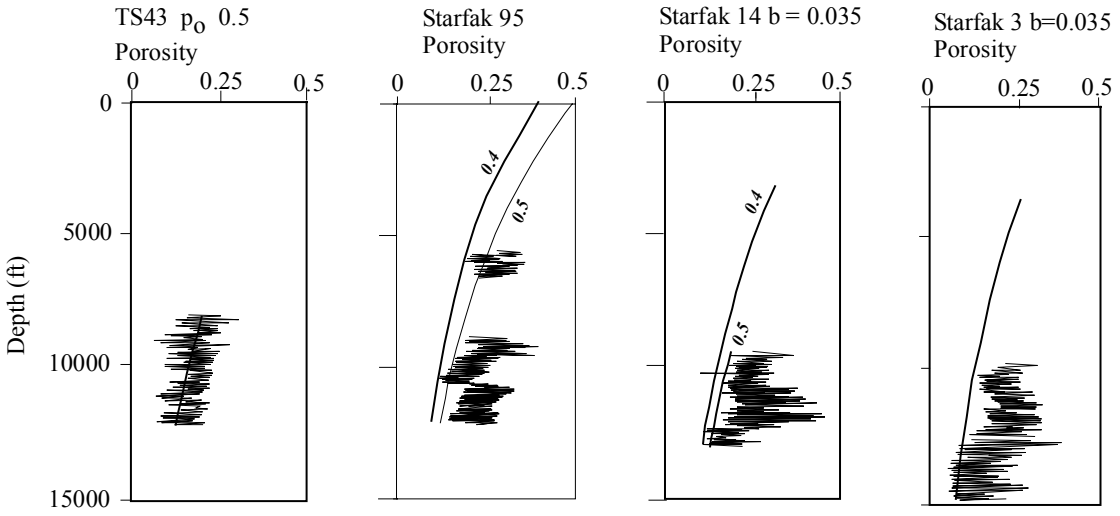

Figure 11. Sonic log - derived (left) and density log - derived (right three) porosity profiles for four wells, Tiger Shoals study area. Unless otherwise indicated, the hydrostatic compaction curves are based on initial porosity of 0.4 and long-term sediment compressibility (b) of 0.0368 Mpa^{-1}.

has persisted during deposition of the most recent 4000 feet of sediment, or about 4 million years. Fluid overpressure is calculated according to

$$P_f = P_{lith} - (\ln(\phi_0/\phi))/\beta \qquad \text{(Eqn. 13)}$$

(Hart et al., 1995), where fluid pressure (P_f) is related to lithostatic pressure (P_{lith}), in situ porosity ϕ, initial porosity ϕ_0 (taken as 0.4), and long-term compressibility β (3.6×10^{-2} Mpa^{-1}). In the Starfak 14 well, calculated fluid overpressure in the zone of anomalous porosity in the shale is on the order of 27 Mpa (4000 psi) at a depth of about 11,500 feet, whereas actual fluid overpressure at that depth is about 34 Mpa (5000 psi). Compaction disequilibrium, as determined from density logs, accounts for a large fraction of the fluid overpressure in the Tiger Shoals area. Therefore, fluid overpressures have been increasing along a nearly lithostatic gradient for the past several million years in these deep sediments.

Oil geochemistry: source and maturity. Oils from the study area are here evaluated in terms of source, maturity, and extent of interaction with gas. Other processes that can affect oil composition, such as water washing and biodegradation, are not considered important for these oils. Oil aromaticity (ratio of toluene to n-heptane; Table A3) is 'normal' (about 1.0) to high for these oils, and indicates that aromatics have not been preferentially removed from the oil due to water washing (Thompson, 1987). Biodegradation is also absent in these oils, as demonstrated by nearly ubiquitous Pr/nC_{17} ratios less than one (Table A1) (two ratios are greater than unity, but the higher of these is likely unreliable due to low concentrations of Pr and nC_{17}). In addition, the ratio of total n-alkanes to iso-alkanes in these oils is at least 2:1, again indicative of no biodegradation. Aromatic, sterane, and hopane biomarkers (Table A4) were evaluated for the purpose of determining source and maturity of oil, and evaluating oil-oil correlations, with the ultimate intention of deducing the 'plumbing system' by which the reservoirs were filled.

Both source and maturity biomarkers show remarkable similarity for the oils from the various fields (Figures 12 and 13), although Tiger Shoals and Starfak oils show slightly greater ranges of various ratios than do oils from Amber and Trinity Shoals. Tiger Shoals and Starfak oils may thus be mixtures of slightly different oils than those present at Amber and Trinity Shoals. The oils are sourced from a rather uniform mixture of land plants (C29 steranes) and marine algae and bacteria (C27, C28 steranes and 17α(H) hopanes) of post-mid Cretaceous age (presence of oleanane).

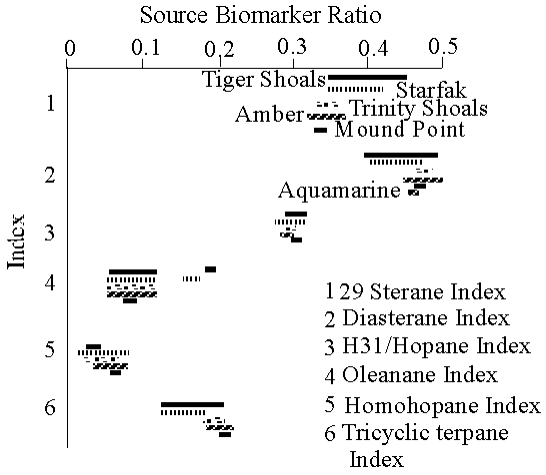

Figure 12. Source biomarker ratios, Tiger Shoals study area. Indices are defined in Table A4 caption.

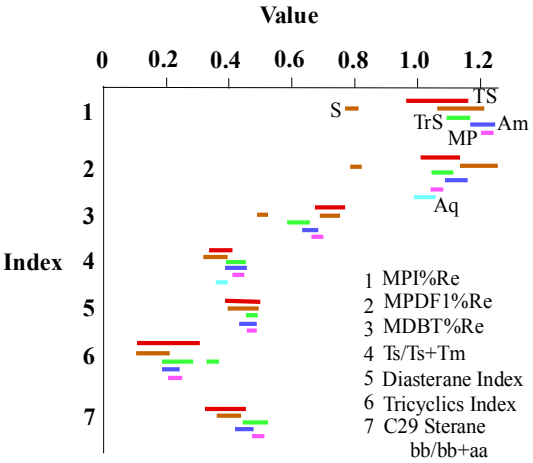

Figure 13. Maturity biomarker ratios, Tiger Shoals study area. TS = Tiger Shoals, S = Starfak, TrS = Trinity Shoals, Am = Amber, MP = Mound Point, Aq = Aquamarine

The source rock was predominantly shale (high diasterane/total sterane and pristane/phytane ratios, as well as low total sulfur content (0.09% and 0.13% in two samples)), with moderate salinity porewater (low gammacerane ratio). Various oil-oil correlation indices, such as the homohopane index and the tricyclic triterpane/(total triterpane) index, show little variability between fields (Figure 12). The oils and condensates are characterized by a very narrow range of whole-oil $\delta^{13}C$ values (-26.4 +/- 0.27 permil PDB; Table A1), which varies little from one field to another. Tertiary shale, such as a Sparta equivalent, was probably the primary if not the sole source for all the oils.

Gas-washed oils and their related condensates show a characteristic relationship to one another on a plot of aromaticity versus paraffinicity, as demonstrated by Thompson (1987) (Figure 14).

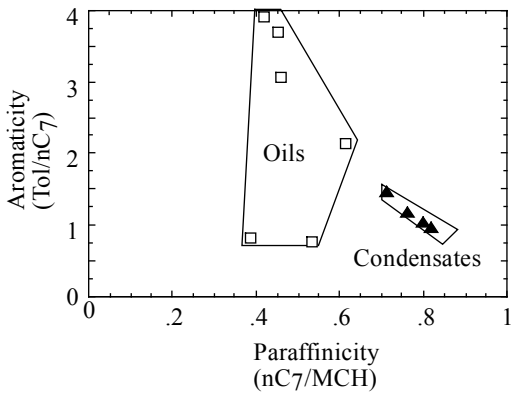

Figure 14. Aromaticity vs paraffinicity (after Thompson, 1987), Tiger Shoals field liquids. Oils and condensates from other fields in the study area show the same relationships.

The vapor phase condenses an 'evaporative fraction' that is highly paraffinic and less aromatic than its parent, whereas the converse is true of the residual oil. Such a relationship is demonstrated by data from oils and condensates from the Tiger Shoals and other fields (Table A3, Figure 14). Origin of condensates by gas washing of oil is also consistent with the close spatial association of the two fluids at Tiger Shoals, and with their similar sources as indicated by carbon isotopic and DMCP data (Figure 15; isotope data in Table A1). The presence of only low-aromatic paraffinic condensates at Tiger Shoals, according to Thompson's (1987) model, suggests the oil fractionation was a single-batch process, rather than a series of mixing-fractionation steps. The latter process results in aromatic condensates, which were not found anywhere in this transect.

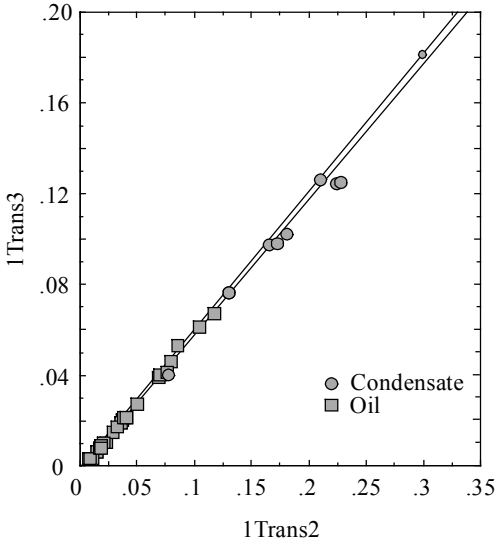

Figure 15. Dimethylcyclopentane isomers 1Trans3 vs 1Trans2 for oils and condensates, Tiger Shoals study area. The ratios for the two fluid types are nearly identical, indicating a common source.

The oils exhibit a wide range of calculated maturities, depending on the biomarker used (Table A4, Figure 13). Methylphenanthrene indices give the highest, and probably most reliable, oil maturities, between 1.0 and 1.2% R_o equivalent (Figure 13) for all but one sample (Starfak RobL-2/650, Vermilion 31, well #10), which has equivalent vitrinite reflectance of 0.79%Ro using the MPI-1 index (Table A4). This general middle to late oil window maturity is consistent with the relative abundance of lighter compared to heavier n-alkanes as shown by steep 'n-alkane slopes' of –0.29 to –0.33, which Kissin (1987) noted as typical of oils having late oil window maturity. Condensates show low maturities relative to the oils, according to the single-valued MPR

index (Radke et al., 1987). As noted above, the condensates are believed to have originated as an evaporative fraction during gas washing, and their compositions have been altered by phase fractionation. Thus, their maturities as indicated by biomarker data may be inaccurate. In summary, the aromatic data show that the oils in the different fields have similar sources, and were generated at largely the same thermal conditions.

Several biomarker ratios, most notably the 24-ethylcholestane 20S/(20S+20R) ratio (Table A4, Figure 16), indicate significantly lower oil maturities relative to those determined from the alkylated phenanthrenes. According to the 20S/20S+20R ratio, many of the oils show equivalent vitrinite reflectances similar to thermally immature sediments. This ratio reaches equilibrium at a value of 0.55, corresponding to an equivalent vitrinite reflectance of 0.7%Ro (Peters and Moldowan, 1993).

A plot of the 20S/(20S+20R) ratio versus depth (Figure 16) shows, for the Tiger Shoals oils, decreasing (less mature) values with decreasing depth, an effect attributed to sediment contamination during migration by Curiale and Bromley (1996) in the case of oils from Vermilion 14. Thus, migration contamination may also be responsible for much of the low apparent maturity indicated by some of the biomarker ratios in the Tiger Shoals study area.

Oils also show a range of 20S/(20R+20S) ratios at a given depth in most fields in the study area (Figure 16), indicating lateral variability. If these ratios indeed reflect migration contamination, and vary in a consistent way across a reservoir, they could be used to indicate flow direction, the oils having flowed from locations of high ratios (less contamination from sediment) to locations of low ratios. A map of the 20S/(20R+20S) ratio (Figure 17) for restricted depth intervals, and in some cases individual reservoirs, from each field shows spatial variations indicative of different flow directions for different fields. Inasmuch as these data are useful for determining oil flow direction, they indicate that each field is characterized by a localized 'plumbing system' rather than a central feeder zone away from which oil flowed to the various fields. Clearly, more data from individual reservoirs, and use of other biomarker ratios that also are affected by migration contamination, would be useful in determining reservoir filling directions.

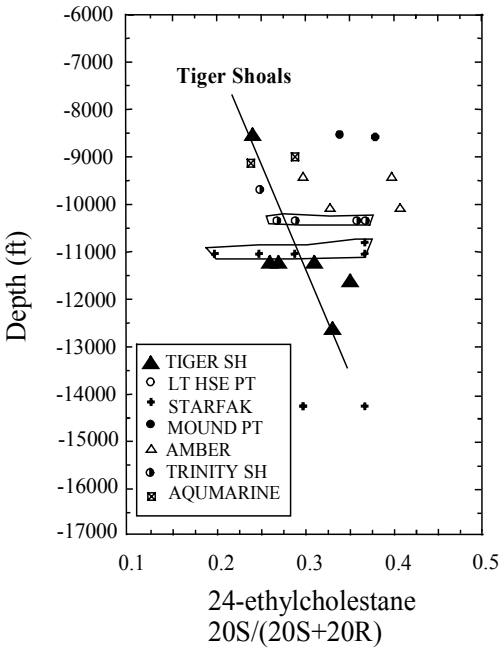

Figure 16. 20S/20S+20R ratio vs depth, Tiger Shoals study area oils. All values are anomalously low for the maturity of the oils. The best-fit line is solely for Tiger Shoals oils. It illustrates the upward decrease in 20S/(20S+20R), indicating that the oils were contaminated with the "biological" epimer 20R by interaction with sediment during their ascent.

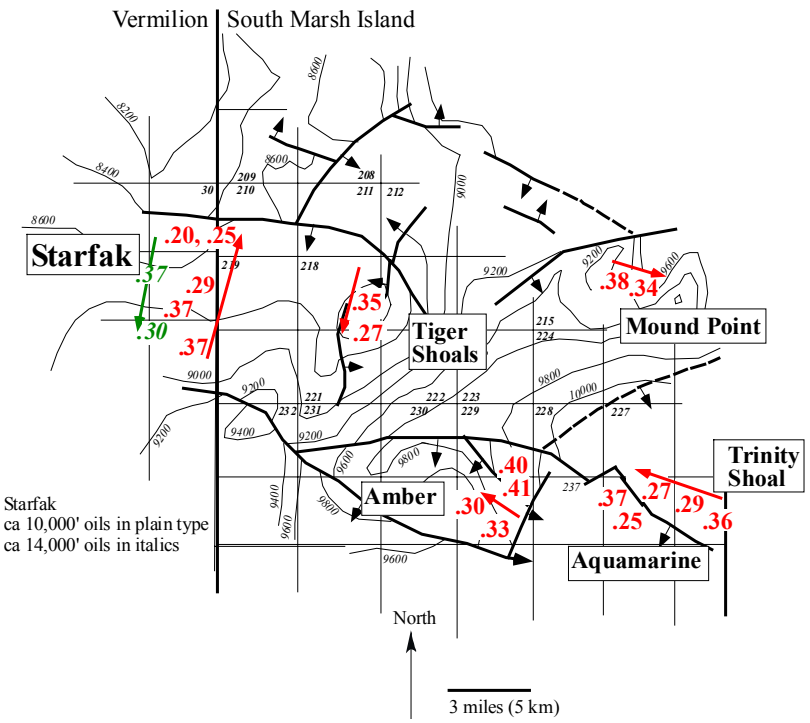

Figure 17. Structure contour map of Tex L marker, Tiger Shoals study area, showing 24-ethylcholestane 20S/20S+20R ratios. Although the data are sparse, they suggest oil flowed away from nearby faults into reservoirs.

Timing of migration. As described previously, nearly all Tiger Shoals oils are unbiodegraded. The presumed sterilization isotherm of 70 C is currently at a depth of about 5500 feet. Using a sedimentation rate of 0.25 mm/yr, applicable to the past several million years, this filling could have taken place no longer ago than 3.6 Ma for oils in the 'N' sand at 8500 feet. Deeper reservoirs, such as the V sand at 11,000 feet, could have filled as long ago as 6.7 Ma. However, the narrow range of maturities and source indicators for the Tiger Shoals oils indicates the filling probably was a relatively brief event. Thus, it is probable that all the Tiger Shoals study area oils migrated around 3.6 Ma.

Biodegraded gas is present in the D, H, L, and O reservoirs, the deepest sand being at 9000 feet (data in Table A2; see discussion in next section). If the sterilization temperature is 70 C and the geothermal gradient has remained the same since the Miocene, the biodegraded gas must have entered the 'O' sand before it was buried to a depth of 5500 feet, or at least 4.2 Ma. Thus at least some of the sampled gases evidently migrated before the oils that are present at the same depth range (i.e., 'N' oils at less than 3.6 Ma). This difference in migration timing implies a prolonged and complex history for gas washing and oil migration, which is not unexpected. Alternatively, the apparent difference in migration timing could simply reflect difference in the actual sterilization temperatures for gas versus oil, implying the involvement of different bacteria.

Gas source. Compound specific carbon isotopic data (Table A2) from five Tiger Shoals gases (D, H, L, O, and T sands) were analyzed by means of a plot of $\delta^{13}C_{compound}$ vs 1/Carbon number of each compound, as described by Chung et al. (1988) (Figure 18). Propane-ethane fractionation is normally used to evaluate gas maturity (after James, 1983). Propane, ethane, and (preferably) n-butane $\delta^{13}C$ data

can also be extrapolated to the ordinate to determine the $\delta^{13}C$ of a fictive 'infinite carbon number' source compound from which the gas was derived (Figure 18). The ethane-propane pair (+/- n-butane) also can be fitted on the 'Chung plot' with a line that extrapolates to $\delta^{13}C$ of thermogenic methane, which would have formed in isotopic equilibrium with the wet gas compounds (Figure 18; Table A5).

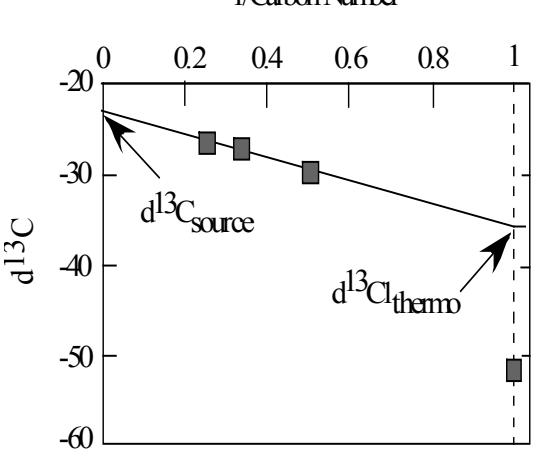

Figure 18. Gas compound $\delta^{13}C$ vs 1/Carbon number for n-butane, propane, ethane, and methane, showing the method of Chung et al. (1988). Sample shown is from SEI Block 330 field. Source $\delta^{13}C$ and extent of bacteriogenic methane mixing are determined through extrapolation of best-fit line through wet gas data.

The calculated thermogenic methane $\delta^{13}C$ is then utilized as an endpoint for computing the percentage of bacteriogenic methane (taken at -70 permil) present in the methane fraction. However, the use of only two points – ethane and propane $\delta^{13}C$ - to compute these parameters makes such computations susceptible to the effects of biodegradation, which in many instances selectively raises the propane $\delta^{13}C$ value (James and Burns, 1984). This results in erroneously high calculated gas source $\delta^{13}C$ values, calculated gas source maturities that are lower (i.e., greater ethane – propane ^{13}C fractionation) than is actually the case, and, for the same reason, lower (and even negative) computed fractions of bacteriogenic methane mixed with thermogenic gas. Such is the case for all but the T sand sample, which has a computed maturity of 1.2% Ro equivalent (based on Faber, 1987), 11% bacteriogenic methane, and a source $\delta^{13}C$ of –27.3 permil, within 1 permil of the average oil $\delta^{13}C$ value. Thus, the gas and oil may have essentially the same source; more analyses of unbiodegraded gas samples are needed. As noted above, samples from the D, H, L, and O sands have experienced biodegradation.

Gas washing. Tiger Shoals area oils have been extensively 'gas washed', giving rise to the abundant gas condensates that have been produced from this area. Analysis of n-alkanes by the method described in the previous section indicates that between 85% and 91% of n-alkanes (nC_{10+}) by mass have been removed from the Tiger Shoals area oils. Break numbers for oils from the study area are remarkably uniform and high, between 22 and 24 (Table A1). By comparison, oils from South Eugene Island Block 330 have break numbers of 10 to 16 (Meulbroek et al., 1998; later section in this report), and were computed to have been gas washed at pressures up to 6500 psi by up to 14 moles of gas per mole of oil (Meulbroek et al., 1998). The much higher break numbers of Tiger Shoals area oils implies considerably higher pressure of gas washing than at SEI330, on the order of 10,000 psi or more, with gas:oil molar ratios on the order of 100:1 (P. Meulbroek, pers. comm.). This molar ratio corresponds to a gas-oil mass ratio of about 7.5:1, or a volume ratio of about 30:1 at reservoir PT conditions. Pressures of 10,000 psi are presently known in the Tiger Shoals area only in the zone of 'hard' overpressure, at or below 11,000 feet.

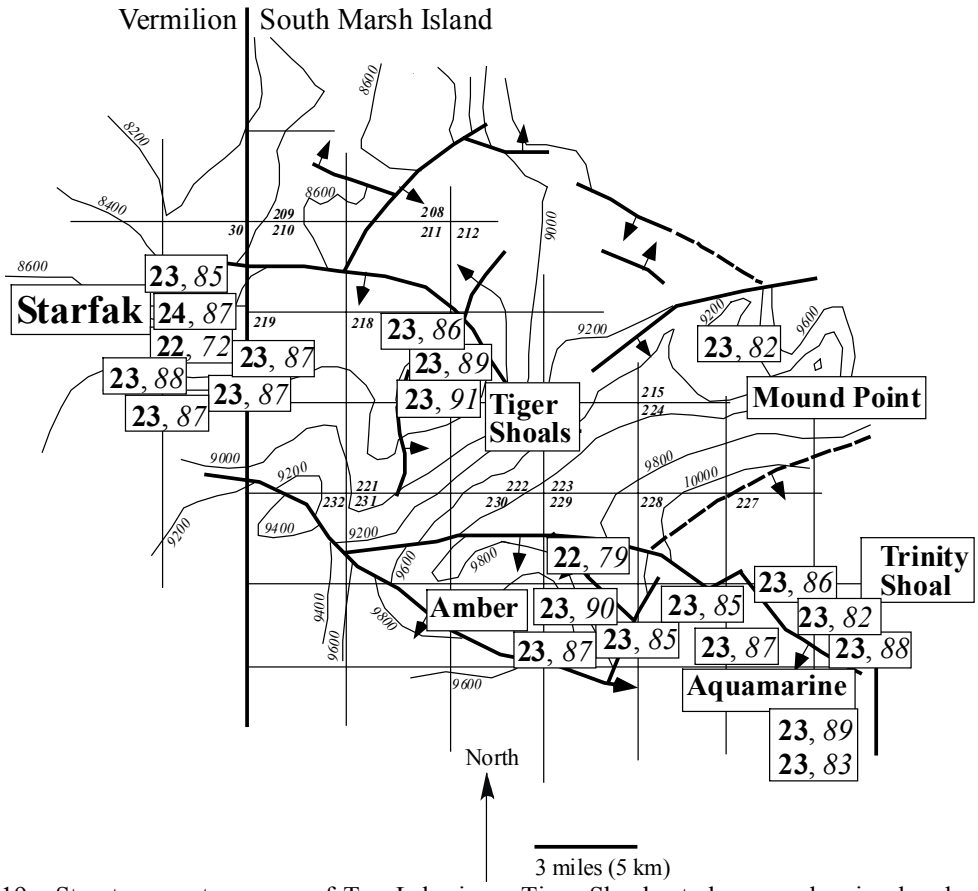

Figure 19. Structure contour map of Tex L horizon, Tiger Shoals study area, showing break number (first number) and percent n-alkane depletion (second number, italics) for sampled oils.

Gas washing has affected the Tiger Shoals area oils to similar extents, regardless of location or depth (Table A1, Figure 19, 20). The similarity in both break numbers and mass depletion of n-alkanes points to similar pressure-temperature-compositional conditions during gas washing of all the oils, in spite of the evidence that each field was characterized by an individual plumbing system. This uniformity in P-T-X conditions of gas washing over a large area in which fluids migration was primarily vertical would not be expected if gas washing were taking place in faults, as gas washing sites in an array of faults would not be expected to be at limited to the same narrow depth range everywhere, nor to have nearly homogeneous ratios of gas to oil. The homogeneity of mixing and the uniformity of PTX conditions of gas washing indicate that it probably took place in a relatively flat-lying sand, where migrating gas and oil were well-mixed at relatively constant ratios. The lack of variation of PTX conditions of washing despite the range of current sample depths

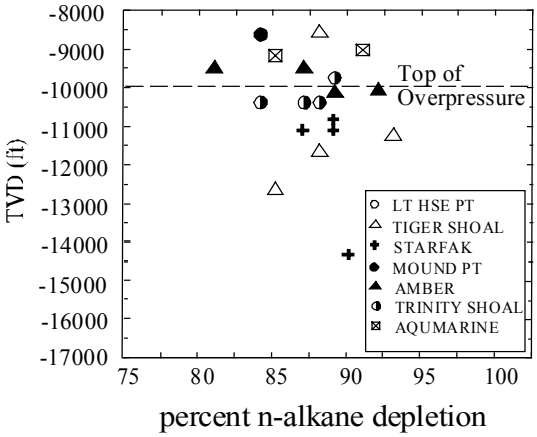

Figure 20. Percent n-alkane depletion vs. depth, Tiger Shoals study area. Depletion shows no evident relationship to top of overpressure.

indicates gas washing took place at some single deeper level in the system, and oils then migrated to their present locations.

Pressures during gas washing were high, possibly in excess of 10,000 psi, and large quantities of gas were involved. The paraffinicity of condensates relative to initial oils (Figure 14) implies a one-stage (batch) phase separation for the gas washing at Tiger Shoals. Determining the geologic setting of gas washing at Tiger Shoals narrows down to determining which sand(s) were at the requisite pressure, 10,000 psi, at the necessary time, no more than 3.6 Ma. Backstripping the sediments to their depths at 3.6 Ma, and back-extrapolating fluid pressures of overpressured sediments along a lithostatic gradient on the basis of the porosity profiles, it is evident that the Rob L sand may have served as the site of gas washing if the washing took place on the order of 3.6 Ma. Deeper sands below the Rob L are not known on the basis of available data, but they would have been at pressures higher than 10,000 psi for all of the time interval during which migration and washing took place, and so are not considered likely sites for gas washing. Conversely, the shallower '12000 sand' (Figure 9), the only other viable candidate for the site of washing in the Tiger Shoals stratigraphic section, is at the appropriate pressure at the present time, but gas washing in this sand does not account for the presence of gas-washed oils in the deeper Rob L sand at the Starfak field.

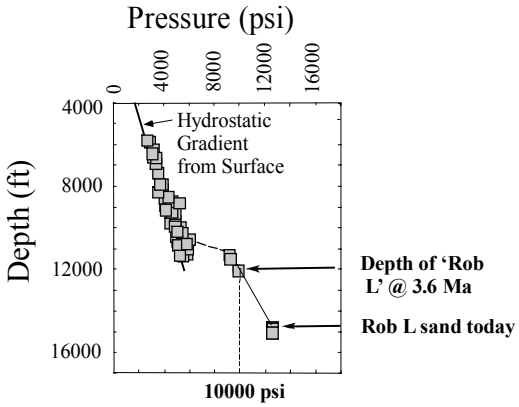

Figure 21. Reconstruction of fluid pressure in Rob L sand at maximum age of gas washing, 3.6 Ma.

Thus, gas washing of the Tiger Shoals oils probably took place in the Rob L sand, in the Pliocene (Figure 22).

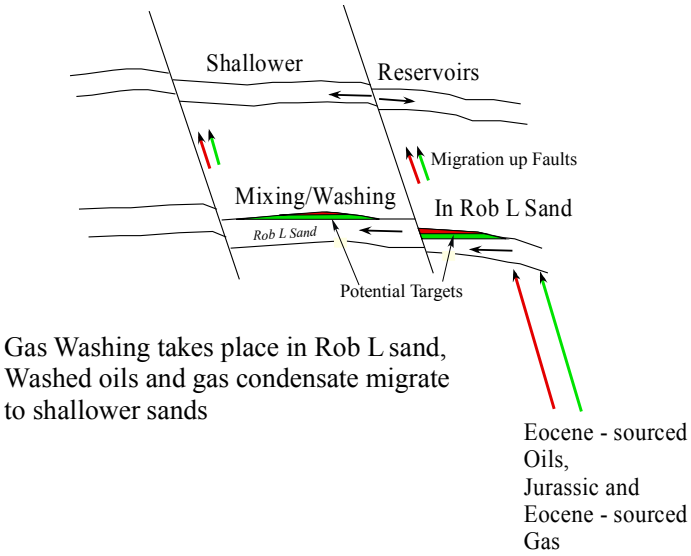

Figure 22. Schematic gas washing model of oil (green) and gas (red) at Tiger Shoals. Oil and gas ascend from source, mix, equilibrate, and separate in the Rob L sand, and then migrate up faults to shallower reservoirs.

SMI9 field

The South Marsh Island 9 (SMI9) field was discovered in the 1960's, and is currently operated by Chevron. In support of this investigation, Chevron has made available several structure contour maps, logs for several wells, reservoir pressure data, compound specific isotopic data for eight gas samples, and 32 oil samples, which have been analyzed by GC and HRGCMS at Woods Hole.

Geology. The SMI9 field has initial reserves 14.4 MMbo and 135 Bscf gas. Production is from a section of late Miocene deltaic sands from 8000 to 18,000 feet depth, flanking and dipping away from a vertical, nearly cylindrical diapir that extends nearly to the seafloor (Figures 23, 24). A system of northwest – to northeast-striking faults cuts the reservoir sands into a number of small fault blocks.

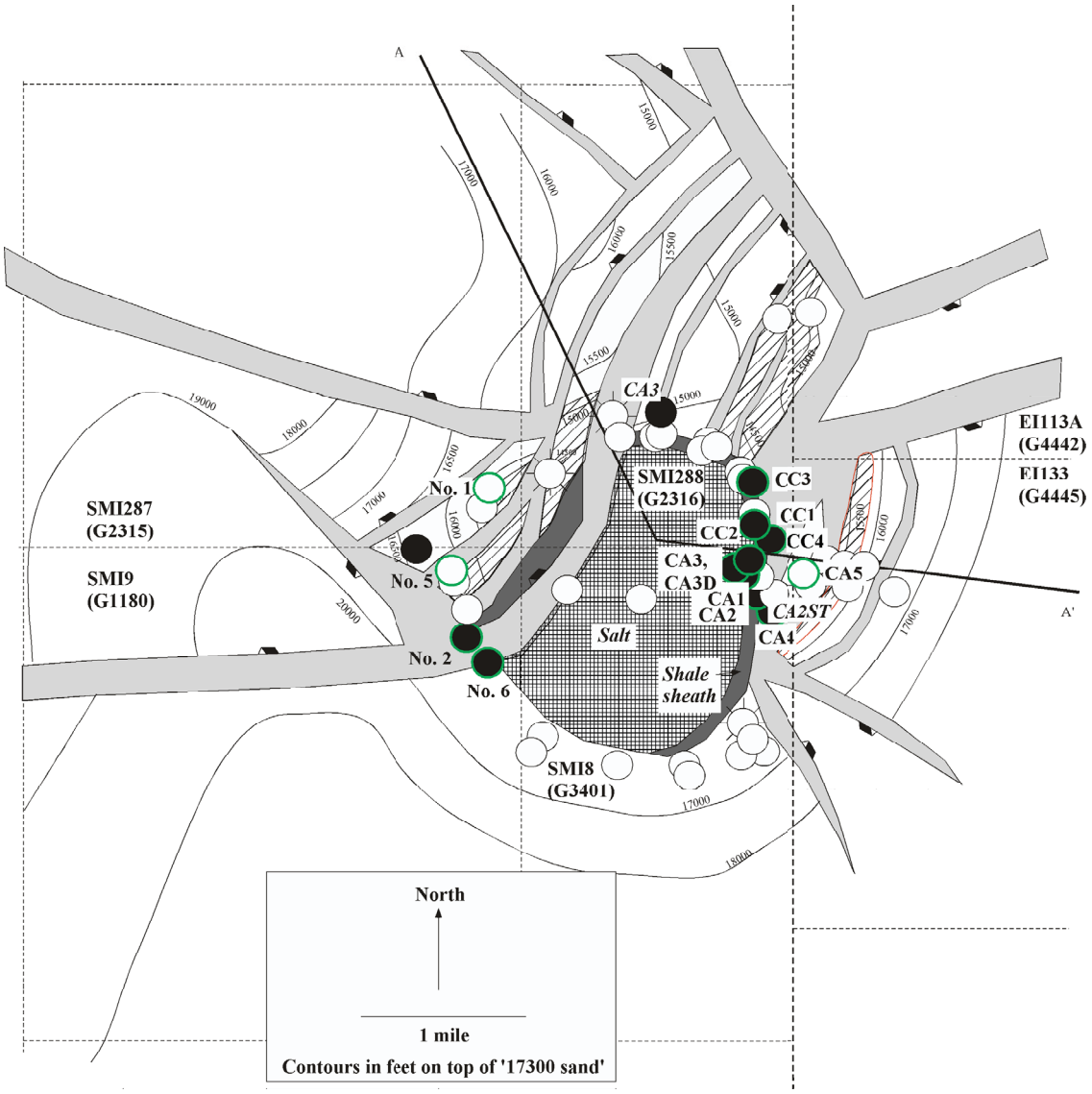

Figure 23. Structure contour map, top of 17300 sand, SMI9 field. Oil sample locations are shown in filled circles.

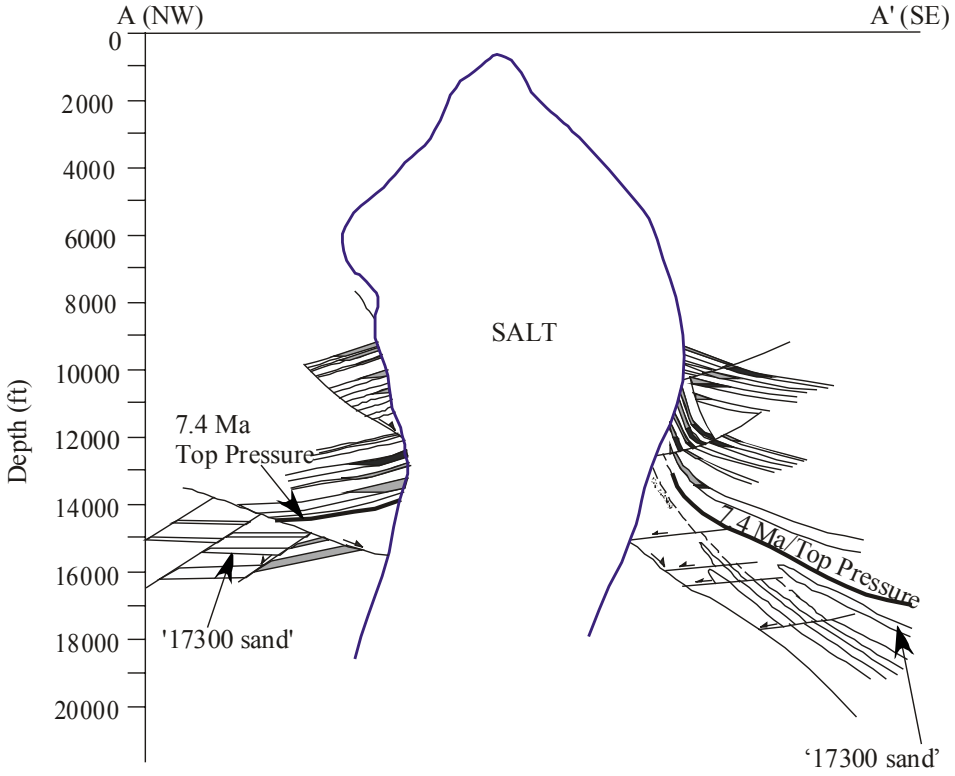

Figure 24. Northwest-southeast cross section through SMI9 field. Section location marked on Figure 23.

Fluid pressure. Initial reservoir pressures show a hydrostatic gradient from the surface to a depth of about 13,000 feet (Figure 25). Given that most of the production, hence pressure measurements, are within a kilometer of the diapir at the structurally highest portion of the sands, the geometry of the top of overpressure away from the diapir is not well constrained. Chevron cross sections (e.g., Figure 24) show that the top of overpressure is parallel to stratigraphic units. Logs from which porosity profiles may be computed are not currently available for this study.

Oil chemistry. In general terms, the oil source is likely primarily Eocene shales (Hood et al., 1995). Whelan and Eglinton (Vol. III, this report) have found that SMI9 oils have oleanane/C32 hopane ratios and dibenzothiopene/phenanthrene ratios compatible with oils sourced from Tertiary shales. Maturity, as determined from methylphenanthrene index (MPI1 and MPI2) estimates are in the range of 0.95 – 1.05% Ro equivalent (Whelan and Eglinton, Volume III). Similar maturities are noted for oils from SEI330 in this same dataset; they are somewhat higher than those previously reported by Whelan et al. (1994) for SEI330. This difference may be attributable to different analytical methods for determining methylphenanthrene isomer concentrations (Whelan, pers. comm); what is important in this context is that the maturity of SMI9 oils is similar to that of SEI330 and Jolliet oils. SMI9 oils have n-alkane slopes, which are crudely related to maturity if not affected by phase changes or fractionation, that are similar to those of SEI330 oils (table A1). Their n-alkane slopes are markedly lower (less negative) than are those of Tiger Shoals oils, suggesting that the maturity of SMI9 oils is much closer to that of SEI330 oils

than to that of Tiger Shoals oils (Re = 1.0 to 1.2% R_o equivalent).

Timing of filling. SMI9 oils were collected over a range of depths, from hydrostatically–pressured to hard–overpressured sands. None of the oils shows evidence for biodegradation in terms of their Pr/nC_{17} ratios (Table A1). All ratios are less than one, and many are significantly less. The fact that none of the shallower oils show evidence of biodegradation, even though they are as little as 1700 feet deeper than the maximum likely depth of bacterial activity (at the 70 C isotherm, at 8500 feet), indicates that the oil currently in the reservoirs may have migrated there within the past 1 Ma (using a sedimentation rate of 0.7 mm/yr), when the reservoirs were already buried deeper than the 70 C isotherm.

Gas source. Stable isotope data from gas samples from several reservoirs indicate varying amounts of mixing of thermogenic gas with bacteriogenic methane (Table A5, Figure 26). Based on the 'Chung analysis', the methane component in the SMI9 gases is between 14 and 41% bacteriogenic (assuming $\delta^{13}C$ of bacteriogenic methane is uniformly -70 permil). Hydrogen isotope data corroborate this range of bacteriogenic methane contents (Figure 26). Figure 26 indicates there may be a small range of $\delta^{13}C$ and δD values for the bacteriogenic methane end member. Maturity of gas, based on propane and ethane $\delta^{13}C$ values, is between 1.7 and 2.0% R_o equivalent (Table A2). Gas source $\delta^{13}C$ values are between –20 and –22 permil (Table A5), on the order of 4 to 6 permil higher than whole-oil $\delta^{13}C$ values from the same reservoirs (Table A1; Figure 27). It is unlikely that the gases sourced either from cracking of that oil or from the same sediment that sourced the oils; rather, different sediment sources for gas and oil are indicated.

SMI9 gas compositions show complex geographic and depth variations. $\delta^{13}C$ of ethane shows a small range of values on the eastern side of the diapir, regardless of depth (Figure 28), whereas ethane in the CA3 sample to the north (in SMI288) shows considerably higher $\delta^{13}C$. This sample also has the highest maturity, at 2.0% Ro. This sample also has among the lowest percentages of bacteriogenic methane (23%). One well, the CA3 in SMI8, has significantly different percentages of bacteriogenic methane (14% vs 41%) over a 2000 foot vertical distance. Overall, the 'plumbing system' of gas, and of gas-washed oils, at the SMI9 field is complex, drawing on different systems depending on position relative to the diapir.

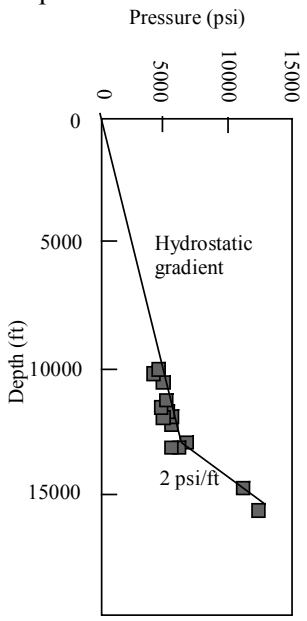

Figure 25. BHP versus depth, SMI9 field.

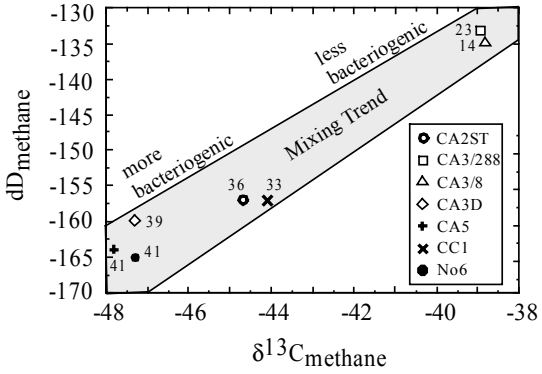

Figure 26. Methane δD vs $\delta^{13}C$ for SMI9 gases. Numbers shown next to samples are percent bacteriogenic methane (assumed $\delta^{13}C$ of –70 permil) in samples as determined by analysis after Chung et al. (1988).

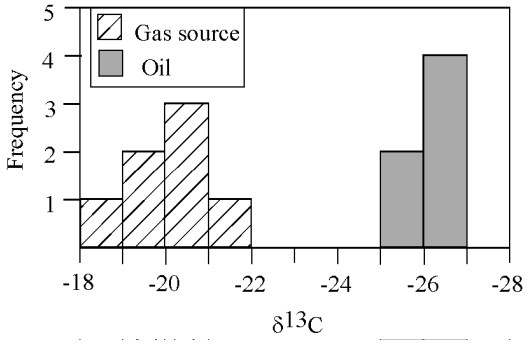

Figure 27. Comparison of computed gas source $\delta^{13}C$ (after Chung et al., 1988) with measured whole-oil $\delta^{13}C$ values, SMI9 field. Gas and oil are shown to have different sources.

Gas washing. All of the oils are gas-washed; n-alkane mass depletion in these oils ranges from 20% to 65%, and break number accordingly ranges between 15 and 21. Extent of gas washing at a given depth covers a wide range; however, overall amount of gas washing shows a slight decrease with increasing depth (Figure 29). The two least-washed samples come from a fault block on the west side of the diapir, and may represent a different part of the plumbing system than the other samples. These least-depleted oils are in the deepest reservoir, at hard overpressure. The break numbers of the washed oils overlap at the low carbon number end with SEI330 oils (Meulbroek et al., 1998) and at the high carbon number end with Tiger Shoals oils (previous section). As break number is primarily a function of pressure at which the oil was gas washed, the pressures of gas washing of SMI9 oils was probably higher than 6200 psi and less than around 10,000 psi. At 1 Ma (the timing of migration), these pressures would have existed at depths between 11,500 and 14,000 feet, assuming compaction disequilibrium. Subsequent burial by 2300 feet of sediments in the past 1 Ma places the sediments in which the oils were gas washed to depths between 13,800 and 16,300 feet. This depth range for gas washing is applicable only near the diapir, where the pressure measurements were made.

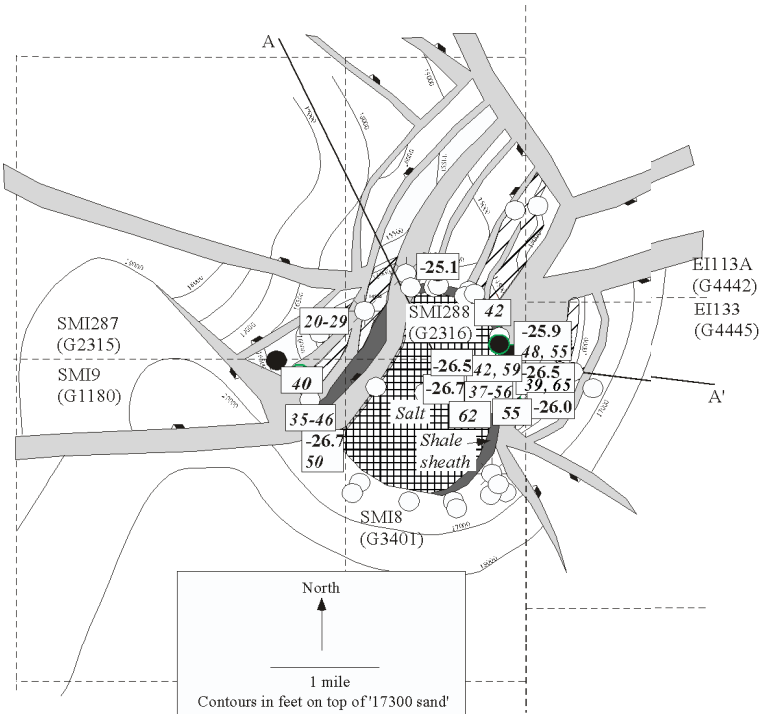

Figure 28. Structure contour map on 17300 sand, SMI9 field, showing $\delta^{13}C$ of ethane (plain font) and percent n-alkane depletion (italics). Except for the sample north of the diapir, ethane isotopic composition is relatively uniform. Extent of n-alkane depletion by gas washing is somewhat less on the west side of the diapir.

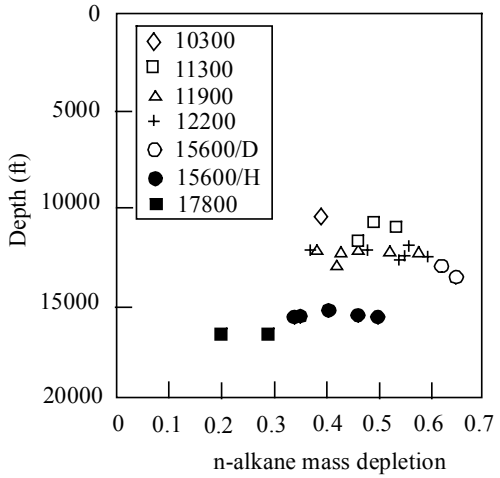

Figure 29. N-alkane mass depletion vs depth, SMI9 field.

Oils having the lower break numbers were possibly gas washed near the top of overpressure at the time of washing. Oils having higher break numbers were gas washed significantly below the depth of top of overpressure at the time. Some gas-washed oils have a relatively low break number of 15 but currently lie in the hard-overpressured '17800 sand' at depths of about 15,000 to 15,700 feet. These oils were likely washed at shallower depth and subsequently buried.

SEI330 Area

For the purposes of this report, the 'SEI330 Field' extends southeast of South Eugene Island Block 330 to incorporate the South Eugene Island Block 341 and 360/361 Fields (Figure 1). The SEI330 Field proper is described in full first, followed by descriptions of the somewhat less well-characterized SEI341 and SEI360/361 Fields.

SEI330 Field Proper

Geologic setting. The South Eugene Island Block 330 field contains initial reserves of 307 Mmbo and 1.5 Tcg gas in four-way closures and fault traps in a Plio-Pleistocene salt withdrawal minibasin about 120 km offshore Louisiana (Figures 30, 31). The geology of the field is described in detail by Holland et al. (1990) and Alexander and Flemings (1995), and the field is placed within a larger geologic context by Rowan (1995). Hydrocarbons are produced primarily from a section of deltaic sands at depths of 4500 to 8000 feet, mostly on the downthrown side of a growth fault (the 'A' fault) – antithetic fault system. Reservoir sands are designated alphabetically, from GA (shallowest) to OI (deepest, Figure 32).

Fluid Pressure. Like Tiger Shoals and the SMI9 field, the SEI330 reservoirs straddle the top of overpressure. Initial reservoir BHP measurements define three pressure compartments in the downthrown side (Figure 33; Hart et al., 1995, Losh et al., 1999). The GA and HB sands are hydrostatically pressured. Beneath the HB sand lies a compartment (IC – LF sands) characterized by fluid pressures that are about 500 to 700 psi above hydrostatic, but which has an internal hydrostatic water pressure gradient. A third compartment, containing the NH and OI sands, lies at 'hard overpressure', at pressures on the order of 0.75 times lithostatic. Thick shales separate these compartments (Figure 32). In addition, the 'A' fault defines a profound lateral seal to all fluids at the depth of the reservoir section; water pressures differ by up to 1800 psi across the fault (Figure 33). In the fault and on the upthrown side, fluid pressures are as much as 0.95 times lithostatic.

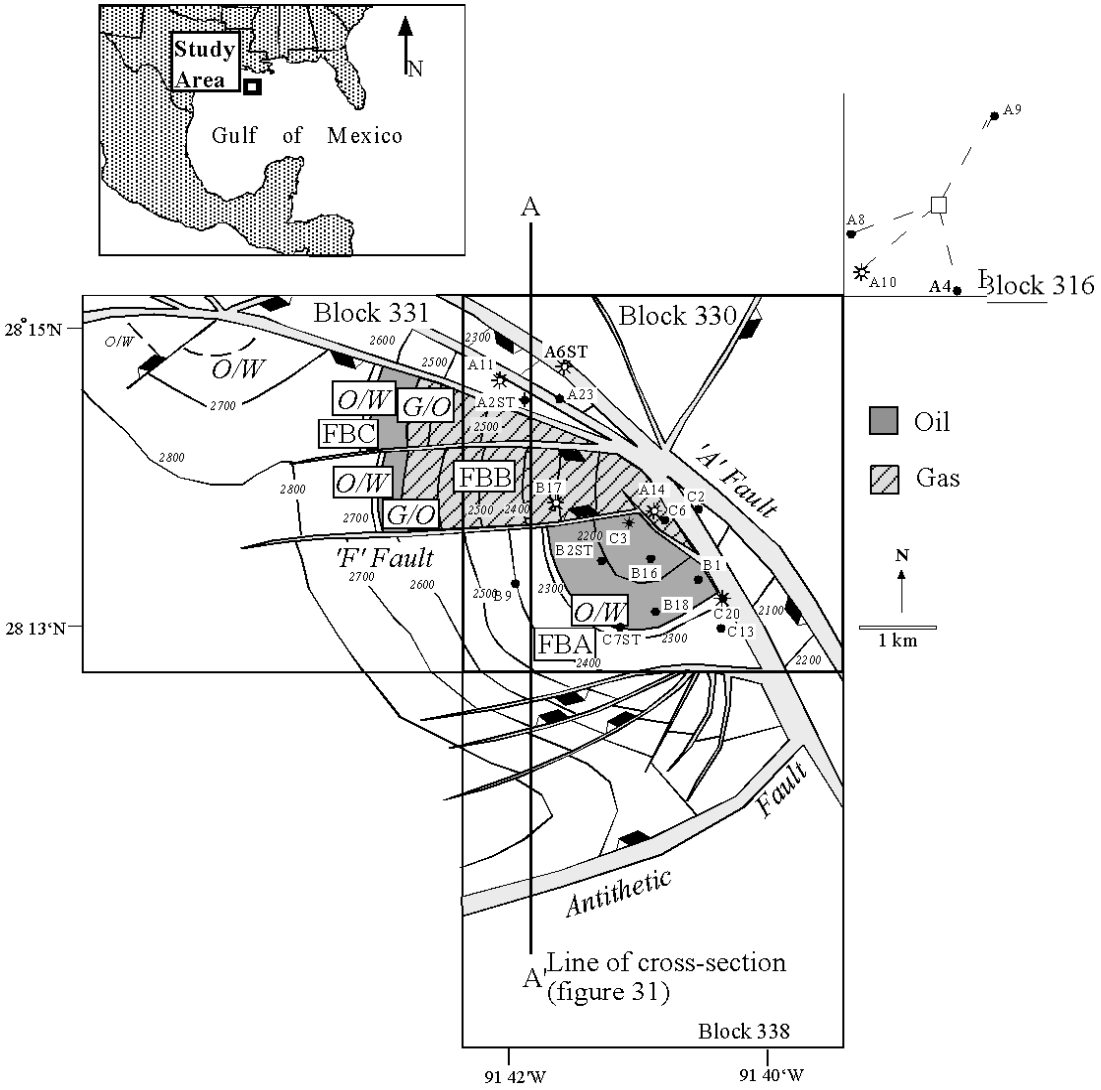

Figure 30. Structure contour map, top of OI1 sand, SEI330 Field, showing locations of selected wells from which oil, gas, and brine samples were collected.

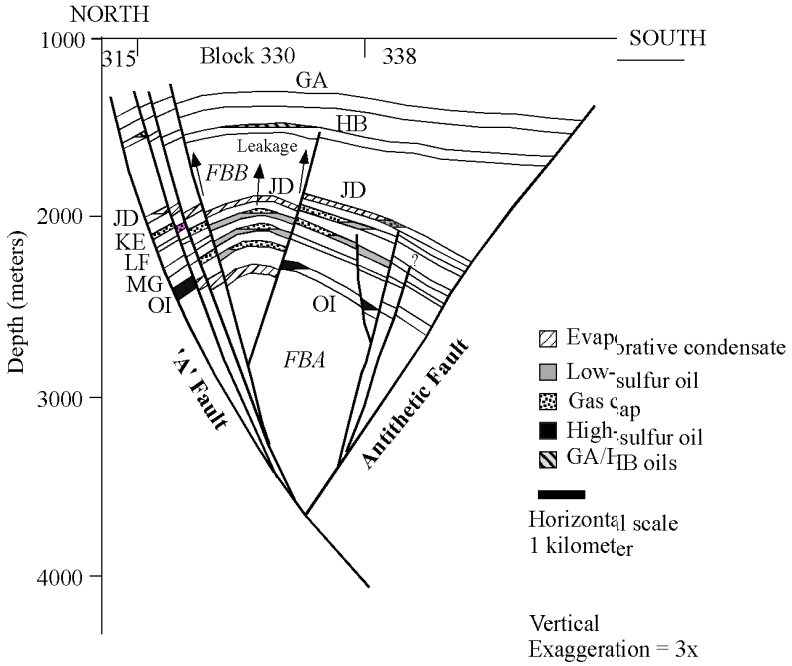

Figure 31. North-south cross section, SEI330 Field. Fluid types are shown for individual reservoirs.

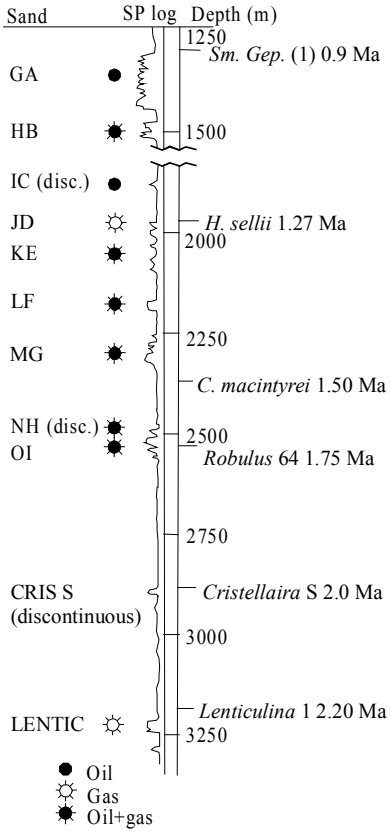

Figure 32. Composite log, SEI330, downthrown to 'A' Fault, modified from Holland et al. (1990).

Porosity profiles on both upthrown and downthrown sides of the 'A' fault in Block 330 correspond to the pressure compartments described above (Figure 34; Hart et al., 1995; Gordon and Flemings, 1998). Overpressure at Block 330 is thus largely attributable to compaction disequilibrium (e.g., Cathles, 1999), modified by pressure redistribution as a result of tilting of sands (Stump, 1998) and localized unloading due to minor fluid flow across the 'A' fault into downthrown compartments (e.g., Hart et al., 1995). Because fluid pressure history is recorded by the sediment porosity at Block 330, the timing of inception of overpressure in the different compartments can be deduced. In the NH and OI sands, overpressure began to develop between 0.5 and 0.7 Ma (Figure 35), based on 'arrested compaction depths' shown in the Figures, combined with the sedimentation rate. In the middle compartment, overpressure began to develop at about 0.15 Ma. Pressure evolution has direct impact on interpretation of gas washing at SEI330. If the pressure field has changed over time, then the depth at which gas washing took place will also vary, depending on when it happened. Thus, to better interpret gas washing, a first

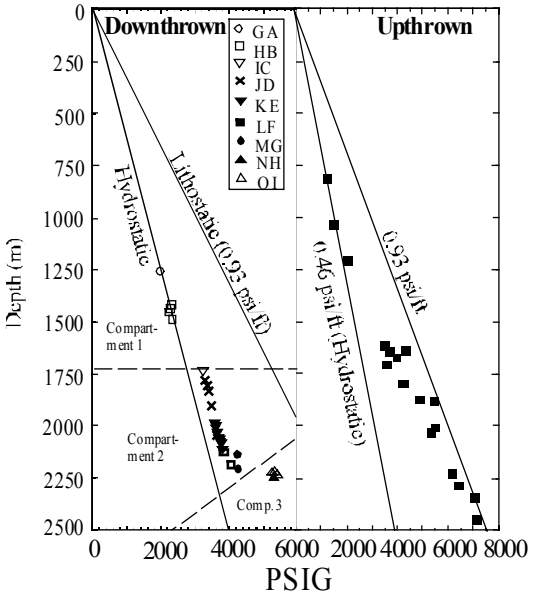

Figure 33. Initial reservoir pressures, derived from BHP (downthrown side) as well as gas kicks in mud (upthrown side). Pressures on the downthrown side are corrected to hydrostatic equivalents.

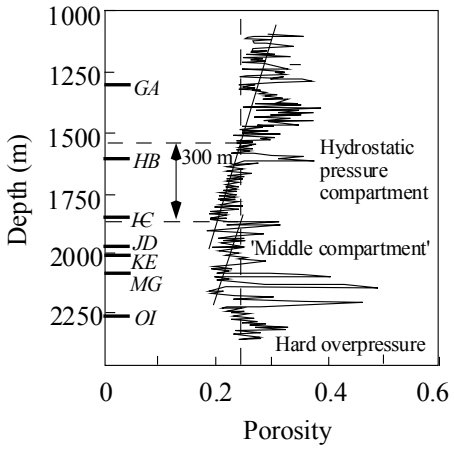

Figure 34. Porosity vs depth, SEI330, downthrown side to 'A' Fault. Similar relationships between porosity and fluid pressure exist in the upthrown side of the fault.

approximation of pressure history for SEI330 sediments is here determined on the basis of compaction disequilibrium. Largely consistent with the results of Gordon and Flemings (1998) and Hart et al (1995), the depth of arrested sediment compaction is determined by projecting porosity from undercompacted sediments upward along a constant porosity profile to the intersection with the hydrostatic compaction trend. The pressure in that sediment during burial is then determined as hydrostatic between the surface and the depth of arrested compaction, and increasing at a lithostatic gradient below that (Revil and Cathles, 2001). The results of this approximate forward modeling of pressure evolution on both sides of the 'A' fault are shown for different 'snapshots' in time in Figure 35.

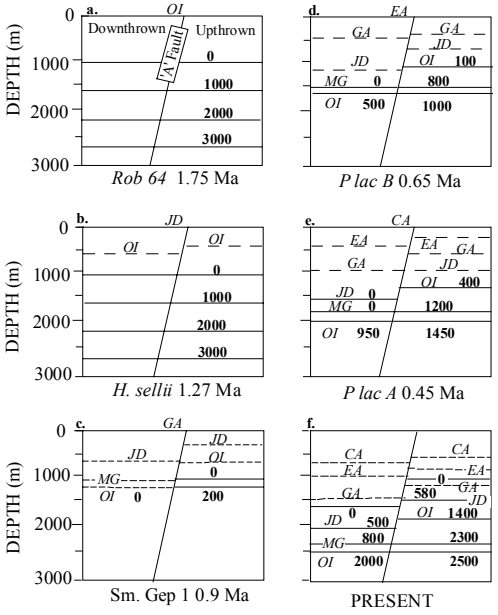

Figure 35. Fluid pressure evolution, SEI330, based on porosity log interpretations, from OI sand deposition (Rob 64) to present. Italics denote sands, numbers denote fluid overpressure in psi.

Hydrocarbon chemistry. Whelan et al. (1994) demonstrated that the SEI330 oils all have similar source and maturity. Oils were generated within Mesozoic carbonate rocks, now buried to 14 km, at thermal maturities of 0.8 +/- 0.05% Ro equivalent. Relatively minor chemical variations between reservoirs indicate that the immediate source of the oils, from secondary reservoirs between the Mesozoic source rocks and the Block 330 sands, were distinct from one another. Whole-oil carbon isotopic values occupy a narrow range, -27.0 +/- 0.15 permil (table A1). Condensate $\delta^{13}C$ values lie in the same range. They also have DMCP isomer ratios identical to those of the oils (Figure 36), indicating a common source. Gas condensates lie in several sands, notably the JD, which contains 1.2 Tscf gas. The

condensates formed by means of evaporative fractionation, as indicated by their systematically higher paraffinicity and lower aromaticity relative to SEI330 oils (Whelan et al., 1994; Meulbroek et al., 1998).

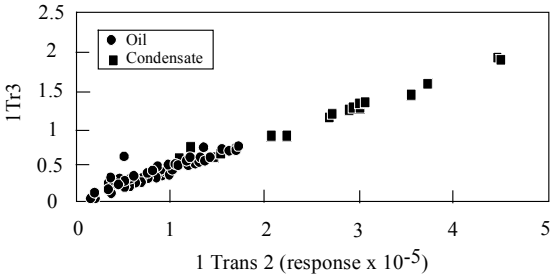

Figure 36. DMCP isomers, SEI330 oils and gas condensates.

Timing of filling. Oils in the GA and HB sands have experienced moderate biodegradation, as indicated by the loss of n-alkanes and most isoprenoids, but not steranes (e.g., Peters and Moldawan, 1993; Schumacher, 1993; Whelan et al., 1994). Oils from deeper sands have Pr/nC_{17} ratios mostly less than one (table A1). Those from the OI and NH sands are on the order of 0.5, indicating no biodegradation, compatible with lack of unresolved complex as shown by gas chromatography (Whelan et al., 1994). Sterilization temperature in these sands is about 65 C (Figure 37).

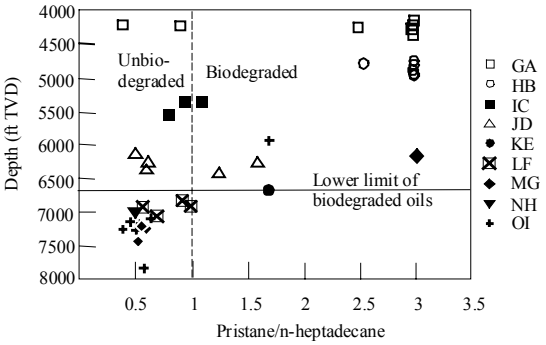

Figure 37. Pr/nC_{17} ratios, SEI330 oils. Highest temperature for biodegraded oil is about 65 C.

Oils below the JD sand, and in particular those in the OI sand, have not experienced temperatures below 65 C; thus the reservoirs filled after they were buried below 1800 meters depth. This constrains the OI sand to have filled within the past 230,000 years, and the shallower sands to have filled within the past 100,000 years.

Gas source. Gas source and maturity are well-constrained at SEI330. The 'Chung plot' yields gas source $\delta^{13}C$ between –23 and –24.5 permil, from 2.5 to 4 permil higher than $\delta^{13}C$ of oils or condensates from the same reservoirs (tables A1 and A5). Thermogenic gas was not derived from cracking of the oil represented in the reservoirs, and it was likely derived from different sediment, or from a different fraction of the kerogen, than was the oil. Percentage of bacteriogenic methane is low (10 to 15%) in all samples but one, the A6ST/KE sample taken just next to the 'A' fault (table A5). Gas samples from this fault were demonstrated to contain significant percentages of bacteriogenic methane (Losh et al., 1999), which locally may vent into reservoirs. Gas maturity was shown by Whelan et al. (1994) to lie between 1.4 and 1.7% Ro equivalent.

Gas washing. Gas washing has affected some, but not all, of the SEI330 oils (Meulbroek, 1997; Meulbroek et al., 1998). Most of the gas washed oils are in the OI sand; a few such oils are also found in the NH, MG, and LF sands (Figure 38). Oils from the 'A' fault zone in the Pathfinder well (A20ST; Anderson et al., 1994) show little or no gas washing, at least for nC_{10} and heavier n-alkanes, despite being sampled over a wide range of pressures (consistent with work of van Graas, et al., 2000). Break numbers for the gas washed oils range from 10 to 16, and n-alkane mass depletion in the fractionated oils ranges from 3 to 15%. Equation of state modeling indicates these oils were gas washed at pressures on the order of 5500 to 6200 psi, or depths of 2.4 to 2.9 km, under the present geothermal gradient at SEI330 (Meulbroek et al., 1998, P. Meulbroek, pers. comm.). Although gas is currently migrating along the 'A' fault (Holland et al., 1990), oils in the reservoirs are not presently being gas washed to any significant extent.

Oils in the Block 330 reservoirs differ from one another, and show chemical

variations within individual sands (Figure 38; Losh et al., 2002). Much of the fluid migrated from the antithetic fault on the south side of the SEI330 minibasin, although a significant fraction migrated via the main, south-dipping growth fault as well. The geochemical variations indicate that the 'plumbing system' supplying the downthrown sands was complex, with different parts of the fault system linking deep hydrocarbon accumulations with specific shallower sands within the reservoir section.

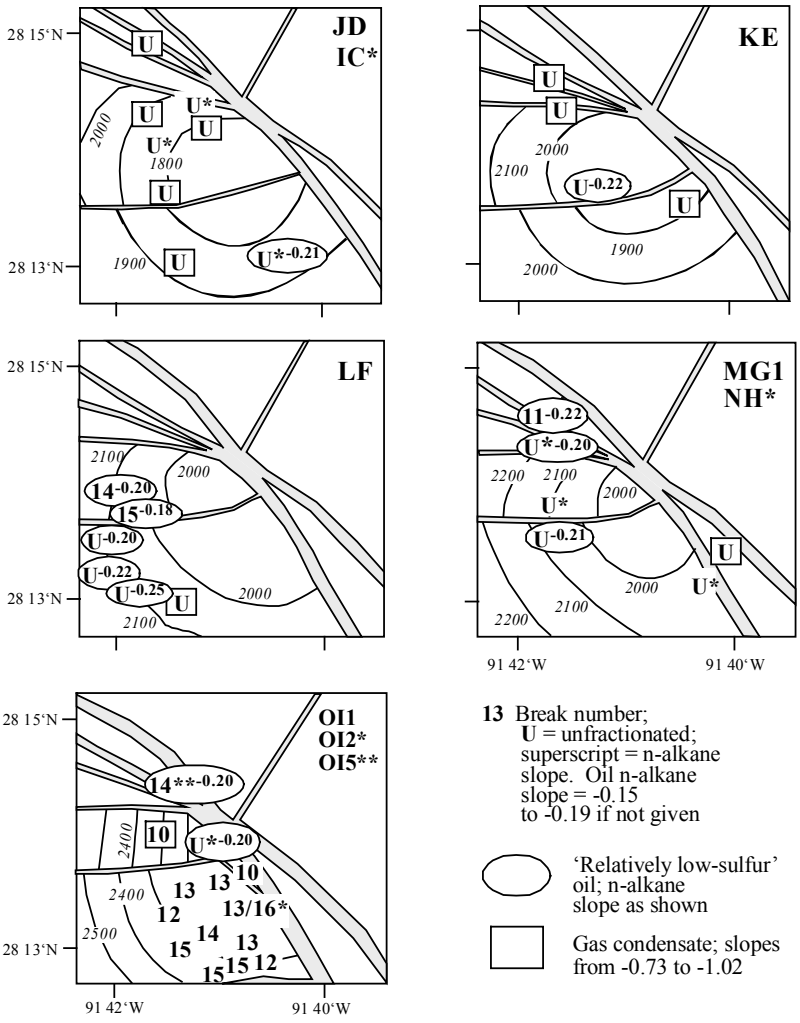

Figure 38. Structure contour maps on selected sands, SEI330, showing distribution of gas-washed oils. Break numbers are shown for gas-washed oils. Also shown are the distributions of gas condensates and low- vs high-sulfur oils, as identified by Whelan et al. (1994) and Losh et al. (2002).

Application of gas washing analysis to exploration. The excellent database at SEI330 allows us to integrate hydrocarbon chemistry and known constraints on fluid pressure, migration timing, and burial history to demonstrate the usefulness of EOS modeling of gas washing. The analysis of gas washing can provide a valuable tool for risking targets, especially in a field in which deeper exploration is contemplated. From equation of state modeling, we can estimate the conditions of gas washing in terms of

pressure, temperature, and composition. Of particular interest for exploration is the determination of the maximum depth at which one may find the gas-washed oil that is present in shallower reservoirs. To do this, the fluid pressure profile that is appropriate to the time and location of gas washing must be used. For the gas washing results presented above, a hydrostatic fluid pressure gradient to 1.5 km depth, underlain by a lithostatic gradient, was assumed for computing the depth at which gas washing took place. According to the fluid pressure reconstruction method described previously, that pressure profile corresponds to that which prevailed in the downthrown side of the 'A' fault about 300,000 years ago. However, since then, the fluid overpressure at a given depth has decreased slightly because the continued deposition of sandier, well-drained sediments has depressed the top of overpressure. In addition, there is a pronounced difference between the fluid pressure profiles on the upthrown and downthrown sides of the 'A' fault. Finally, for the maximum depth of sediment containing fractionated oil to be accurately known, the subsequent burial of the sediments in which the gas washing happened must also be taken into account.

The relationship between estimate of washing depth, location, and timing of gas washing, is shown graphically in Figure 39. As described previously, the OI oils were gas washed at depths between 2.4 and 2.9 km, assuming a fluid pressure profile appropriate to the downthrown side at 300kA. Today, the same fluid pressures exist at depths of 2.5 to 3.0 km, respectively. The change in washing depth due to the change in fluid pressure profile with time is shown by the "no burial" trends on Figure 39. Additionally, sediments on the downthrown side of the 'A' Fault were buried 600 meters since 300 kA (based on Alexander and Flemings, 1995). The combined effects of the change in fluid pressure profile and of post-washing burial are taken into account in the shaded areas on Figure 39. The "Downthrown Path" area corresponds to the fluid pressures and burial depths of sediments in which gas washing would have taken place on the downthrown side of the 'A Fault' in the past. As described previously, the fluid pressures on the upthrown side of the 'A Fault' are substantially higher than on the downthrown side at depths of one to three km. The elevated fluid pressure on the upthrown side, combined with the slightly different burial history for the upthrown side (500 m in 300kA) accounts for the shaded "Upthrown Path" area on Figure 39.

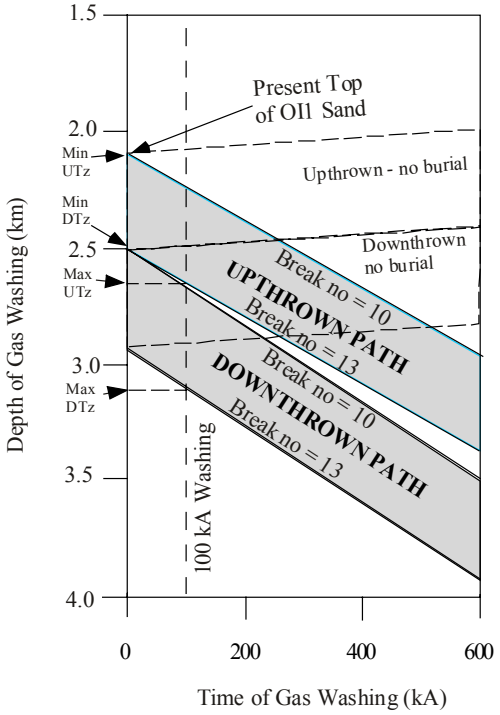

Figure 39. Depth of gas washing vs time of washing, upthrown vs downthrown sides of 'A' Fault, Block 330

To determine the present depth of sediment in which gas washing took place, the timing of gas washing must be constrained. At SEI330, the lack of biodegradation of oil below 2 km indicates the reservoirs filled within the past 100,000 years or so. If washing took place at 100 kA, the sediment in which gas washing of OI oil took place would now be at depths of ~2.65 – 3.1 km (for oils having break numbers of 10 to 13, respectively) if washing took place on the downthrown side. If washing took place on the upthrown side at 100kA, the sediments in which washing took place would now be at

depths of ~2.2 – 2.65 km, for oils having break numbers of 10 to 13, respectively. If gas washing took place a longer time ago, then the sediment in which it took place would be presently at a greater depth.

This technique can be used to assess exploration risk. Consider the scenario in which oils having break numbers of 13 are present in shallow reservoirs (e.g., the LF), but the OI reservoir had not been drilled yet, although it was being considered as a potential target. Furthermore, the chemistry of JD condensates indicates they originated from gas-washed oils. Although the OI sand is not identified as the "washing sand" at SEI330, the existence of gas-washed oil in the OI sand is compatible with the presence of condensates in the JD sand, and with the geologic reconstruction shown in Figure 39.

Figure 40 shows the present depth of sediment in which gas washing took place at 100kA, based on Figure 39. The top and bottom of the zone in which gas washing took place is shown for both upthrown and downthrown sides of the 'A Fault.'

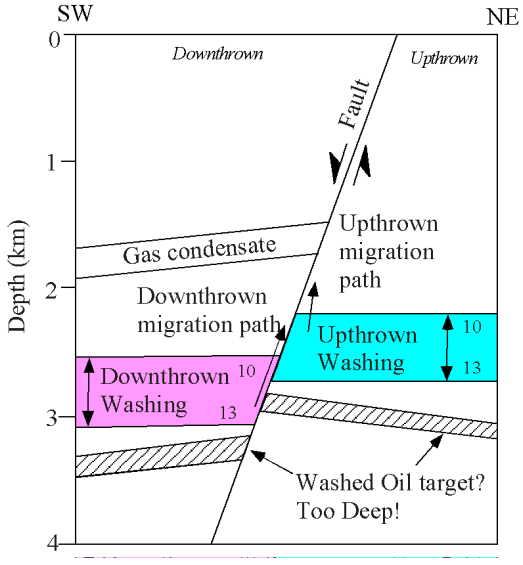

Figure 40. Schematic cross-section across 'A' Fault, SEI330, showing regimes of gas washing of oils in Block 330 reservoirs. Depths of washing for break numbers of 10 and 13 are shown.

If a 'washing sand' target were being considered on the upthrown side at a depth of 3 km, for example, the reconstruction indicates that this sand would be unlikely to have been the site of gas washing and so would not have a high probability of containing washed oil.

This technique has the capability of identifying 'missing' oil, if gas-washed oil has been sampled and if genetically related evaporative condensates are present. For example, the composition of gas-washed OI oils indicates an average of 12 moles gas/mole oil, or a volumetric gas:oil ratio of about 18:1 at reservoir conditions (Meulbroek et al., 1998). At Block 330, the volume of JD condensate to gas-washed OI oils is similar to that determined from modeling of gas washing of OI oil, or about 15:1 (1.2 Tscf: 120 MMBO). Thus, within the uncertainly of the calculations, little if any oil or condensate would be identified as 'missing' in this system. However, if only 10 million barrels of gas-washed oil were present in the OI reservoir instead of 120 MMBO, a potential 'missing' resource of 110 MMBO would be identified by this analysis in order to account for the volume of the JD condensate. The maximum depth of this 'missing' residual oil is identified as 2.6 km on the upthrown side or 3.1 km on the downthrown side of the 'A' fault. Thus, this analysis can point not only to depths of targets but, if the appropriate fluids have been sampled, it can constrain potential volumes of hydrocarbon in the target as well.

Migration routes for fractionated oils can also be deduced by this method, if their distribution is known. For example, if gas washing took place at 100kA, and a fractionated OI oil having break numbers as low as 10 were present in a downthrown sand at a depth of 3.0 km, it is clear from Figure 40 that it could not have been washed in the upthrown side and subsequently migrated across the fault. Rather, the oil would have to have been gas-washed on the downthrown side, ruling out the upthrown side as a migration route for gas-washed oil and its associated condensate into the downthrown reservoir sequence. This insight can aid in risking upthrown targets. In this case, it would indicate that other oils that migrated as part of the same petroleum system as the gas-

washed oils may be more likely to lie in other downthrown reservoirs rather than in upthrown sands. Clearly, this technique must be used in conjunction with well-defined geologic constructions and all available knowledge of fluid geochemistry in order to be most useful.

SEI341 and SEI361 Fields.

Geology. The SEI341 and SEI361 fields are operated by Chevron, and are only partly characterized here. Available reservoir data consist of structural geologic maps of selected sands, well logs, and reservoir BHP and temperature data. The SEI341 field (Figure 41), put into production in 1982, has initial reserves of 84 Mmbbo and 225 Bscf gas (MMS, 1999). It lies in Upper Pleistocene aggradational deposits; no paleontological data are available. Samples were obtained from depths of 5650 to 7380 feet. The sedimentary section differs somewhat from that at SEI330 and shows significant lateral variation within the field. In the A12 well, sands are abundant to depths of about 6000 feet, then are underlain by thick shale to depths of about 7800 feet, then underlain by a deep sandy interval about 500 feet thick. Sands in the A10 well (Figure 41), which typifies the downthrown, producing fault block, are less abundant, with shale dominating the 5000-7000 foot interval.

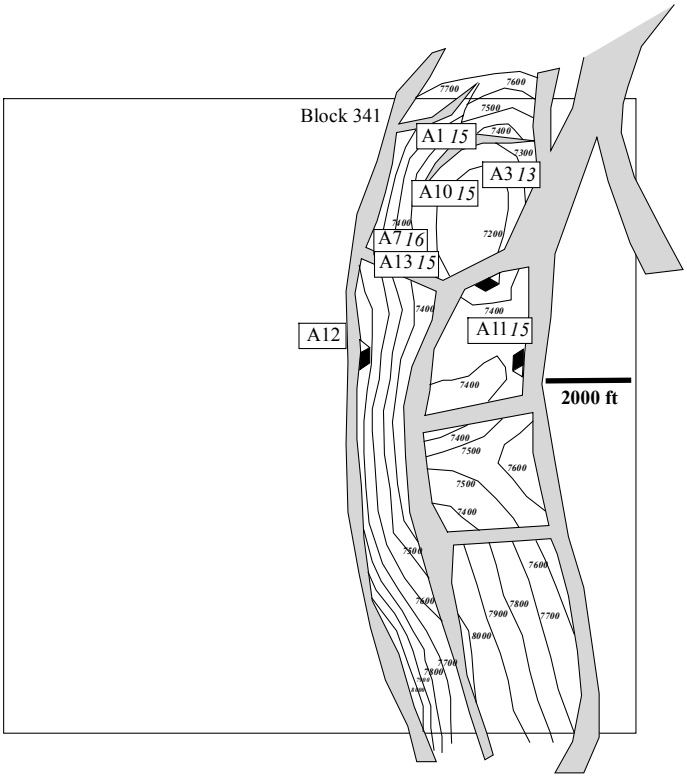

Figure 41. Structure contour map, top of '7400 sand', SEI341. Locations of oil samples are shown, as is the A12 well, discussed in the text. All samples are from the 7400 sand, except for A7, from the '6000 sand' and A11, from the '6400 sand'. Break numbers (italics) are shown for samples from which they could be determined.

Available BHP measurements (Figure 42) are consistent with the top of overpressure being at about 5500 feet, based on measurements made in the same fault block in which the shale-dominated A10 well is located. Overpressure of about 1250 psi is observed at 6000 feet in that block, whereas sediments at 7200 feet in that block show maximum (probably pre-production) overpressures on the order of 1890 psi. A sonic log from the A12 well, which as noted above contains abundant sands in an upthrown block,

indicates an average shale porosity of about 23% at 7200 feet and 25% at 7900 feet, corresponding to calculated overpressures of 1210 psi and 1900 psi, respectively (assuming an initial porosity of 0.4 and using Issler's (1992) equation for porosity and Hart et al (1995) for calculation of fluid pressure). The somewhat lower overpressures at a given depth in the upthrown well are compatible with the greater depth of onset of overpressure due to greater sand abundance. Thus, compaction disequilibrium accounts for much, if not all, of the fluid overpressure at SEI341. Temperature data, not known to be Horner-corrected, indicate a geothermal gradient of about 25 C/km, such that the 70 C

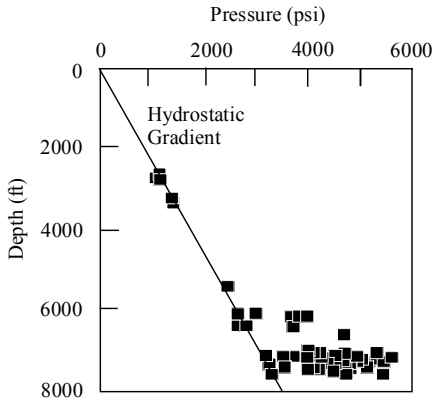

Figure 42. BHP measurements, SEI341 Field. Maximum measured pressures allow estimation of pre-production reservoir pressures; sub-hydrostatic pressures have been culled.

"sterilization temperature" for bacterial activity in oil is at a depth of about 2 km (6600 feet), shallower than all but two samples. The lack of biodegradation of any of the SEI341 samples indicates relatively recent migration of oil to the reservoirs.

The SEI361 field, put on line in 1985, has initial reserves of 31 MMbbo and 107 Bscf gas. It lies at shallow depth (<5000 feet; samples were taken from depths of 3110 ft to 4594 ft) in complexly-faulted late Pleistocene sands (Figure 43), in a generally shaly section atop a salt sill. The scarcity of sand atop the salt suggests the area was a relative high during deposition, such that predominantly shales accumulated there. BHP measurements show overpressures as shallow as 3500 feet, with overpressure on the order of 1400 psi at a depth of 6000 feet. Density-log shale porosity in the A18 well is 0.3 at a depth of 4700 ft SSTVD (sonic log porosity for the same interval is about 0.33), corresponding to fluid pressure of 3220 psi, or an overpressure of about 1100 psi. This pressure is consistent with the BHP data, which suggests a lithostatic (0.93 psi/ft) fluid pressure gradient below about 2600 feet. No deeper porosity log data are available to verify the relationship between porosity and fluid pressure, but it appears from the existing data that compaction disequilibrium accounts for fluid overpressure at the SEI361 field. Temperature data (not known to be Horner corrected) show scatter, but the best fit line through the data, given seafloor temperature of 20 C, defines a geotherm of about 27 C/km. This gradient is somewhat higher than normal for this region, and may reflect the proximity to subjacent salt, which elevates heatflow in overlying sediments. The data indicate the sterilization isotherm of 70 C is at a depth of 1.85 km (6070 feet), at greater depth than any of the analyzed oils. Most oils are at temperatures of about 50 – 55 C.

Oil geochemistry: *SEI341*. Several geochemical markers indicate the SEI341 oils are from a Mesozoic marly source, and are of peak oil window maturity similar to oils at SEI330. They are all unbiodegraded. These oils display a relatively wide range of n-alkane slopes, from –0.15 to –0.3; the reason for this range of slopes, given similar maturity and source for the oils, in unclear. All samples show effects of gas washing, having a narrow range of break numbers, from 13 to 16 (Table A1, Figure 41), corresponding to n-alkane depletions of 0.05 to 0.33. Based on comparison with SEI330, gas washing of the SEI341 oils probably took place not far below the deepest reservoir sand.

Oil Geochemistry: SEI361. Oils from this field are largely marl- to carbonate-sourced and have middle- to late-oil window maturity comparable to oils throughout the area. Most of the oils are biodegraded to the extent that

they have lost original n-alkanes and isoprenoids, but at least two of the oils show no compositional evidence of biodegradation in terms of n-alkane/isoprenoid ratios (Figure 44), indicating they migrated into the relatively cool reservoirs very recently. Biodegradation may also be hindered by poor hydrologic communication throughout the reservoir section, as indicated by the shale-rich nature of the section and the presence of shallow overpressures, but its near-absence is

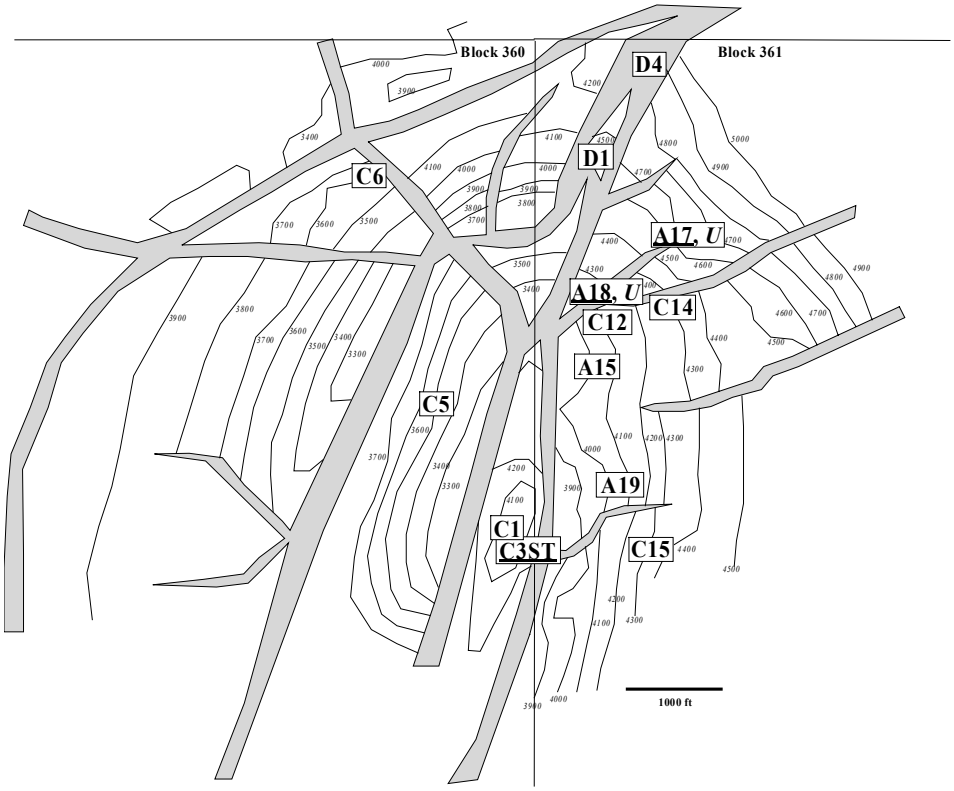

Figure 43. Structure contour map, '3700 sand' SEI361 Field, showing well locations of samples. Unfractionated samples are shown by 'U', in italics. Underlined samples are those that have low Pr/nC17 ratios. The remainder of the samples are too biodegraded to allow an assessment of gas washing; even the C3ST sample (Pr/nC17 of 1.07) has a curved n-alkane profile at all carbon numbers that precludes a confident determination of gas washing.

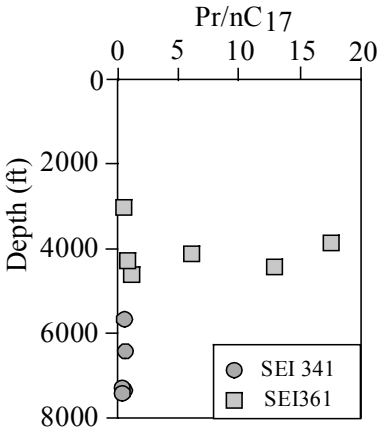

Figure 44. Pr/nC_{17} vs depth, SEI341 and SEI361 oils. Most SEI360/361 oils have no pristane or nC_{17}.

not expected unless migration from depth is very recent. The unbiodegraded oils (A17 and A18) also show no evidence of gas washing. This analysis could not be carried out on the bulk of SEI360/361 oils due to their biodegradation. Many of the biodegraded oils show evidence for the addition of light oil/condensate (nC_{8-10}), which suggests recent migration of vapor phase. There are insufficient data to address whether this represents leakage of

condensate-bearing gas from a reservoir, or gas washing and vapor migration from depth.

Jolliet Field (GC 184)

Geology. The Jolliet field is owned by Conoco, Texaco, and Oxy USA. Production began in 1989, and for a time retained the world record for water depth (1700 feet) in which a tension leg platform produced oil. The Jolliet Field and overlying Bush Hill vent system are developed within the geologic context of a Plio-Pleistocene salt withdrawal minibasin, part of which is still partly floored by salt (Figures 45, 46). The vents have been extensively described by Brooks et al. (1984), Brooks et al., (1986), Kennicutt et al. (1988), MacDonald et al. (1994), Sassen and MacDonald (1994), Sassen et al. (1993), Sassen et al. (1999), and Sassen et al. (2001). The Jolliet Field has been described by Cook and D'Onfro (1991). Initial reserves were 32 Mmbbo and 152 Bscf gas. Approximately 25 stacked slope fan and channel and levee deposits comprise the reservoir sequence, with most production coming from the Trim A – Ang B interval (0.6 – 1.8 Ma), at depths of 4000 – 8000 feet SSTVD. Production is from four-way closure and normal fault traps associated with a salt ridge (Figure 45, 46), as well as from some reservoirs in the downthrown side of a pre-Trim A thrust fault that predates the normal faults. The normal fault traps began to form over 600 kA (pre-Trim A), as shown by expansion across the faults (Figure 46); some of the faults are active today. Fluid pressures prior to production were elevated relative to hydrostatic in all sampled reservoirs, but quickly dropped to or below hydrostatic in many reservoirs as a result of production that started in 1990. Pre-production top of overpressure was at about 4500 feet bsf, or about 6000 feet SSTVD (L. DiCarlo, pers. comm., 2001). Temperatures in the Jolliet reservoirs define a "normal" geotherm of 21 C/km (Figure 47).

The normal fault system that transects the reservoirs consists of several linked strands that each has several tens to 200 feet of throw (Figures 45, 46). In the case of the HJ sand, they divide the reservoir into blocks in which the gas-water contacts are at different elevations. In this sand, the maximum gas column height is about 350 feet (Figure 45). At the pressure-temperature conditions of this reservoir, this column would require a seal to have a mercury injection pressure of about 1540 psi. Since nearly all shales, and shale-dominated fault gouge, have injection pressures higher than this, the HJ sand is probably not at leakpoint with respect to seal capacity. Furthermore, although the western fault block may be filled to its synclinal spill point, not all of the fault blocks in the HJ sand are filled to structural capacity. Thus, the HJ sand represents a reservoir that is only partially filled by the plumbing system that supplies the field and overlying vent system.

Pressure. Initial reservoir static BHP measurements in the Jolliet field indicate that all production is from initially overpressured sands. Local fluid pressure gradient is between 0.82 psi/ft from 6500 – 8000 feet, and 0.95 psi/ft from 8500 – 10600 feet (Figure 47). The pressure gradient shows no pronounced change across the thrust fault.

Bulk density logs for several wells indicate that compaction is retarded at shallow depths (<4500 feet), and porosity decreases very gradually to values of 22-23% at depths of 11,800 feet. No porosity discontinuity is noted at the thrust fault. Using the relation between porosity and effective stress of Hart et al (1995), the calculated fluid pressure of 8395 psi at 11,800 feet compares favorably with the measured pressures on the order of 8430 psi. Fluid overpressure at Jolliet is due largely if not entirely to compaction disequilibrium, with compaction being slowed if not arrested at shallow depths.

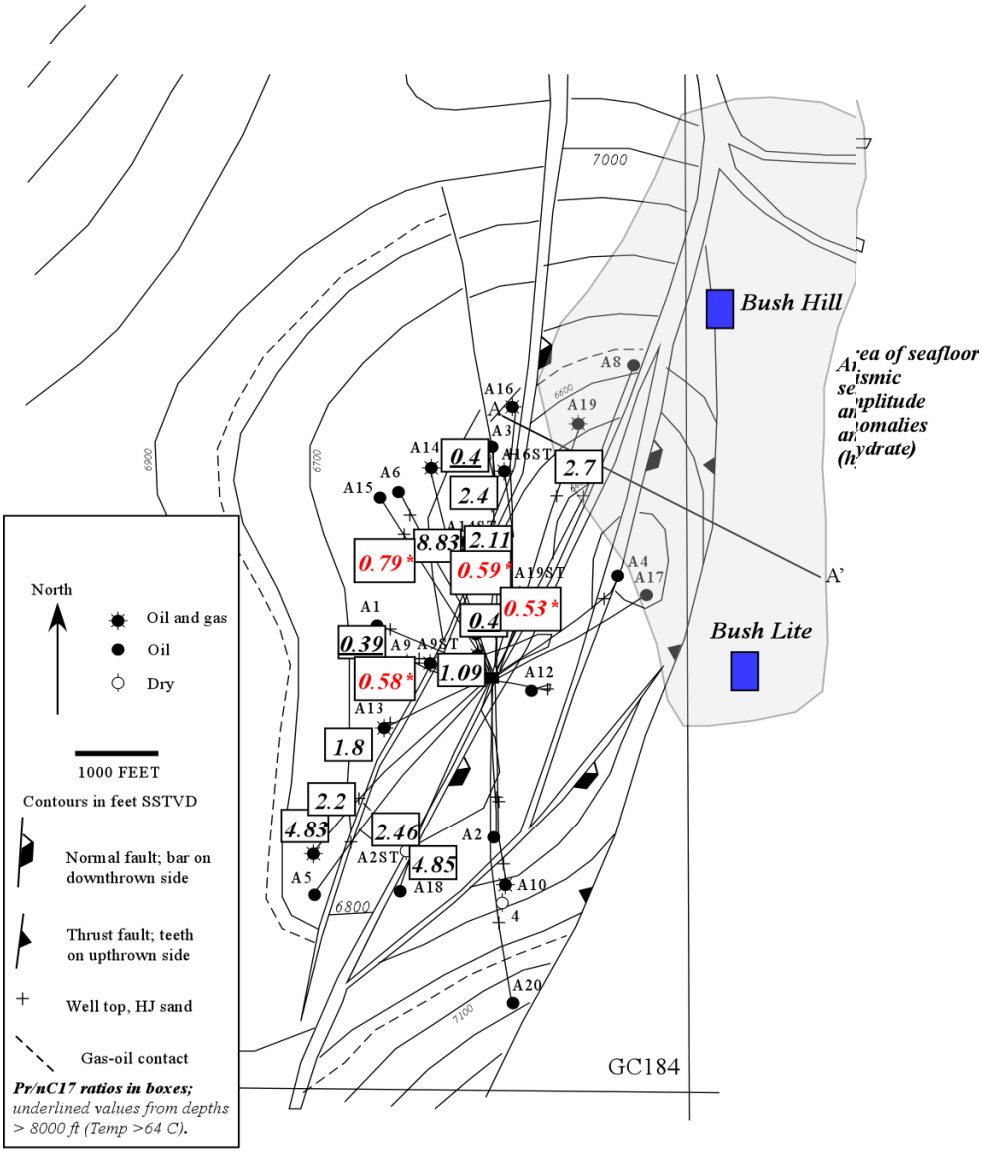

Figure 45. Structure contour map, top of HJ sand, Jolliet Field. Sample locations are shown, with Pr/nC17 values, discussed in test. Asterisked samples are unbiodegraded oils that are in cool (ca. 50 C) reservoirs. Underlined samples are from deep (8000+ ft) reservoirs. Shaded area corresonds to area of seafloor seismic amplitude anomalies (Roberts, 1996); locations of seafloor vents Bush Hill and Bush Lite are also shown.

Hydrocarbon chemistry. Jolliet oils are sourced from Mesozoic carbonates, as indicated by Thompson et al (1990) and Whelan et al., Volume III. Jolliet oil n-alkane slopes are similar to those of SEI330 oils (-0.15 to-0.26; table A1), indicative of similar thermal maturity (ca 0.85% +/- 0.05% Ro; Whelan et al., 1994). Whelan (Part III of this report) indicates MPI1-based maturities of 0.9 to 1.0% Ro for Jolliet oils, but also indicates higher maturities for SEI330 oils than in the 1994 publication. As noted for the SMI9 oil maturities, the difference may be attributable to different interpretation techniques (J. Whelan, pers . comm); what is noteworthy is that the maturities of the SMI9, SEI330, and Jolliet oils are nearly

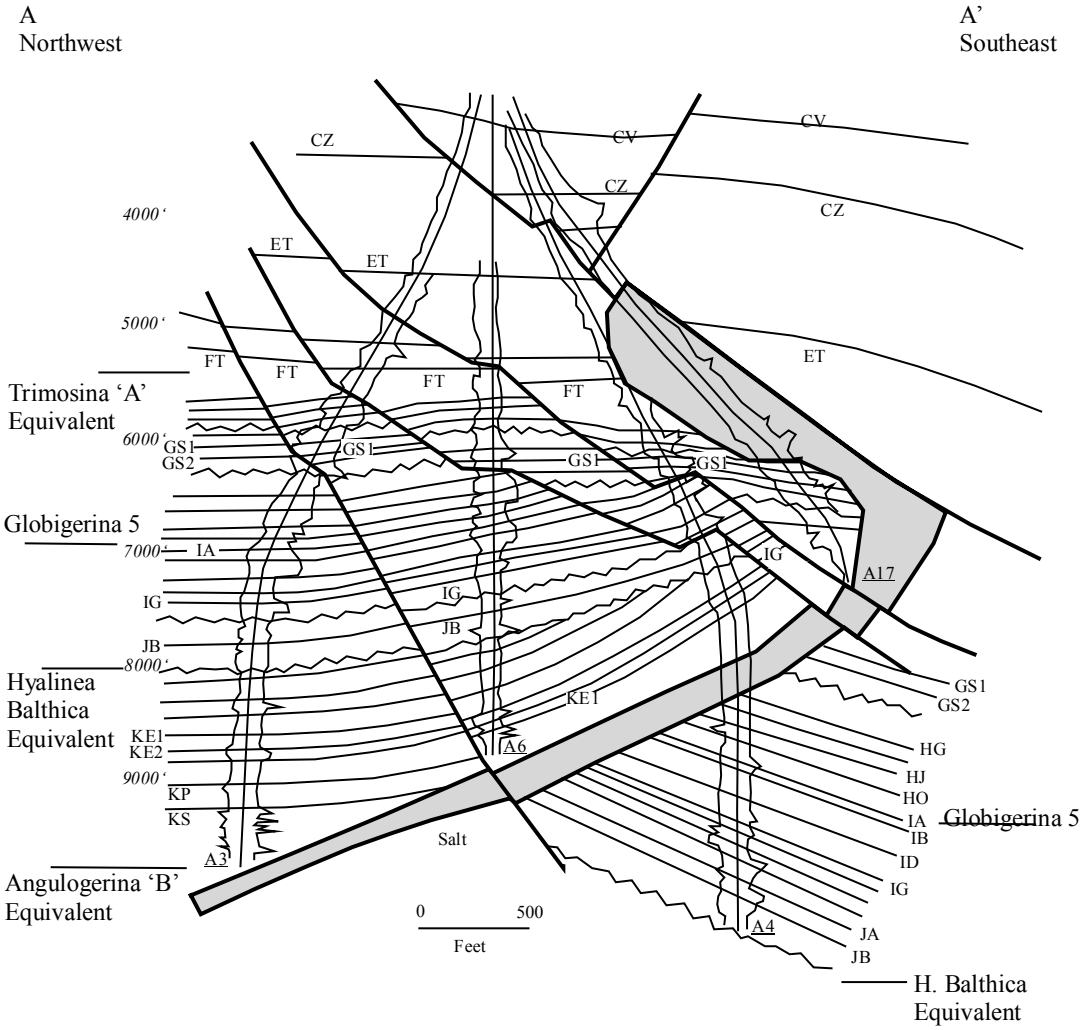

Figure 46. Northwest – southeast cross section (see Figure 44 for location), Jolliet Field, modified from Cook and D'Onfro (1991). Selected sands are shown, with easterly-dipping normal faults that offset an older thrust fault (gray shading denotes chaotic shaly gouge associated with thrust and other faults).

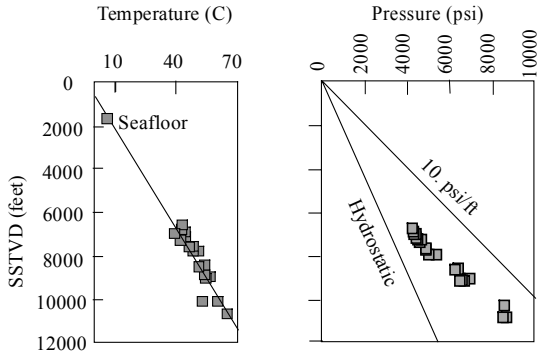

Figure 47. Temperature (left) and BHP (right) measurements vs depth, Jolliet Field.

identical, as determined by MPI1 and MPI2. Jolliet oils show a range of pristane/nC_{17} ratios, indicative of varying degrees of biodegradation. All of the reservoirs are at temperatures below 70 C; some are as cool as 45 C. Particularly noteworthy is the presence of a wide range of Pr/nC_{17} ratios in a narrow depth range (Figure 48). Low ratios, 0.6 or less, characterize unbiodgraded oils, and are found in a cluster near faults just south of the structural high that dominates the field (Figure 45). Higher ratios are found in oils mainly from the flanks of the structure. The implication of the spatial pattern of biodegraded vs unbiodegraded oils, assuming

that production has not significantly disrupted it, is that 'fresh' oils have been injected into the reservoirs in a spatially coherent fashion. In all cases, gas that is produced with the oil is unbiodegraded.

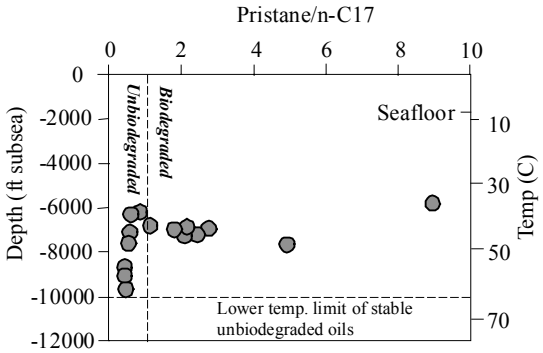

Figure 48. Pristane/nC17 vs depth, Jolliet Field. Unbiodegraded oils are present at temperatures as low as 45 C, implying recent migration.

Several Jolliet samples show two distinctly different slopes on molar fraction plots (Figure 49), indicating that they are mixtures of 'normal oil' and light oil or condensate of unknown origin. Oils that are not evidently mixed with any significant amount of condensate are also unbiodegraded (table A1), whereas n-alkane plots for oils that are mixed with condensate show that the oil experienced biodegradation prior to mixing with the light unbiodegraded oil. Thus, the n-alkane patterns show three episodes of oil migration: an older one, which is sufficiently old that biodegradation has taken place, and two younger ones: normal, unbiodegraded oil (n-alkane slopes of -0.15 to –0.20), and an unbiodegraded liquid of condensate composition (n-alkane slopes about –0.5) that has been variably added to oil. These later unbiodegraded liquids may have migrated at the same time as the gas, probably within the past 5000 years, as discussed below. The n-alkane patterns for oils not mixed with condensate show loss of n-alkanes heavier than nC_{26} or so (Figure 49b), probably through paraffin precipitation, which is known to pose problems for production at Jolliet.

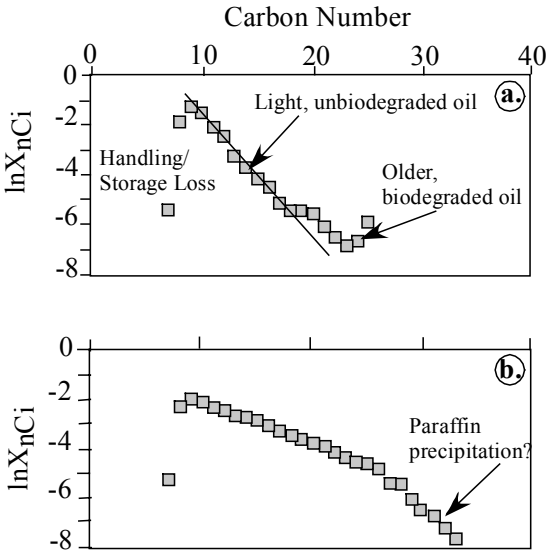

Figure 49. Molar fraction plots, Jolliet oils: a) unbiodegraded condensate/light oil, with relatively steep n-alkane slope mixed with older, biodegraded oil having less steep n-alkane slope (A6 well, GJ sand). b) Unbiodegraded oil, n-alkane slope –0.20 (A14ST well, GS1/GS2 sand). Light end losses in both oils are probably due to separator artifacts or handling/storage losses.

Gas source. Compound specific isotope data from 17 Jolliet gas samples indicate the gases have similar maturities (1.2 – 1.35% Ro; table A2) and similar fractions of bacteriogenic methane. From a simple Chung plot analysis (Figure 50), $\delta^{13}C$ of thermogenic methane lies in a narrow range from –36.3 to –38.8 permil, and between 25 % and 33% of the methane is bacteriogenic, assuming $\delta^{13}C$ of the end member methane is –70 permil (table A5). Scatter in the δD-$\delta^{13}C$ plot indicates that the isotopic composition of bacteriogenic methane is moderately variable here. Gas source $\delta^{13}C$ is similar to that of SMI9 gases, between –21.2 and –22.0 permil. The isotopic composition of the gases indicates that biodegradation is absent, as all gases are well fit by straight lines in the C_2 – C_4 range on the Chung et al. (1988) plot. If biodegradation had taken place, propane $\delta^{13}C$ would have shown a shift to anomalously high values (James and Burns, 1984), which would have readily shown on the Chung plot.

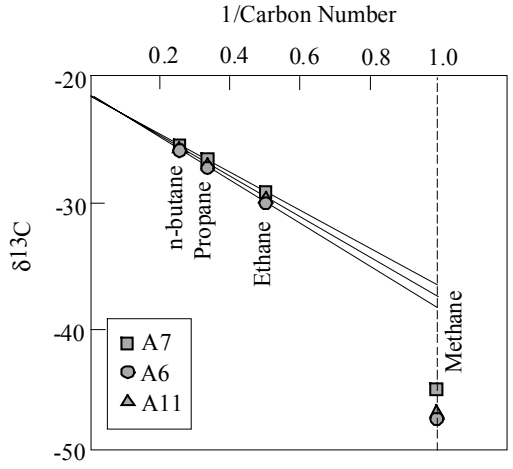

Figure 50. 'Chung plot' for three Jolliet gases, showing linear fit for wet gas components and presence of isotopically light methane mixed with the gas.

Oil and gas are currently venting to the seafloor in several locations at Bush Hill (GC184/185). Echo sounding of the water column shows the area of active gas venting to the seafloor to be on the order of 600 meters across (Sassen et al., 2001). The vent system is developed within an extensive, thick, mound-like accumulation of gas hydrate. This hydrate covers an elliptical area measuring about 600 x 1500 meters, centered on the main vents, and is perhaps on the order of 200 meters thick (Sassen et al, 2001). Uranium-series dating of carbonate precipitated as a result of oil oxidation in shallow sediments show the GC185 vents to have been active for at least 3200 years (Aharon et al, 1997). Where sampled, the mound consists of Structure II hydrate, indicating an origin from thermogenic gas. A thermogenic gas origin is confirmed by molecular and compound specific stable isotopic analysis of hydrate. Hydrate, vent gas, and underlying reservoir gases have been shown to be correlative, and the reservoir gas composition can be taken to represent the gas that supplies the vent-hydrate system.

Migration timing constraints imposed by lack of biodegradation. Using the lack of biodegradation to determine the maximum length of time that gas has been present in the reservoirs requires knowledge of rates of such bacterial activity, both in terms of metabolic rates and in terms of availability of nutrient to the bacteria. Chapelle and Lovley (1990) noted that geochemical modeling in deep aquifers shows that organic matter is degraded at much slower (2-4 orders of magnitude) rates than would be computed on the basis of metabolic rates determined in the laboratory. This difference could be due to the effects of increased pressure and temperature in situ, to a decrease in the availability of necessary reactants to sustain metabolism, or to a difference in the type of bacteria that grow in the subsurface, or all three.

Bacterial abundance, hence metabolic rates (in terms of CO_2 produced per volume of sediment per time) decreases strongly with depth (Parkes et al., 1994). Parkes et al link bacterial population to productivity of the sampled sediments; hence to nutrient supply as measured in terms of TOC, but also to temperature. However, in spite of similarities in amount of organic matter between sample sites noted in the Juan de Fuca ridge as noted by Cragg and Parkes (1994), the diminished bacterial abundance at depth at hydrothermal sites versus at normal geotherms appears to reflect the maturity of organic matter, hence the availability of readily utilizable compounds. Shallow organic matter has carbohydrates, lipids, proteins, and the like that are degraded during early burial, although some of these may persist to depth. The predominant carbon and energy source in deeper organic matter is alkanes (iso-alkanes predominate over n-alkanes (Hunt, 1996)). Some of the n-alkanes are bacterially converted to organic acids, which fuel methanogens (Wellsbury et al, 1997, Zengler et al., 1999). The decrease in available substrate (electron donors) and nutrients (substances essential to cell metabolism, such as S, P, K, and N) with depth clearly affects bacterial activity.

Superposed on this pronounced decrease in population due to diminished substrate and nutrient supply with depth is the effect of adding substrate in the form of oil and gas. These provide a substrate on which bacteria that feed on the buried organic matter can multiply. The most usable

compound type in the oil appears to be the n-alkanes, which are slightly more readily degraded than the isoalkanes that dominate in buried organic matter. But although the type of available organic matter remains basically the same, what is most affected by influx of oil and gas is the abundance of substrate. In itself, such an increase in substrate supply will surely promote growth relative to sediments lacking oil and gas. For example, Parkes et al (1994) noted a pronounced increase in bacterial population, particularly heterotrophs, corresponding to a zone containing thermogenic gas.

The effect of temperature on metabolic rates of thermophiles is minor at most. Thermophilic anaerobic sulfate-reducers collected from vent effluent (Huber et al., 1990), water that was used to flood an oilfield (Stetter et al., 1993), and oil field formation waters (Haridon et al., 1995) were cultured in the lab at reservoir pressure (80 to 420 atm) and temperature (70 to 90 C), with turbidity (significant growth) taking place in a span of 18 to 72 hours. These were grown in an enrichment medium. Given oil and gas as a substrate, and with sediment, oil, and brine providing nutrient (K, N, P, etc.), growth would be expected to be slower (see So and Young, 1999), but the difference in activity is not great. Especially noteworthy was the observation that seawater injected into North Sea and Alaskan reservoirs, at ambient temperatures of 82 to 90 C, was recovered with thermophilic bacteria counts between 10^4 and 10^6 cells/liter (Stetter et al., 1993). Seawater itself contains on the order of 10 cells/liter or less of such bacteria (Huber et al., 1990). If growth, rather than simple flushing out of extant populations, can be demonstrated, this shows that substantial growth of thermophiles took place in situ in a matter of years under the vigorous waterflood conditions prevailing in these reservoirs. At the same time, waterflood conditions are very different from the normal subsurface environment, and this evidence of rapid growth, if valid, is not necessarily applicable to biodegradation in normal oil reservoirs.

The effect of pressure on metabolic activity of subsurface thermophiles does not appear to be strong. The strongest effect was shown by Parkes et al (1994), who demonstrated that the metabolic activity of a sulfate reducer collected at an ambient pressure of 10 Mpa (1500 psi) decreased to about 15% of its in situ level when subjected to pressure of 27 Mpa (4000 psi). This decrease in activity with increased pressure could reflect the present evolutionary status of the bacteria on its burial path. Related bacteria now at 4000 psi may be just as efficient because they have evolved to function under increasing pressure during burial, as discussed by Jannasch and Taylor (1984). However, Jannasch and Taylor also postulate a relatively small decrease in overall metabolic activity of barophiles relative to bacteria that live at atmospheric pressure. Some biochemical processes are slowed by elevated pressure, but the effects vary with the type of microbe. Barophiles cultured at deep – sea vents (pressure of 4000 psi, temperature of 20 – 90 C) show rates of growth similar to those of aerobes at atmospheric pressure. The pronounced diminution of metabolic activity with pressure hypothesized by Whelan et al. (1986) and Chapelle and Lovley (1990) was based on observations of Jannasch and Taylor (1984) on barotolerant, not barophilic, bacteria. Wirsen and Molyneaux (1999) found that growth rates of deep-sea barophiles, that are slow-growing under ambient, nutrient-poor (oligotrophic) conditions, were significantly increased at all pressures up to 6000 psi by the addition of a readily utilizable food (yeast extract). As would be expected, the effect of elevated pressure on growth rate of barophiles was positive relative to STP. The effect of increased pressure on metabolism of C. thermocellum was studied by Berberich et al (2000). Relative to STP, growth rates in propane gas were undiminished at pressures of 1.5 Mpa (220 psi), but were slowed by about 80% when a phase change to supercritical state occurred around 2.9 Mpa. Finally, the incubation of enrichment cultures from oilfields at varying pressures to 420 atm (ca 6000 psi) are reported to have little effect on growth rates (Stetter et al. 1993; Haridon

et al. 1995). The overall implication of these studies is that large (thousands of psi) increases in pressure may slow metabolism by as much as an order of magnitude, but the effect is probably less.

Different types of bacteria appear to grow at different rates. During burial, the primary mechanism for energy production changes from sulfate reduction to the less-efficient methanogenesis (Lovley and Chapelle, 1995, Wellsbury et al., 1997, Zengler et al., 1999). Methanogens tend to grow much slower than sulfate reducers, perhaps owing to the much smaller energy output of methanogenesis. So and Young (1999) found a doubling time of 3 days for anaerobic sulfate-reducing bacteria grown on hexadecane, whereas data of Zengler et al. (1999) imply a doubling time of about 75 days for methanogens grown on the same substrate.

The conclusion of these lines of evidence are that pressure and temperature do not exercise substantial inhibitory effects on growth of thermo/barophilic bacteria that are present in oil reservoirs, that bacteria do grow more slowly on n-alkane substrate than on enrichment medium, and that methanogens grow more slowly than sulfate-reducers. Allowing for the most conservative conditions (increased pressure slows activity by an order of magnitude; methanogens have a doubling time of 75 days at STP on hexadecane), a doubling time of two years would be perhaps the slowest metabolic rate allowed by the data. In this instance, a single bacterium per cubic centimeter would grow into a colony of 10^7 cells/cm^3, a population that would significantly biodegrade oil, in about 46 years. Sulfate reducers, with a doubling time of 3 days on hexadecane, would grow into such a colony in about 2 years. While this may be long relative to the sorts of growth rates typically determined for bacteria in the laboratory, it is very short on a geologic timescale.

Chapelle and Lovley (1990) report that in situ activity of sulfate reducing bacteria in deep aquifers, as indicated by geochemical modeling, is 2 to 4 orders of magnitude less than determined from laboratory cultures. They noted that, if even relatively slow metabolic rates measured in the laboratory actually prevailed in situ, then all of the organic matter in the deep aquifers they studied would have been degraded long ago. This observation also applies to oil biodegradation studies. Given that the metabolic rates of bacteria in laboratories, even when scaled down to account for effects of pressure, are such that large populations of bacteria could grow in a matter of years, then why are biodegraded oils still in existence? In the GOM, most oils that have been biodegraded have experienced only mild to moderate extent of biodegradation (Biodegradation index of 3, Peters and Moldawan, 1993), in spite of having experienced the conditions necessary for biodegradation for thousands to, perhaps, millions of years. In many biodegraded oils, n-alkanes are still present, so the effect of different substrate (i.e., n-alkane vs aromatics) on growth rates is moot. The idea that microbes are highly specific with respect to substrate (i.e., degrading hexadecane but not decane; Zengler et al., 1999) does not appear very applicable to reservoirs, where a consort of microbes act on different types of petroleum compounds, and where progressive biodegradation through alkanes to aromatics is typically the case given enough time and exposure to the necessary conditions.

Clearly, some process in the oil and gas legs acts to retard bacterial attack on oil and gas. It has long been believed that in situ oil biodegradation takes place primarily at the oil-water contact. It may be that bacteria do not metabolize hydrocarbons as efficiently in oil-saturated, but water-wet, sands, where the water that supplies sulfate to sulfate-reducers or oxygen and hydrogen to acetogens/methanogens is bound to mineral surfaces and thus has different physical properties than does water in pore spaces. However, water saturation in the oil or gas leg is almost always high enough that free water is present. It may also be that, especially in the case of gas, the bacteria that live on mineral surfaces and water that lines the pores do not have ready access to the bulk

of hydrocarbon that is in the pore space, particularly in cases where there is little movement of pore fluid or gas once the reservoir is filled. In such cases, the rates of biodegradation may be slowed because of diminished availability of substrate, leading to lower populations of bacteria. Thus, the observations of Chapelle and Lovley (1990) may be relevant to oil and gas accumulations. If this is the case, and actual rates of biodegradation are, for instance, 3 orders of magnitude less than determined from laboratory cultures, then for methanogens, the time required to significantly biodegrade hydrocarbons may be on the order of thousands to tens of thousands of years. Since the limiting factor in this case is substrate and nutrient availability, the type of bacteria (methanogen vs sulfate reducer) may not be a primary factor in determining rate of biodegradation. Thus, at Jolliet, the lack of gas biodegradation constrains the accumulation to be only less than several thousand years (ca 5000) old. This estimate is compatible with the 3200-year radiometric date of seep-related carbonate at Bush Hill. Although hydrocarbon venting has been going on for much longer elsewhere in the area (carbonate in GC140 yields ages as high as 197 kA), the Jolliet field/Bush Hill vent system appears to be a very young feature.

Gas washing. None of the Jolliet samples show evidence of gas washing, although depletion at nC_{10} or less is pronounced. This depletion is also observed in low molecular weight naphthenes and aromatics, and is attributed to fractionation during production or sample handling. In the case of mixed biodegraded and unbiodegraded liquids, only the later, unbiodegraded liquid is known to be unfractionated. The older, biodegraded oil may have been gas washed, but subsequently lost its n-alkanes to bacterial activity. The available data only allow us to conclude that the n-alkanes in the present oil do not show effects of gas washing.

The lack of gas washing at Jolliet suggests that gas and oil have migrated separately to the reservoirs. Copious amounts of gas have vented and are venting at the seafloor in western GC185 (e.g. Sassen et al., 2001) from the surface manifestation of same 'plumbing system' that controls distribution of Jolliet oils at depth. This large volume, combined with the computed field GOR of 4906 scf/bbl, indicates the presence of adequate gas (on the order of 15 moles gas per mole oil) in the system to produce at least moderate washing under the ambient reservoir pressures. The oils evidently did not interact with gas during migration or within the reservoirs, implying separate migration times and/or conduits for oil and gas. Different migration times for oil versus gas are indicated by the occurrence of unbiodegraded gas with biodegraded oils (assuming similar kinetics for gas and oil biodegradation), whereas different migration routes are indicated by the existence of unbiodegraded, unwashed oils in the same reservoirs as unbiodegraded (ie, contemporaneous) gas.

Other fields.

Oils from other locations within the transect area show variable amounts of n-alkane mass depletion due to gas washing. Generally the depletion decreases with increasing distance from the shoreline, consistent with the pattern displayed by the depletion data from the four detailed study areas (Table A1; Figure 1).

IV. b. Large-scale gas washing patterns

Several patterns emerge from the combined field data, and are discussed in turn: 1) gas and oil come from different sources, presumably generated at different times and/or in different sediments in a particular setting, 2) reservoirs have filled relatively recently, regardless of age of the sediment or of the oil generation, 3) break number shows a strong positive correlation with extent of gas washing ($r^2 = 0.95$), as determined by n-alkane mass depletion calculations, 4) extent of gas washing shows

no consistent relationship to present depth of the samples, either in absolute terms or with respect to the top of overpressure extent of gas washing decreases dramatically from nearshore, where it is extreme, to deepwater, where it is absent, and 5) extent of gas washing and n-alkane break number, which is a proxy for pressure of gas washing, both decrease with distance from the shore.

With the possible exception of Tiger Shoals, gas and oil are sourced from different sediments or from different organic matter types within the same sediment. In either case, there is a distinction in time and/or space between oil and gas migration at a particular location. For example, at SEI330, the oils and gases have maturities on the order of 0.85% +/- 0.05Ro and 1.5 +/- 0.2%Ro, respectively (Whelan et al., 1994). Whole-oil $\delta^{13}C$ values are 3 to 4 permil less than those of gas in the same reservoirs. The bimodality of these maturities and the exclusive presence of oils having early–oil window maturity constrains those oils to have been generated in Mesozoic source rock, then expelled prior to the sediments entering the gas window. The isotopic difference between gas source and whole oil may be due either to different source sediment/organic matter, or to the gases being derived from a ^{13}C – enriched asphaltic fraction in residual oil in the Mesozoic source (J. Whelan, pers. comm). In either case, however, the oil must have been expelled from the source rock prior to gas generation. This scenario appears to apply to the other fields as well.

As noted, biodegradation is not known, at least from the Pr/nC_{17} ratios, in most of the samples analyzed in this study (Figure 51). In a number of instances, the oils are from reservoirs that are at temperatures only slightly higher than that at which biological activity in oils ceases, about 70 C. In a subsiding basin, this relationship indicates that the oils filled the reservoir only after it was buried to temperatures higher than the sterilization temperature. It is noteworthy that, even in systems in which oil was generated millions to tens of millions of years ago, such as at Tiger Shoals or at SMI9 (Volume 5 of this report), the lack of biodegradation indicates that the oil currently in the reservoirs arrived there within the past

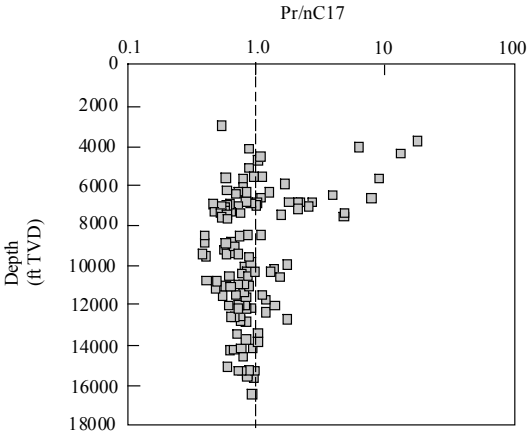

Figure 51. Pristane/n-heptadecane vs depth, transect samples. Biodegraded oils plot at values less than 1; the large majority of transect oils, regardless of depth, are essentially unbiodegraded. Use of the ratio total n-alkanes/total isoprenoids corroborates this observation.

four million years, at Tiger Shoals, or within the past two million years, at SMI9. No tectonic control for this relatively recent filling is known: in the above-noted areas, salt withdrawal was largely completed during the periods of rapid sedimentation, millions of years ago. It may be that these older reservoirs are continually being 'topped off', and just as continually leaking, such that any oil that was emplaced early, at temperatures lower than that of sterilization, has been displaced by more recently-migrated oil. If the oils are displaced in this manner, the rate of 'flushing out' must be low, in order to account for the low rate of leakage of oil and gas at the seafloor in the inner to middle shelf. The timing of gas washing is not so constrained, however, since these oils may have been gas washed millions of years ago and then subsequently stored in a secondary reservoir prior to their Plio-Pleistocene migration. However, Plio-Pleistocene gas washing of these oils is not precluded on the basis of this evidence, and a straightforward history of washing during migration to the present reservoirs is probable.

Extent of gas washing shows a pronounced correlation with n-alkane break number (Figure 52). Thompson (1987) and

Meulbroek (1997) showed that the fugacity of n-alkanes in vapor is strongly pressure-dependent.

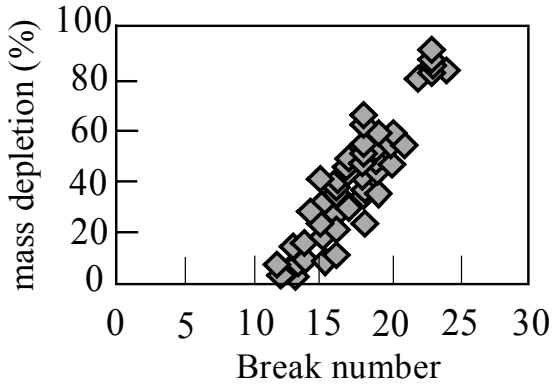

Figure 52. Break number vs n-alkane mass depletion, transect samples, showing strong correlation.

Thus, the 'solubility' of n-alkanes in vapor drops off sharply with increasing molecular weight at a given pressure, and the highest-molecular weight compound to be partitioned in the vapor phase signifies the pressure at which fractionation occurred. Mass of vapor relative to mass of oil also affects the break number, in that even a sparingly soluble compound will show depletion if enough 'solvent' (vapor) is present. However, Thompson (1987) and Meulbroek (1997) showed that this effect on break number is weak compared to that of pressure, and that large fractions of vapor in the vapor+oil system may increase break number by one or two carbon number units relative to small fractions of vapor. Temperature also affects fugacity; Meulbroek's (1997) modeling incorporates temperature in the form of a geothermal gradient. Effect of subsurface temperature variations on break number, like that of compositional variations, is secondary to that of pressure differences encountered in the subsurface. Break number is primarily a proxy for pressure during gas washing.

The relationship between break number and extent of gas washing is strong. It is to be expected: the higher the pressure at which gas washing takes place, the higher the fugacity of a given compound is in the vapor phase, leading to greater partitioning of compounds into the vapor phase. However, such a correlation is not required, in that high vapor:liquid ratios at relatively low pressure can produce strong depletions in low-molecular weight hydrocarbons, leading to substantial extent of gas washing in oils that have low break numbers, as shown by Meulbroek (1997). So it is noteworthy that, although there is scatter at individual locations, such a strong correlation exists over the entire transect. It may be that the physical nature of gas – oil interaction may be different at high pressure than at low pressure, allowing for a more efficient uptake of compounds into the vapor phase at high pressure. Alternatively, since the extent of gas washing is related to the amount of vapor that interacts with the liquid, as well as to the pressure-temperature conditions of washing, it may be that gas is more plentiful in the migration pathway of oil in the deeper reaches of the petroleum system. The ubiquity of gas washing, especially in nearshore areas where oils are strongly fractionated, indicates there is an adequate supply of gas to fractionate oils everywhere in the subsurface. Finally, if gas washing is enhanced by porous flow through sandy sediments as opposed to fracture or fault-controlled flow through shales, as indicated at Tiger Shoals, then conditions favorable for gas washing are generally found over a much greater stratigraphic thickness and to much greater depth nearshore, owing to the prograding wedge-like nature of the deltaic complex during the Cenozoic. Maximum break numbers are higher nearshore, presumably indicating that gas washing commenced at greater depths there, although at any given location it persisted over a range of depths corresponding to a range of break numbers.

Pressure of gas washing, as proxied by the break number, is not related to present – day depth of reservoir (Figure 53). Thus, gas washing of reservoired oils is probably not taking place. There also is little if any evidence that gas washing takes place primarily at the top of overpressure. In one instance where pressure, hence depth, of gas washing has been modeled at SEI330 (Meulbroek et al., 1998),

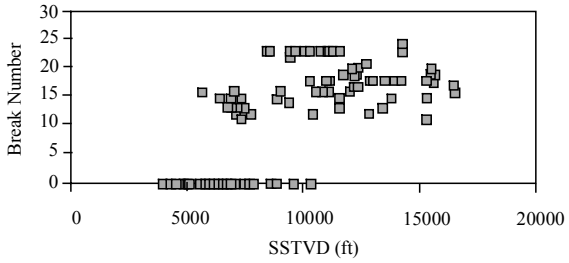

Figure 53. Oil break number vs depth, transect samples. No correlation is evident, whereas one would be expected if the oils were being gas washed in their current locations.

the OI oils were found to have been fractionated over 1 km below the depth of the top of overpressure at the time at which the oils were washed. These oils currently lie at hard overpressure. At Tiger Shoals, oils are gas washed to similar extent regardless of depth, and oils in hard overpressure are as fractionated as those in hydrostatically-pressured reservoirs. The lack of relationship between present depth and break number (Figure 53) in individual fields as well as over the entire transect, combined with the conclusion (above) that the sampled oils mostly migrated into their respective reservoirs relatively recently in the reservoirs' burial history, indicates that oils are not gas washed in but, rather, below the reservoirs in which they currently lie. The oils were likely gas washed as they migrated to their current locations. This conclusion is consistent with the lack of gas washing in oils above the OI sand at SEI330: once in the reservoirs, these oils have evidently been sequestered from gas washing.

Maximum n-alkane break number, as well as extent of gas washing, shows a pronounced decrease with distance from the shoreline (Figures 54, 55). The depletion trend cuts across tectonostratigraphic boundaries, implying that gas washing is not specific to any one province or to a particular type of province (detachment, minibasin, etc). The extent of gas washing may have more to do with the difference in timing of generation of oil relative to gas, with oils generated in the late oil window (as at Tiger Shoals) being still at great depth in the migration pathway

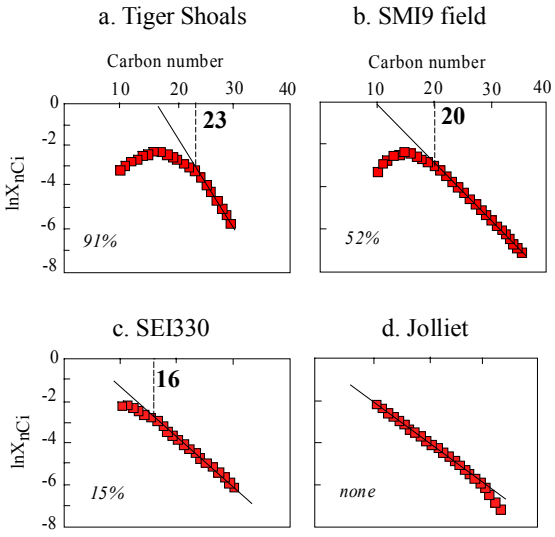

Figure 54. Representative n-alkane molar fraction plots from the four main study areas, from north (a) to south (d). Decreased break number and extent of n-alkane depletion from north to south are clearly shown.

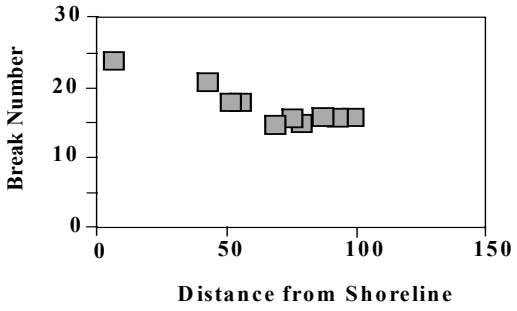

Figure 55. Maximum n-alkane break number at a given locality vs distance (miles) from Louisiana shoreline.

when gas generation began. In this way, gas can more immediately interact with oil, not having to migrate as far to reach it as in settings where the oil was present at greatly shallower depth than where the gas was being generated. Alternatively, as noted above, the increased extent of gas washing nearshore may, like break number, simply reflect the greater thickness of sediment conducive to gas washing.

Break number and extent of gas washing are not evidently related to oil compositional parameters in a gross sense. Maturity of SMI9, SEI330, and Jolliet oils are all nearly the same, but the extent of gas washing, and the depth at which it occurred, varies substantially between those fields. Oil source varies from predominantly Tertiary shale at Tiger Shoals to Mesozoic carbonate at SEI330, but the gradient in gas washing does not show any discontinuity across oil source terrane boundaries.

The location of gas washing may be controlled by the distribution of porosity and permeability in the migration pathway, with suitable conditions being found at greater depths in the sedimentary section nearshore. Although there is nothing to preclude gas washing taking place in faults, it is likely that sand layers play a major role in gas washing, especially the profound depletions that are observed nearshore. Thus, the highest break number in a particular field may reflect the depth of the deepest hydrocarbon-bearing sand, which in turn may be the deepest continuous sand encountered by the ascending petroleum (Figure 56). Break numbers that are lower than the maximum at a given location may reflect gas washing in migration conduits such as faults or at the inlet point into the reservoir itself.

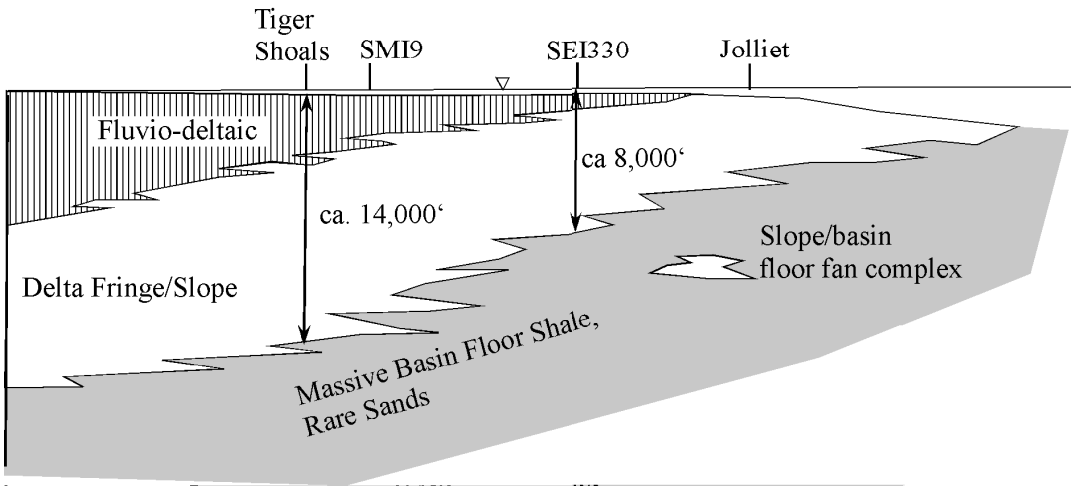

Figure 56. Schematic cross section along transect, showing relationship between depth of gas washing and lithostratigraphy. Oil and gas may mix within sands as gas flows past, mixes with, and separates from oil.

Although first-order sand abundance is linearly related to distance from the shoreline, sand distribution over distances of several miles, particularly in areas undergoing active salt tectonism, is irregular (e.g., Weimer et al., 1998). Thus, in sedimentary sections deposited in such areas, the depth of gas washing, hence break numbers and n-alkane mass depletions, may vary considerably over relatively short distances, reflecting the lateral variability in depth to the deepest sand in the migration pathway. According to the modeling carried out by Meulbroek et al. (1998), the maximum depth of gas washing at SEI330 is on the order of 2.9 km, if washing took place on the downthrown side of the ‘A’ fault. This depth corresponds to the Lenticulina 1 sand. It is not likely that gas washing in the SEI330 ‘plumbing system’ took place any deeper than this sand. However, gas washing could take place, and oil-bearing sands found, at greater depth at other nearby fields owing to the heterogeneity of sand distribution. Deeper gas washing could point to the existence of deep oil-bearing sand at other locations in the area (as at Tanzanite, SEI346; Petzet, 1998), and samples from shallow reservoirs in other fields should be evaluated for evidence of deep gas washing. A similar

rationale applies to deep prospectivity for oil at Tiger Shoals. Given that all the oils there were gas-washed at pressures on the order of 10,000 psi, probably in the Rob L sand, and that each field is evidently characterized by its own feeder system from depth, then it is likely that any traps in the Rob L sand beneath a given field would contain oil.

Quantification of the pressure-temperature-composition conditions of gas washing of a particular oil, or of separation of a particular condensate from an oil, can be developed into and utilized as an exploration tool for deep oil in an existing field or prospect. In particular, if a condensate is modeled as having separated from an oil at a given pressure, then the depth of the oil paired with that condensate can be constrained by taking into account the fluid pressure evolution, the timing of gas washing (proxied by migration timing), and the burial history since migration. If gas washing is indeed linked to sands, then trap analysis at the appropriate depth may ascertain the likelihood and the volume of gas-washed oil remaining at depth. Further constraint on this volume may be provided by mass balance of known condensate vs washed oil, as indicated for SEI330. In order to successfully reconstruct the physical and chemical conditions that prevailed during gas washing, a determination of the original, unfractionated oil composition is needed. Ideally, this is obtained from a sample of such an oil from the area being studied, but it can also be estimated through the methodology outlined in Appendix B, given samples of fractionated oil and condensate derived from fractionation of that oil. Equation of state modeling of liquid-vapor fractionation can then reproduce the known oil and condensate compositions as a function of PTx conditions.

The existence of a separate gas phase at depth substantially greater than the top of overpressure is mandated by the equation of state modeling of gas washing, coupled with the reconstruction of fluid pressure profiles at the time of gas washing in different study areas. Thus, separation of gas from oil is not in itself an adequate explanation for the development of overpressure in the study areas.

The substantial gas washing of transect oils has implications for the deep plumbing system in the Gulf of Mexico. At least two distinct hydrocarbon phases, liquid and vapor, exist throughout much of the basin. These phases evidently mix and separate relatively late in the oil migration history, and at depths that are shallow relative to the oil source rock. This finding does not preclude the possible involvement of gas in primary migration, as suggested by Price et al (1983). Gas involved with mobilization of oil from its source rock may remain dissolved with the oil, or it may exsolve at depth. In either event, the compositional effect of gas washing, if it occurred, overprints any signal due to the exsolution of co-generated gas from oil.

V. Conclusions

The work described in this report demonstrates the utility of combined chemical and geologic studies of oil and gas in elucidating the deep plumbing system in the Gulf of Mexico basin. The original impetus for this work was the hypothesis that gas exsolution from oil is responsible for the development of fluid overpressure. Modeling and documentation of phase separation expanded into applications not envisaged in the original proposal. The value of this work lies in the insights it gives into the deep plumbing system, below the top of overpressure down to the hydrocarbon sources. Gaseous solution of oil in source rocks notwithstanding, gas and oil are for the most part separately generated, and migrate as separate phases to relatively shallow depths in the basin, where they may mix and separate, resulting in gas-washed oils. The depth and extent of gas washing vary at any given location, but the maximum depth and extent show a systematic decrease with distance from the shoreline. This first–order

variability probably represents the spatial distribution of suitable sites for gas washing, and may reflect the depth of a laterally continuous sand in which phases mix and separate. It also may reflect the spatial variability in effective gas:oil ratios in the migration pathway. The greater volume of gas generated near the shoreline relative to the continental slope may account for part of the greater extent of gas washing nearshore, but the absence of gas washing at the Jolliet Field, where sands are laterally discontinuous but where gas is plentiful, suggests that sand distribution may be the primary factor controlling depth and extent of gas washing in the transect.

VI. Recommendations

Further study along the lines described in this report is recommended along two parallel lines. First, the various components of the gas washing system should be investigated further so that the model results have greater predictive power. More detailed and rigorous EOS modeling of phase separation, and comparison to the range of sample compositions, is needed to better understand PTX conditions of gas washing and to increase robustness of the tentative links between gas washing and geologic features. This modeling will be carried out in the near future, as the technology for such intensive work is just now becoming available. In the other direction, incorporation of geologic and chemical data into an integrated 3D finite element fluid flow model, properly done, will further elucidate connections between sedimentation, faulting, hydrocarbon generation and migration, phase separation, and overpressure development – all important elements in the petroleum system that affect the chemistry of petroleum and that are involved in gas washing. Second, expansion of the types of analysis presented in this report to other parts of the Gulf of Mexico, and to other petroleum basins, will broaden and deepen the pool of data from which the preliminary conclusions in this report are drawn. Third, field testing of the insights developed herein will result in refinement of, and increased confidence in, the gas washing technology as a tool for risk reduction in oil and gas exploration and exploitation. Ideal tests are exemplified by the SEI361 Field and by the Tiger Shoals study area. In both cases, specific predictions are made regarding the pressure or depth of sediments in which gas washing has taken, or is taking, place. If seismic interpretation discloses suitable traps, and stratigraphic relations and seismic attributes are indicative of adequate reservoir and seal, then the predictions made herein can be tested with the drill bit. Alternatively, confidence in the methodology can be enhanced by "reverse testing", whereby the existence of known deep oil or gas reservoirs can be predicted on the basis of the chemistry of shallower fluids or vice versa. This is the case at SEI330, where the JD condensate is compatible with the existence of gas-washed oil at the depth of the OI sand; if only the JD condensate were known, the OI accumulation could have been predicted. Other field tests involving genetically related condensates and gas-washed oils can be carried out to further test the concept and to increase understanding of the petroleum system in the Gulf of Mexico. It is recommended that a project be funded that will incorporate all the above elements into a cohesive and comprehensive investigation of gas washing, with the intention of developing and employing a technology that breaks through into routine exploration and exploitation applications.

Acknowledgments

The work described herein would not have been possible without the generous cooperation of numerous people, including Pete Kelley and Steve Krause of Texaco

(now ChevronTexaco), Mark Beeunas, Mark Kamm, and David O'Bright of Chevron (now also ChevronTexaco), Dave Owens of Pennzoil (now Devon Energy), and Kate Weissenberger, Bob Lynn, and Tom McClurg of Conoco (now ConocoPhillips). Discussions with Jean Whelan, Peter Meulbroek, and Martin Schoell have been very helpful.

References

Aharon, P., Schwarcz, H., and Roberts, H., 1997, Radiometric dating of hydrocarbon seeps in the Gulf of Mexico; Geol. Soc. Amer. Bull., v. 109, p. 568-579

Alexander, L., and P. Flemings, 1995, Geologic evolution of a Pliocene – Pleistocene salt withdrawal mini-basin, Eugene Island, Block 330, offshore Louisiana: Amer. Assoc. Petrol. Geol. Bull. v. 79, p. 1737-1756

Anderson, R., Flemings, P., Losh, S., Whelan, J., Billeaud, L, Austin, J., Woodhams, R., 1994, The Pathfinder drilling program into a major growth fault in Eugene Island 330, Gulf of Mexico: Implications for behavior of hydrocarbon migration pathways, in CD-ROM prepared under U.S. Dept. of Energy contract DE-FC22-93BC14961

Berberich, J., Knutson, B., Strobel, H, Tarhan, S., Nokes, S., Dawson, K., 2000, Toxicity effects of compressed and supercritical solvents on thermophilic microbial metabolism; Biotech. and Bioengr., v. 70, p. 491-497

Berner, R.A., and Berner, E.K., 1996, Berner, Global environment : water, air, and geochemical cycles, Prentice Hall, Upper Saddle River, N.J.

Bodvarsson, G., 1969, Temperature of water flowing through fractures, Jour. Geop. Res., v. 74, p. 1987-1992

Brooks, J., Kennicutt, M., Fay, R., Mcdonald, T., and Sassen, R., 1984, Thermogenic gas hydrates in the Gulf of Mexico; Science, v. 225, p. 409-411

Brooks, J., Cox, H., Bryant, W., Kennicutt, M., Mann, R., McDonald, T., 1986, Association of gas hydrates and oil seepage in the Gulf of Mexico; Org. Geochem., v. 10, p. 221-234

Chapelle, F., Lovley, D., 1990, Rates of microbial metabolism in deep Coastal Plain aquifers; Appl Environ. Microbiol., v. 56, p. 1865-1874

Chung, M., J. Gormly, and R. Squires, 1988, Origin of gaseous hydrocarbons in subsurface environments: theoretical considerations of carbon isotopic distribution, in M.Schoell, ed., Origin of methane in the earth, Chemical Geology, v. 71, p. 97-103

Cook, D., D'Onfro, P., 1991, Joliet Field thrust structure and stratigraphy, Green Canyon block 184, offshore Louisiana; Trans. Gulf coast Assoc. Geol. Socs., v. 41, p. 100-121

Cragg, B., Parkes, R.J., 1994, Bacterial profiles in hydrothermally active deep sediment layers from Middle Valley (NE Pacific), sites 857 and 858; in Mottl, M., Davis, E., Fisher, A., and Slack J., eds, Proc. Ocean Drilling Program Scientific Results, v. 139, p. 509-517

Cragg, B., Parkes, R.J., Fry, J., Weightman, A., Rochelle, P., Maxwell, J., 1996, Bacterial populations and processes in sediments containing gas hydrates (ODP Leg 146, Cascadia Margin); Earth Planet. Sci. Lett., v. 139, p. 497-507

Curiale, J., Bromley, B., 1996, Migration induced compositional changes in oils and condensates of a single field; Org. Geochem., v. 24, p. 1097-1113

Diegel, F., Karlo, J., Schuster, D., Shoup, R., Tauvers, P., 1995, Cenozoic structural evolution and tectonostratigraphic framework of the northern Gulf coast continental margin, in M.P.A. Jackson, D/G. Roberts, and S. Snelson, eds., Salt tectonics: a global perspective: AAPG Memoir 65, p. 109-151

Engelder, T., Leftwich, J., 1997, A pore-pressure limit in overpressured south Texas oil and gas fields, in Surdam, R., ed., Seals, Traps, and the Petroleum System: AAPG Memoir 67, pp. 255-268

Faber, E., 1987, Zur Isotopengeochemie gasformiger Kohlenwasserstoffe; Erdol, Erdgas, Kohle, v. 103, p. 210-218

Gatenby, G., 2001, Phase changes: A major aspect of deep water hydrocarbon migration; Proc. GCSSEPM Foundation 21st Ann. Res. Conf., P. 453-468.

Gordon, D., Flemings, P., 1998, Generation of overpressure and compaction-driven fluid flow in a Plio-Pleistocene growth faulted basin, Eugene Island 330 field, offshore Louisiana; Water Resources Research, v. 10, pp. 177-196

Haridon, S., Reysenbach, A., Glenat P., Prieur, D., Jeanthon, C., 1995, Hot subterranean biosphere in continental oil reservoirs; Nature, v. 377, p. 223-224

Hart, B., P. Flemings, and A. Deshpande, 1995, Porosity and pressure: Role of compaction disequilibrium in the development of geopressures in a Gulf Coast Pleistocene basin: Geology, v. 23, p. 45-48

Holland, D., J. Leedy, and D. Lammlein, 1990, Eugene Island Block 330 field - U. S. A., offshore Louisiana; in Beaumont, E., and Foster, N., eds., Structural Traps III: Tectonic Fold and Fault Traps: Amer. Assoc. Petrol. Geol. Treatise of Petroleum Geology, p. 103-143

Hood, K. ; Wenger, L ; Gross, O ; Harrison, S; Goodoff, L., 1995, Northern Gulf of Mexico; an integrated approach to source, maturation, and migration; Amer. Assoc. Petrol. Geol. Abstr. w/Prog. vol. 4, p. 109-110

Huber, R., Stoffers, P., Cheminee, J., Richnow, H., Stetter, K., 1990, Hyperthermophilic acheaeobacteria within the crater and open sea plume of erupting MacDonald seamount; Nature, v., 345, p. 179-181

Hunt, J., 1996, Petroleum Geology and Geochemistry, W.H. Freeman and Co., New York, p. 125-127

Issler, D., 1992, A new approach to shale compaction and stratigraphic restoration, Beaufort-Mackenzie basin and Mackenzie Corridor, northern Canada; Amer. Assoc. Petrol. Geol. Bull., v. 76, pp. 1170-1189

James, A., 1983, Correlation of natural gas by use of carbon isotopic distribution between hydrocarbon components: Amer. Assoc. Petrol. Geol. Bull., v. 67, p. 1176-1191

James, A., Burns, B., 1984, Microbial alteration of subsurface natural gas accumulations; Amer. Assoc. Petrol. Geol. Bull., v. 68, p. 957-960.

Jannasch, H., Taylor, C., 1984, Deep-sea microbiology; Ann. Rev. Microbiol., v. 38, p. 487-514

Kennicutt, M., Brooks, J., Denoux, G., 1988, Leakage of deep, reservoired petroleum to the near surface of the Gulf of Mexico continental slope; Marine Chem., v. 24, p. 39-59.

Kissin, Y., 1987, Catagenesis and composition of petroleum: Origin of n-alkanes and isoalkanes in petroleum crudes: Geochim. et Cosmochim. Acta, v. 51, p. 2445-2457

Losh, S., L. Eglinton, M. Schoell, and J. Wood, 1999, Vertical and lateral fluid flow related to a large growth fault, South Eugene Island Block 330 field, offshore Louisiana; Amer. Assoc. Petrol. Geol. Bull. vol. 83, p. 244-276

Losh, S., Walter, L., Meulbroek, P., Martini, A., Cathles, L., Whelan, J., 2002, Reservoir fluids and their migration into the South Eugene Island Block 330 reservoirs, offshore Louisiana; AAPG Bull., vol. 86, pp. 1463-1488.

Lovley, D., Chapelle, F., 1995, Deep subsurface microbial processes, Ann. Rev. Geoph. v. 33, p. 365-38

MacDonald, I., Guinasso, N., Sassen, R., Brooks, J., Lee, L., Scott, K., 1994, Gas hydrate that breaches the seafloor on the continental slope of the Gulf of Mexico; Geology, v. 22, p. 699-702

McBride, B., 1998, The evolution of allochthonous salt along a megaregional profile across the northern Gulf of Mexico basin; Amer. Assoc. Petrol. Geol. Bull., v. 82, pp. 1037-1054

McKenna, T., 1997, Fluid flow and heat transfer in overpressured sediments of the Rio Grande embayment, Gulf of Mexico Basin; Gulf coast Assoc. Geol. Soc. Trans. v. 47, p 351-366.

Meulbroek, P., 1997, Hydrocarbon phase fractionation in sedimentary basins: unpub. PhD thesis, Cornell University, 344 pp.

Meulbroek, P., Cathles, L., Whelan, J., 1998, Phase fractionation at South Eugene Island Block 330; Org. Geochem., v. 29, pp. 223-239

MMS, 1999, Assessment of conventionally recoverable hydrocarbon resources of the gulf of Mexico and Atlantic Outer Continental shelf as of January 1, 1995; OCS Report MMS 99-0034, CD-ROM

Parkes, R.J., Cragg, B., Gale, S., Getliff, J., Goodman, K., Rochelle, P., Fry, J., Weightman, A., Harvey, S., 1994, Deep bacterial biosphere in Pacific Ocean sediments; Nature, v. 371, p. 410-413

Peters, K., and Moldowan, J., 1993, The Biomarker Guide: Interpreting Molecular Fossils in Petroleum and Ancient Sediments: Prentice Hall, Englewood Cliffs, NJ, 323 pp.

Petzet, A.G., 1998, Anadarko find, technology gains renew subsalt hopes; Oil and Gas Jour., v. 96, no. 33, pp. 116-117.

Price, L., Wenger, L., Ging, T., Blount, C., 1983, Solubility of crude oil in methane as a function of pressure and temperature; Org. Geochem., v. 4, pp. 201-221.

Radke, M., 1988, Application of aromatic compounds as maturity indicators in source rocks and crude oils; Marine and Petrol. Geol., v. 5, pp. 224-235.

Revil, A. and L. M. Cathles, 2001, The porosity-depth pattern defined by 40 wells in Eugene Island South Addition, Block 330 Area, and its relation to pore pressure, fluid leakage, and seal migration: Petroleum Systems of Deep-Water Basins: Global and Gulf of Mexico Experience, Houston, Texas, GCSSEPM, p. 687-712.

Roberts, H. 1996, Surface amplitude data: 3D seismic for interpretation of seafloor geology (Louisiana slope); Gulf Coast Assoc. Geol. Socs. Trans. v. 46, pp. 353-362.

Rowan, M., 1995, Structural styles and evolution of allochthonous salt, central Louisiana outer shelf and upper slope, in M.P.A. Jackson, D.G. Roberts, and S. Snelson, eds., Salt tectonics: a global perspective: AAPG Memoir 65, p. 199-228.

Sassen, R., MacDonald, I., 1994, Evidence of structure H hydrate, Gulf of Mexico continental slope, Org. Geochem., v. 23, p. 1029-1032

Sassen, R., Roberts, H., Aharon, A., Larkin, J., Chinn, E., Carney, R., 1993, Chemosynthetic bacterial mats at cold hydrocarbon seeps, Gulf of Mexico continental slope, Org. Geochem., v. 20, p. 77-89

Sassen, R., Sweet, S., Milkov, A., DeFreitas, D., Salata, G., McDade, E., 1999, Geology and geochemistry of gas hydrates, central Gulf of Mexico continental slope; Trans. Gulf Coast Assoc. Geol. Socs., v. 49, p 462-468

Sassen, R., Losh, S., Cathles, L., Roberts, H., Whelan, J., Milkov, A., Sweet, S., DeFreitas, B., 2001, Massive vein-filling gas hydrate: relation to ongoing gas migration from the deep subsurface in the Gulf of Mexico; Mar. Petrol. Geol. v. 18, p. 551-560

Schumacher, D., 1993, Eugene Island Block 330 Field, offshore Louisiana: Geochemical evidence for active hydrocarbon recharging; Amer. Assoc. Petrol. Geol. Ann. Convention Abstr. w/Prog., New Orleans, April.

Silverman, S., 1965, Migration and segregation of oil and gas; Young, A., Galley, G., eds., Fluids in Subsurface Environments; Amer. Assoc. Petrol. Geol. Mem. 4, pp. 53-65

So, C-M., Young, L. Y., 1999, Isolation and characterization of a sulfate-reducing bacterium that anaerobically degrades alkanes; Appl. Environ. Microbiol., v. 65, p. 2969-2976

Stetter, K., Huber, R., Blochl, E., Kurr, M., Eden, R., Fielder, M., Cash, H., Vance, I., 1993, Hyperthermophilic bacteria are thriving in deep North Sea and Alaskan oil reservoirs; Science, v. 236, p. 822-824

Stump, B., Flemings, P., Finkbeiner, T., Zoback, M, 1998, Pressure differences between overpressured sands and bounding shales of the Eugene Island 330 Field, (Offshore Louisiana USA) with implications for fluid flow induced by sediment loading; Mitchell, A., Grauls, D., Swarbrick, D., Dainelli, J., organizers, Overpressures in Petroleum Exploration, Workshop Proceedings, Pau, France

Thompson, K., 1987, Gas condensate migration and oil fractionation in deltaic systems: Marine and Petrol. Geol., v. 5, p. 237-246

Thompson, K., Kennicutt, M.C., Brooks, J., 1990, Classification of offshore Gulf of Mexico oils and gas condensates; Amer. Assoc. Petrol. Geol. Bull., v. 74, pp. 187-198.

van Graas, G., Gilje, A., Isom, T., Tau, L.A., 2000, The effects of phase fractionation on the composition of oils, condensates and gases; Organic. Geochem., v. 31, pp. 1419-1439.

Wellsbury, P., Goodman, K., Barth, T., Cragg, B., Barnes, S., Parkes, J., 1997, Deep marine biosphere fuelled by increasing organic matter availability during burial and heating; Nature, v. 388, p. 573-576

Weimer, P., Varnai, P., Budhijanto, F., Acosta, Z., Martinez, R., Navarro, A., Rowan, M., McBride, B, Villamil, T., Arango, C., Crews, J., Pulham, A., 1998, Sequence stratigraphy of Pliocene and Pleistocene turbidite systems, northern Green Canyon and Ewing Bank (offshore Louisiana), northern Gulf of Mexico; AAPG Bull. v. 82, no. 5B, pp. 918-960.

Whelan, J., Oremland, R., Tarafa, M., Smith, R., Howarth, R., Lee, C., 1986, Evidence for sulfate-reducing and methane-producing microorganisms in sediments from sites 618, 619, and 622; Bouma, A., Coleman, J., Meyer, A., et al., Init. Repts. Deep Sea Drilling Project, v. 96, p. 767-775

Whelan, J., Kennicut, M., Brooks, J., Schumacher, D., Eglinton, L., 1994, Organic geochemical indicators of dynamic fluid flow processes in petroleum basins; Organic Geochem., vol. 22, pp. 587-615

Wirsen, C., Molyneaux, S., 1999, A study of deep-sea natural microbial populations and barophilic pure cultures using a high-pressure chemostat; Appl. Environ. Microbiol. v. 65, p. 5314-5321

Zengler, K., Richnow, H., Rosello-Mora, R., Michaelis, W., Widdel, F., 1999, Methane formation from long-chain alkanes by anaerobic microorganisms; Nature v. 401, p. 266-269

Appendix A. Data Tables

Table A1. Sample descriptions, GRI transect samples. Depth is in feet SSTVD. $\delta^{13}C$ is for whole oil in permil relative to PDB. Mass depletion is calculated for nC_{10+}

Sand	Well	Depth	Pr/nC_{17}	Break no	Slope	mass depl	$\delta^{13}C$	Sulfur (%)
SEI330								
GA-2	A13D	4297					-26.65	0.88
GA-2	B16D	4228	.57				-27.45	1.11
GA-2	B18D	4254					-27.1	1.23
GA-2	B1D	4198					-27.05	1.19
GA-2	C10D	4213					-27.1	1.08
GA-2	C13D	4223					-27.0	1.0
GA-2	C15D	4208					-26.65	1.04
GA-2	C1D	4197					-26.95	0.94
GA-2	C2D	4290					-26.9	0.87
GA-2	C5D	4259	8.16				-26.8	0.87
GA-2	C6D	4205	-				-26.7	0.91
HB-1	A13ST	4765	-				-26.35	0.9
HB-1	A18D	4821	-				-27.1	1.04
HB-1	A2	4767	-				-27.35	0.98
HB-1	B17D	4822	-				-26.85	1.29
HB-1	B18	4833	-				-26.75	1.45
HB-1	B2(ST)	4767	-				-27.15	1.29
HB-1	C2	4779	-				-27.2	1.23
HB-1	C3D	4754	-				-26.85	1.17
HB-1	C4E	4759	1.78				-26.9	1.36
HB-1B/2	B16	4757	-				-27.3	1.6
HB-3	B3(ST)	4900	-				-27.25	1.26
J-1-D	A19ST	6250	1.00	U	-1.02		-27.35	0.02
JD	B7A	6360		U	-0.94			
JD	B17	6078	.46	U	-1.02		-26.95	0.01
JD	B3ST	~5900	.40					
JD	A5	6319		U	-0.94			
JD	A11	6391		U	-0.48			
JD	B7AST			U	-0.23			
JD	A1	6402		U	-0.89			
KE	C18	6672	.90	U	-0.22			
KE	A5	6628		U	-0.89			
KE	A6ST	6300		U	-0.95			
KE	C17	6250		U	-0.73			
LF	A21	6894		15	-0.18	0.08		
LF	B14	7037		13.9	-0.20	0.12		
LF	B4	7078	.49	U	-0.2		-27.15	0.69
LF	B5ST	6800	.57	U	-0.25			
LF	B6ST	~6900	.63	U	-0.22			
LF	B7	6837	.46	U	-0.64		-26.85	0.03
LF	C20	6420	.35					
LF	C21	6374	.26					
MG-1-2	A20	7247	.29	U	-0.22		-27.2	0.51
MG-1-2	B9D	7302	.49	U	-0.21		-27.2	0.35
MG-4	B9	7424	.30	U	-0.23		-26.3	0.32
MG	C15	6100	.83	U	-0.75			
NH	B10ST	6666	.33	U	-0.16		-27.3	1.09
NH	A3	7614		U	-0.2			
NH	C18	7717		U	-0.16			
OI-1	B12D	7050	.31	12.6	-0.17	0.04	-27.3	0.9
OI1	C21	7102		13.5	-0.16	0.09		
OI1, 2	B11	7050		15.9	-0.19	0.10		
OI1	B11	6949		13	-0.19	0.03		
OI1	B13	7432		13.1	-0.18	0.05		
OI1	B3	7327		14	-0.17	0.11		
OI-1	B15D	7145	.34	13	-0.18	0.05	-26.75	0.92
OI-1	C14D	7048	.35	13	-0.18	0.10	-27.0	0.89
OI-1	C16	7257	.25	11.6	-0.17	0.07	-27.25	0.95
OI-1	C17ST	7226	.27	13	-0.17	0.06	-27.2	0.93
OI-1	C4	5933	.89					

Sand	Well	Depth	Pr/nC$_{17}$	Break no	Slope	mass depl	$\delta^{13}C$	Sulfur (%)
OI-1	C7A	7616	.31	13	-0.17	0.05	-27.35	0.89
OI-1	C9D	7168	.27	13.8	-0.15	0.08	-26.9	0.89
OI1	C19	7142		13.1	-0.18	0.07		
OI-1-2	A14A	7066	.42				-27.0	0.1
OI-1-2	A4	7836	.45	U	-0.73		-26.75	0.03
OI2	A14	7166		U	-0.2			
OI5	A2ST	7302		13.6	-0.23	0.15		
Jolliet (GC184)								
GS1/GS2	A14DST	6231	0.59	U	-0.18			
GS1/GS2	A15D	6085	0.79	U	-0.15			
GJ A6	A6	5708	8.83	U	-0.53*			
HJ1	A9DST	6674	1.09	U	-0.26			
HJ1	A13	6857	1.8	U	-0.24*			
HJ1	A14ST	6902	2.11	U	-0.20*			
HJ1/HM1	A11D	6869	2.2	U	-0.21*			
HO3/IA7/IB7	A8	6836	2.7	U	-0.16*			
IF A12	A2DST	7107	2.46	U	-0.23*			
IF1	A11	7578	4.83	U	-0.27*			
IF/A12	A18	7478	4.85	U	-0.26*			
KE1/KE2/KI	A1	8900	0.39	U	-0.15			
KP3/KQ3	A7	8562	0.4	U	-0.15			
KS3	A3ST	10090	0.4	U	-0.20			
*Oil mixed with condensate oil, except A6 and A3DST								
SMI9 field								
10200/A	SMI288/CA3	10179					-25.75	
10300/P	EI133/CA5	10420					-26.47	
10300/P	EI133/CA5	10420	0.85	16	-0.262	0.39		
11300/CP8/P	SMI8/A3D	10972	0.81	18	-0.29	0.53		
11300/CP8/P	SMI8/A3D	10714	0.71	18	-0.2	0.49		
11300/P	SMI8/CA3D	10682					-26.47	
11900/P	SMI8/A1D	12122	0.83	17	-0.21	0.43		
11900/P	SMI8/A1D	12133	0.85	19	-0.215	0.43		
11900/R	SMI288/CC1	12130	0.73	17	-0.21	0.48	-26.57	
11900/R1	SMI288/CC1	12125	0.75	19	-0.22	0.52		
11900/R1	SMI288/CC1	12126	0.74	19	-0.24	0.58		
11900/R1	SMI288/CC4	12117	0.72	17	-0.21	0.46		
11900/R1	SMI288/CC4	12120	0.75	17	-0.2	0.38		
11900/T	SMI288/CC3	12841	0.75	18	-0.18	0.42		
12200/O	SMI8/CA2	12170	0.73	17	-0.17	0.37		
12200/O	SMI8/CA2	11748	0.81	19	-0.295	0.56		
12200/O	SMI8/CA2ST	11636					-26.59	
12200/O	SMI8/CA2	12180	0.74	19	-0.195	0.48		
12200/O	SMI8/CA4	12640	0.65	21	-0.2	0.54		
12200/O	SMI8/CA4	12110	0.6	20	-0.2	0.55		
12200/O	SMI8/CA4	12640	0.67	CURVED				
12200/P	SMI8/CA3	12126	0.81	20	-0.44			
12200/P	SMI8/CA3	12130	0.8	18	-0.405			
12200/R	SMI288/CC4	12352	0.75	20	-0.25	0.59		
15600/A	SMI9/6	15651	0.87	19	-0.2	0.5	-26.26	
15600/D	SMI8/CA1	12886	0.82	18	-0.31	0.62		
15600/D	EI133/CA5	13525	0.7	18	-0.29	0.65		
15600*/H	SMI9/2D	15534	0.93	20?	-0.20?	0.46		
15650*/H	SMI9/2D	15579	0.9	19?	-0.17	0.35		
15700*	SMI9/2	15652	0.86	18?	-0.16?	0.34		
15750*/H	SMI9/5	15302	0.96	15	-0.29	0.4		
15750/H	SMI9/5	15310	0.86	11	-0.46			
15800	SMI9/5	15376	0.71	18?	-0.26?			
15800	SMI9/5	15378	0.77	CURVED				
17800BFBM	SMI287/1	16500	0.93	16	-0.2	0.20		
17800	SMI287/1	16510	0.93	17	-0.2	0.29		
RFT	SMI288/6	13242	0.68	CURVED				
CP-9	SMI288/7ST	11710	0.81	18	-0.24	0.46		

Sand	Well	Depth	Pr/nC$_{17}$	Break no	Slope	mass depl	δ^{13}C	Sulfur (%)
Tiger Shoals Study Area								
Tiger Shoals								
N1 MDL/300(oil)	72	8528	.746	23	-0.31	0.86	-26.4	
Q-1/390 (GC)	172	9473	.837	-	-0.90		-26.2	
T-1/250 (GC)	4	10526	.818		-0.98		-26.0	
T-1/900 (GC)	83	10526	.799				-26.2	
U N-1/300(oil)	72	11619	.74	23	-0.31	0.86	-26.4	
V/550 (oil)	76	11210	.388	23	-0.32	0.91	-26.7	
V/580 (oil)	121	11210	.395	23	-0.32	0.91	-26.7	
Y/400 (GC)	118	11892	.629		-0.68		-26.3	
12000A/150 (oil)	186	12200	.572	24	-0.24	0.83	-26.7	
Starfak								
T2A/475	V31/1	10820	.398	23	-0.29	0.87	-26.8	
U/450 (9921)	V30/4	11062	.706	23	-0.28	0.85	-26.5	
U/450 (10960)	V30/4	11062	.619	-	-0.28	-	-26.7	
U/500	V31/14	11062	.652	23	-0.30	0.87	-26.7	
U/670	V31/20	11062	.518	23	-0.29	0.87	-26.6	
12000A/670	V31/6	12690	.708		-0.8		-26.7	
ROBL1/655	V31/3	14290	.609		-0.47		-26.6	
ROBL2/670	V31/4	14276	.569	24	-0.34		-27.0	
ROBL2/650/1*	V31/10	14276	.597	23		0.88	-26.9	
ROBL2/650/2*	V31/10	14276	.409		-0.33	0.88	-27.1	
Trinity Shoals								
J/250	171	9679	.826	23	-0.32	0.87	-26.5	
N/100	130	10346	.692	23	-0.31	0.86	-26.5	
N/100	151	10346	.675	23	-0.30	0.85	-26.6	
N/100	178	10346	.682	23	-0.27	0.82	-26.5	
N/100	188	10346	.726	23	-0.31	0.86	-26.5	
N/100	193	10346	.727		-0.62		-25.8	
Amber								
N/360	C7	10109	.668	23	-0.33	0.90	-26.4	
N/144	160	10109	.713	23	-0.31	0.87	-26.4	
TexL4/310	100	9450	.242	22	-0.32	0.79	-26.6	
TexL4/110	A3	9450	.59	23	-0.31	0.85	-26.3	
Mound Point								
M/500	41	8585	1.838	23	-0.31		-26.3	
M/500	70	8585	.622	23	-0.29	0.82	-26.4	
Q1/250	108	9980	.896		-1.08		-26.2	
Lighthouse Point								
Q1	21	9368	.503		-1.38		-26.4	
Q2/800	15	9460	.528		-0.83		-26.4	
Aquamarine								
TexL1/500	153	8992	.774	23	-0.31	0.87	-26.5	
J/500	196	9131	1.051	23	-0.30	0.83		
*/1 – sample no 9926, /2 – sample no 10962								
SMI23								
	E1	13888	1.02	18	-0.16	0.47		
	F4	12373	1.16		-0.70			
	F2	14175	0.93	18	-0.17	0.36		
SMI48								
	C1	12020	1.4		1.02			
	B6	11420	0.80		-0.80			
	C7D	10636	1.55					
	C3	9992	1.72					
	E4D	10256	0.82	18	-0.16	0.22		
SMI66								
	B8	10257	1.34		-0.72			
SMI78								
	B7	14586	0.79		-0.25			
	B7	15074						
SMI79								
	B1	13793	0.81	15	-0.19	0.18		

Sand	Well	Depth	Pr/nC_{17}	Break no	Slope	mass depl	$\delta^{13}C$	Sulfur (%)
SMI79 (cont'd)	C1	12144	0.92		-0.40			
	C3	14156	0.76					
EI238								
	J2	7760			-1.02			
	H2	12820	1.71	12	-0.27	0.03		
	H5D	10400	1.29		-0.24	0		
	C3	9060	0.65	16	-0.23	0.27		
	A6	11010	0.82					
	H5	11580	1.12	13	-0.38			
	H13	13450	1.03	13	-0.21	0.13		
	J1	7437	1.58	-	-0.66	-		
EI252								
	B3	9395	0.66	14	-0.24	0.28		
	B7	8880	0.64	15	-0.24	0.30		
SEI305								
	A1	10400	0.96		-0.31?			
	A3	8950	0.58		-0.42			
	A5	11550	0.68	15	-0.24	0.21		
	B2	11580	0.54					
	B5	10800	0.41	16	-0.20	0.21		
	B7	*12050*	*0.61*	*16*	*-0.22*	*0.21*		
SEI341								
	A3	7381	0.53	13	-0.15	0.05		
	A13	7321	0.62	15	-0.17	0.21		
	A7	5650	0.58	16	-0.30	0.33		
	A10	7267	0.52	15	-0.15	0.09		
	A11	6410	0.68	15	-0.28	0.23		
	A1	7340	0.47	15	-0.15	0.09		
SEI361								
	D1	3829	17.6		-0.76			
	A17	4594	1.07	0	-0.24	0		
	A15	4400	-		-			
	D4	4025	-		-			
	C14	4385	13		-			
	C3ST	3003	0.55		-0.22			
	A19	3110	-		-			
	C5	3506	-		-			
	C15	4179	-		-			
	C12	4087	6.15					
	A18	4244	0.87	0	-0.23	0		

Table A2. Gas geochemical data, transect samples. Molecular data are in volume percent for SMI9 data, mole percent for Jolliet and SEI330. For Tiger Shoals, mole percentages are normalized for n-C_{1-4}

Block/Well	Sand	SSTVD	%N2	%CO2	%C1	%C2	%C3	%iC4	%nC4	%iC5	%nC5	δD_{C1}	$\delta^{13}C_1$	$\delta^{13}C_2$	$\delta^{13}C_3$	$\delta^{13}iC_4$	$\delta^{13}nC_4$	%Ro
SMI9 field																		
SMI9/6	15600/A	15157	9.48	1.29	82.66	4.31	1.5	0.38	0.23	0.069	0.035	-164.6	-47.26	-26.66	-25	-25.11	-24.32	1.75
SMI8/CA2ST	12200/O	11636	9.54	0.51	84.87	3.86	0.87	0.2	0.1	0.029	0	-156.7	-44.67	-26.01	-24.11	-24.35	-23.75	1.8
SMI288/CA3	10200/A	10179	11.29	0.31	85.21	2.27	0.58	0.15	0.11	0.037	0.003	-133.4	-38.87	-25.09	-23.19	-23.49	-23.26	2.0
SMI8/CA3	12200/A	12209	9.54	0.45	84.88	3.57	0.97	0.3	0.16	0.062	0.027	-135.6	-38.77	-26.47	-23.95	-23.5	-23.19	1.8
SMI8/CA3D	11300/P	10682	10.31	0.38	84.06	3.87	0.93	0.24	0.12	0.044	0.003	-160.4	-47.28	-26.68	-24.69	-24.75	-24.5	1.7
EI133/CA5	10300/P	10260	9.4	0.32	85.63	3.38	0.86	0.22	0.11	0.03	0.002	-163.8	-47.76	-26.49	-24.19	-24.75	-24.04	1.8
SMI288/CC1	11900/R	11820	9.89	0.7	81.9	5.06	1.59	0.45	0.25	0.087	0.044	-157	-44.05	-25.86	-24.07	-24.38	-23.38	1.8
Jolliet																		
A8	IA7/IB7	6836	0.32	1.64	88.56	5.91	2.23	0.33	0.55	0.15	0.13	-196.4	-45.83	-29.5	-26.84	-27.52	-25.7	1.3
A3ST	KS3	10090	0.33	0.09	89.62	6.45	2.26	0.32	0.51	0.13	0.12	-191	-44.85	-29.15	-26.67	-27.31	-25.57	1.3
A14ST	HJ1	6902	0.15	1.12	84.91	8.22	3.7	0.51	0.86	0.2	0.16	-200.1	-46.91	-30.16	-27.22	-27.78	-25.85	1.2
A13	HJ1	6857	0.21	0.49	86.34	7.42	3.5	0.53	0.92	0.22	0.18	-199.1	-47.03	-29.89	-27.1	-27.72	-25.77	1.25
A3DST	HO/IA1/IB	7158	0.33	1.34	86.21	6.96	3.2	0.52	0.9	0.21	0.17	-198.8	-46.5	-29.66	-26.99	-27.61	-25.74	1.25
A19ST	HO3/IA7/IB7	7520	0.28	0.37	86.3	7.6	3.34	0.53	0.93	0.23	0.21	-198.5	-46.09	-29.5	-26.92	-27.69	-25.74	1.3
A18	IF/A12	7478	0.22	1.31	85.84	6.74	3.39	0.57	1.05	0.3	0.28	-206	-48.72	-30.03	-27.14	-27.78	-25.79	1.2
A14DST	GS1/GS2	6231	0.27	0.25	90.83	5.09	2.34	0.35	0.58	0.13	0.099	-200.3	-48.09	-29.97	-26.98	-27.65	-25.67	1.2
A2DST	IF A12	7107	0.23	1.18	85.91	7.31	3.38	0.51	0.89	0.22	0.19	-204.1	-48.69	-30.07	-27.12	-27.74	-25.77	1.2
A9	HO1/IA1	6981	0.32	0.23	87.48	7.25	3.08	0.45	0.75	0.17	0.14	-200.5	-47.06	-29.73	-26.99	-27.6	-25.71	1.25
A1	KE1/KE2/KI	8900	0.28	0.15	83.92	8.82	4.02	0.67	1.16	0.33	0.32	-197.2	-45.88	-29.59	-26.86	-27.66	-25.68	1.35
A15D	GS1/GS2	6085	0.23	0.29	89.17	5.46	2.82	0.48	0.86	0.25	0.21	-199.2	-48.07	-29.92	-26.98	-27.68	-25.64	1.2
A7	KP3/KQ3	8562	0.28	0.13	85.13	8.38	3.67	0.6	1.03	0.27	0.25	-194.2	-45.1	-29.36	-26.79	-27.61	-25.62	1.35
A6	GJ A6	5708	0.19	0.23	85.99	7.25	3.76	0.63	1.1	0.3	0.27	-206	-47.24	-30	-27.25	-27.77	-25.88	1.2
A11	IF1	6674	0.25	0.41	85.76	7.71	3.58	0.57	0.99	0.26	0.23	-200.4	-46.94	-29.78	-27.06	-27.68	-25.78	1.25
SEI330																		
C13D	GA2/B	4204			77.4	8.00	4.40	0.73	1.30	0.42	n.d.		-42.0	-28.8	-26.9			
B18	HB1/B	4821			75.9	4.40	2.30	0.43	0.96	0.31	n.d.		-40.7	-28.7	-27.6			
C5	HB1	4809			56.6	4.73	2.43	0.41	0.73	0.23	0.21		-43.7	-27.8	-26.2		-25.5	
A11B	J1D/C	6391			75.6	6.10	2.60	0.38	0.88	0.29	n.d.		-39.4	-28.4	-26.7			
A1B	JD/B	6402			78.5	6.57	2.99	0.46	0.91	0.29	0.32		-40.7	-28.3	-28.2		-24.6	
A1B	JD/B	6402			79.9	6.10	2.40	0.36	0.78	0.28	n.d.		-36.3	-28.7	-27.3			
B17	JD/B	6180			79.7	6.20	2.40	0.36	0.76	0.23	n.d.		-37.2	-28.3	-26.8			
B7A	JD/A	6360			75.2	6.30	2.70	0.41	0.87	0.20	n.d.		-38.1	-28.3	-26.8			
C8D	JD/B	5955			81.5	6.86	2.84	0.41	0.79	0.30	0.26		-39.5	-28.7	-26.6		-26.2	
C8D	JD/B	5955			79.7	6.40	2.60	0.42	0.91	0.30	n.d.		-39.1	-27.6	-27.1			
A5	KE2/B	6628			59.5	4.41	1.54	0.20	0.39	0.13	0.15		-40.4	-27.4	-26.4		-26.0	
C8	MG4/B	6688			78.7	6.40	2.60	0.31	0.89	0.25	n.d.		-36.8	-28.3	-26.8			
A6ST	KE/JD	6048			76.4	4.14	1.46	0.12	0.19	0.02	0.01		-51.7	-29.8	-27.3		-26.7	
B12D	OI-1/A	7050			80.6	5.80	1.60	0.19	0.38	0.12	n.d.		-38.7	-28.0	-26.7			
B12D	OI-1/A	7050			79.8	6.90	2.10	0.25	0.48	0.09	n.d.		-36.5	-28.3	-26.6			
C14	OI-3/A	7305			80.2	6.53	1.97	0.19	0.32	0.07	0.07			-24.3	-23.7	-24.1		
Tiger Shoals																		
62	D	6600			96.17*	3.16	.67						-50.34	-40.96	-38.47			0.4
79	H	7400			95.33	3.89	.78						-47.63	-36.28	-32.88			0.65
49	L	8000			95.41	3.75	.84						-45.09	-35.44	-31.93			0.7
84	O	8900			94.86	4.23	.91						-42.64	-33.75	-29.44			0.85
36	T	10600			94.54	4.28	.81	.18	.19**				-37.44	-30.79	-29.83	-26.87	-27.01	1.2

Table A3. Bulk compositional data, Tiger Shoals oils and condensates, determined by solvent extraction.

SAND/SEG	WELL	FIELD	API	Para*	Aro*	ARO	RES	ASPH	NORM	BRAN	CYCL
N1 MDL/300	72	TIGER SH		0.532	0.776	28.9	2.4	0.4	39	9.7	19.5
Q-1/390	172	TIGER SH	51.4	0.762	1.151	1.8	1.8	0.4	39.1	7.1	49.8
T-1/250	4	TIGER SH	50.9	0.818	0.939	4.6	0	0	33	9.2	53.2
T-1/900	83	TIGER SH	49.1	0.799	1.032	4.5	0	0	59.7	4	31.8
U N-1/300	76	TIGER SH	34.7	0.416	3.915	20.4	1.3	3.6	9.5	4	61.2
V/580	121	TIGER SH	34.3	0.459	3.067	17.4	1.5	2.4	26.5	2.6	49.6
Y/400	118	TIGER SH	43.3	0.709	1.452	27.7	0	0	34.2	1.3	36.8
12000A/150	186	TIGER SH	35.5	0.614	2.153	19.5	4.7	1.6	25.1	6.3	42.8
T2A/475	1	STARFAK	33.7	0.555	2.239	20.9	0.9	0.8	21.3	6	50
U/450	4	STARFAK	34.7	0.53	1.843	12.4	4.6	4.6	33.9	5.8	38.7
U/450	4	STARFAK	35.3	0.565	1.928	12.5	1.7	2.8	27.4	1	54.5
U/500	14	STARFAK		0.477	1.836	8.2	1.2	8.6	25.5	14.6	41.9
U/670	20	STARFAK	31.6	0.33	2.097	4	0.3	0	45.3	5	45.3
12000A/670	6	STARFAK	48.4	0.737	0.106	3	0.5	0	40.6	16.9	38.9
ROB L-1/655	3	STARFAK	49.6	0.807	0.785	10.4	1	0.3	45.1	3.8	39.5
ROB L-2/670	4	STARFAK	39.6	0.7	0.802	11.5	2.1	2.3	29.8	12.3	42.1
ROB L-2/650	10	STARFAK	41.2	0.638	0.785	12.9	2.2	1.2	35.9	2.2	45.6
ROB L-2/650	10	STARFAK		0.629	0.83	19.8	2	0	37.2	7.4	33.5
M/500	41	MOUND PT		0.25	0.455	8.9	7.8	2.8	63.5	5.7	11.4
M/500	70	MOUND PT		0.42	0.54	10.5	2.5	0.9	15.2	7.3	63.7
Q1/250	108	MOUND PT		0.779	0.275	19.6	3	0	35.3	15.1	26.9
TexL-4/310	100	AMBER	33.2	0.449	0.644	19.3	4.8	0.8	10.3	4.6	60.3
TexL-4/110	A3	AMBER	34.4	0.51	2.134	19	3.3	1.5	21.5	3.6	51.1
N/360	C7	AMBER	30.8			21.2	3.6	2.2	11.5	6.4	55.1
N/144	160	AMBER	33.1	0.391	1.422	18.4	2.5	1.2	17.3	3.1	57.6
J/250	171	TRINITY SH	36.3	0.571	0.424	13.7	3	1.2	21.8	3.6	56.7
N/100	130	TRINITY SH	37.4	0.665	0.771	17.6	8.2	7.1	6.1	3	57.9
N/100	151	TRINITY SH	36.7	0.633	0.824	7.9	3.6	0.9	23	3	61.6
N/100	178	TRINITY SH	34.6	0.468	0.97	14.6	3.4	1.3	11.3	5.6	63.8
N/100	188	TRINITY SH	35.2	0.514	0.822	5.7	6.7	4.6	18.1	4.4	60.4
N/100	193	TRINITY SH	48.4	0.733	0.783	4.2	0	0	40.3	6.4	49.1
TexL-1/500	153	AQUA	36.9	0.618	0.469	11.2	1.9	0.8	23.7	2	60.4
J/500	196	AQUA	37.1	0.588	0.45	13.5	2.9	1.5	16.5	4.7	60.9
Q-2/800	15	LT HSE PT	49.1	0.802	0.803	21.3	0	0	14.3	9.5	54.8
Q-1	21	LT HSE PT	47.6	0.783	1.14	2.3	0.8	0	39.3	2.2	55.3

*Para = paraffinicity: n-heptane/methylcyclohexane; Aro = aromaticity: toluene/n-heptane. Methylcyclohexane value includes a relatively minor dimethylcyclopentane peak. ARO = aromatics; RES = resins; ASPH = asphaltenes; NORM = normal alkanes; BRAN = isoalkanes; CYCL = naphthenes.

Table A4. Biomarker source and maturity ratios, Tiger Shoals oils and condensates. Abbreviations: LHP – Lighthouse Point, TIG – Tiger Shoals, STAR – Starfak, MOUN – Mound Point, AMB – Amber, TRIN – Trinity Shoals. Data from Pete Kelley, Texaco. Explanations of ratios are on next page.

SPL	FIELD	SAND	DEPTH	(1)	(2)	(3)	(4)	(5)	(6)	(7)	(8)	(9)	(10)	(11)	(12)	(13)	(14)	(15)
9901	LHP	X		0.27	0.48	0.75	1.21	0.86	0.2	0.79	0.42	0.46	0.35	0.07	0.02	0	0.29	0.27
9902	LHP	Q2/800	9460	0.03	0.36	0.66	1.24	0.64	0.37	0.56	0.36	0.32	0.42	0.94	0.5	0	0.54	0.46
9903	TIG	Q1	9368	0.19	0.44	0.61	1.27	0.55	0.32	0.51	0.27	0.33	0.45	0.91	0.4	0	0.57	0.49
9905	TIG	T1/250	10526	0.25	0.48	0.69	1.33	0.83	0.38	0.76	0.43	0.49	0.36	0.03	0.02	0	0.27	0.31
9906	TIG	T1&t2/950		0.26	0.48	0.93	1.3	1.15	0.41	0.75	0.4	0.46	0.34	0.03	0.03	0	0.25	0.31
9907	TIG	D/900	6566	0.21	0.46				0.38		0.42	0.46	0.34	0.01	0.07	0.03	0.31	0.2
9908	TIG	T1/250	10526			0.75	1.17	0.74		0.66								
9909	TIG	U N1/300	11618	0.35	0.52	1.19	0.73	1.08	0.42	0.72	0.46	0.49	0.35	0.01	0.11	0.05	0.3	0.21
9910	TIG	V/550	11210	0.27	0.49	1.05	1.11	1.11	0.36	0.75	0.4	0.43	0.37	0.04	0.08	0.03	0.3	0.14
9911	TIG	V/580	11210	0.31	0.51	1.05	1.09	1.1	0.35	0.76	0.42	0.4	0.38	0.03	0.09	0.03	0.29	0.14
9912	TIG	Q1/390	9473			0.74	1.24	0.84		0.81								
9915	TIG	T1/900	10526	0.29	0.5	1.2	0.89	1.12	0.49	0.76	0.46	0.41	0.4	0.03	0.03	0.07	0.43	0.31
9916	TIG	Y/400	11892	0.17	0.44	1.03	1.16	1.12	0.39	0.75	0.45	0.41	0.37	0.02	0.02	0	0.34	0.24
9921	STAR	U/450	11062	0.2	0.45	1.21	1.11	1.23	0.38	0.72	0.45	0.47	0.36	0.02	0.08	0	0.28	0.17
9923	STAR	ROBL1/655	14290	0.25	0.48	0.79	1.24	0.94	0.35	0.57	0.42	0.5	0.38	0.02	0.14	0.5	0.28	0.3
9924	STAR	ROBL2/670	14276	0.37	0.54	1.23	1.06	1.22	0.38	0.71	0.42	0.47	0.42	0.05	0.16	0.47	0.31	0.15
9925	STAR	12000A/670	12690	0.13	0.41	0.74	1.09	0.73	0.23	0.46	0.32	0.38	0.41	0.81	0.51	0.38	0.39	0.34
9926	STAR	ROBL2/650	14276	0.3	0.5	0.79	1.13	0.85	0.35	0.54	0.44	0.45	0.39	0.05	0.16	0.45	0.32	0.16
9927	STAR	U/670	11062	0.37	0.54	1.03	1.13	1.1	0.36	0.73	0.38	0.41	0.4	0.03	0.09	0.08	0.31	0.13
10955	TIG	N1 MDL/300	8528	0.24	0.47	1.18	0.72	1.06	0.36	0.66	0.34	0.44	0.36	0.01	0.09	0.44	0.32	0.14
10956	MOUN	M/500	8528	0.34	0.52	1.22	0.55	1.06	0.42	0.68	0.49		0.33	0.05	0.11	0.06	0.31	
10957	MOUN	M/500	8585	0.38	0.54	1.23	0.55	1.07	0.44	0.67	0.46	0.48	0.35	0.02	0.1	0.07	0.3	0.21
10959	MOUN	Q1/250	9980	0.21	0.46	0.62	1.33	0.61	0.38	0.61	0.5	0.48	0.36	0.02	0.09	0.05	0.34	0.24
10960	STAR	U/450	11062	0.25	0.47	1.14	1.16	1.22	0.35	0.69	0.42	0.46	0.35	0.03	0.09	0.02	0.3	0.19
10961	STAR	T2A/475	10820	0.37	0.53	1.14	1.07	1.15	0.34	0.71	0.38	0.43	0.38	0.03	0.09	0.02	0.31	0.15
10962	STAR	ROBL2/650	14276	0.3	0.5	0.79	1.04	0.82	0.32	0.5	0.44	0.47	0.39	0.02	0.17	0.47	0.32	0.17
10963	STAR	U/500	11062	0.29	0.49	1.21	1.13	1.23	0.34	0.74	0.4	0.45	0.39	0	0.1	0.02	0.3	0.17
10964	AMB	N1/360	10217	0.29	0.49	1.18	0.9	1.13	0.42	0.68	0.48	0.49	0.33	0.01	0.04	0.03	0.32	0.19
10965	AMB	N/360	10109	0.41	0.55	1.22	0.84	1.13	0.45	0.67	0.48	0.48	0.36	0.01	0.09	0.07	0.3	0.21
10966	AMB	TEXL4/310	9450	0.4	0.55	1.24	0.61	1.09	0.42	0.66	0.45	0.48	0.37	0.02	0.11	0.48	0.3	0.2
10967	AMB	N/300	10109	0.41	0.56	1.24	0.8	1.13	0.42	0.66	0.47	0.49	0.37	0.03	0.12	0.06	0.31	0.2
10968	AMB	N/300	10109	0.4	0.55	1.25	0.62	1.1	0.44	0.68	0.45	0.48	0.33	0.05	0.12	0.05	0.31	0.21
10969	AMB	TEXL4/110	9450	0.3	0.5	1.21	0.79	1.1	0.41	0.64	0.46	0.5	0.33	0.05	0.11	0.5	0.3	0.22
10970	AMB	N/144	10109	0.33	0.51	1.19	0.79	1.09	0.38	0.67	0.41	0.45	0.35	0.04	0.11	0.05	0.3	0.19
10984	TRIN	N/100	10340	0.27	0.49	1.11	0.98	1.1	0.43	0.63	0.51	0.47	0.34	0.04	0.08	0.07	0.29	0.2
10985	TRIN	N/100	10346	0.37	0.54	1.12	0.95	1.09	0.41	0.63	0.45	0.47	0.36	0.02	0.1	0.05	0.3	0.19
10986	TRIN	J/250	9679	0.25	0.47	1.11	0.93	1.07	0.38	0.6	0.45	0.47	0.34	0.04	0.08	0.06	0.3	0.19
10987	TRIN	N/100	10340	0.29	0.5	1.12	0.93	1.1	0.42	0.64	0.47	0.48	0.34	0.02	0.08	0.03	0.3	0.21
10988	TRIN	N/100	10346	0.36	0.53	1.16	0.88	1.09	0.42	0.63	0.42	0.48	0.34	0.05	0.1	0.04	0.3	0.2
10989	TRIN	N/100	10090	0.3	0.5	1.04	1.17	1.14	0.41	0.7	0.42	0.49	0.32	0.02	0.02	0	0.32	0.35
10990	AQUA	H/500	8457	0.21	0.45	0.73	1.25	0.81	0.62	0.69	0.34	0.45	0.41	0.82	0.1	0	0.6	0.4
10991	AQUA	F/500	8162	0.18	0.44	0.93	1.12	0.97	0.37	0.6	0.47	0.47	0.34	0.02	0.05	0.04	0.27	0.19
10992	AQUA	TEXL1/500	8997	0.29	0.5	1.03	0.99	1.03	0.37	0.57	0.41	0.46	0.34	0.02	0.09	0.46	0.29	0.19
10993	AQUA	J/500	9131	0.24	0.47	1.03	0.99	1.02	0.37	0.57	0.42	0.46	0.32	0.04	0.06	0.06	0.31	0.16
10994	TIG	V/550	11210	0.26	0.48	0.99	1.18	1.12	0.37	0.71	0.44	0.43	0.37	0.02	0.07	0.03	0.29	0.15
10995	TIG	12000A/150	12600	0.33	0.51	0.97	1.05	1.02	0.36	0.68	0.41	0.4	0.45	0.01	0.18	0.4	0.31	0.12
10996	AMB	N1/360	10217	0.39	0.54	1.17	0.94	1.13	0.45	0.69	0.44	0.5	0.35	0.01	0.08	0.08	0.31	0.2
10997	AMB	N/300	10109	0.4	0.55	1.17	0.94	1.13	0.44	0.68	0.47	0.49	0.34	0.02	0.11	0.05	0.31	0.2

Explanation of Ratios, Table A4

(1) 29Ste S/S+R = 24-ethylcholestane 20S/(20S+20R)
(2) Re 29Ste S/S+R = Equivalent %Ro for (1)
(3) Re MPI-1 (<1.35%) = Equivalent %Ro (<1.35%Ro) for MPI1 (Radke, 1988),
(4) Re MPR = Equivalent %Ro for 1MP/P (Radke, 1988)
(5) Re MPDF-1 = Equivalent %Ro for (2MP+3MP)/(1MP+2MP+3MP+9MP)
(6) Ts/Ts+Tm = 18a(H)-22, 29, 30-trisnorheohopane(Ts)/(Ts + 17a(H) – 22, 29, 30-trisnorhopane)
(7) Re MDR = Equivalent %Ro from 4MDBT/1MDBT (Radke, 1988)
(8) 29Ste bb/bb+aa = 24-ethlycholestane ββ/(ββ+αα)
(9) Diast/Tot ster = (C27-30 diasteranes)/((C27-30 diasteranes + C27-30 Regular steranes)
(10) 29Ste/27+28+29 Ste = (29-AAR+AAS+BBR+BBS steranes)/(27- + 28- + 29- AAR+AAS+BBR+BBS steranes)
(11) Gamma index = Gammacerane/(Gammacerane+17a(H)-Hopane)
(12) Oleanane Index = 18a(H)-oleanane/(18a(H)-oleanane + 17a(H)-Hopane)
(13) Homohopane Index = C35R+S Hopane/(sum C31-C35 R+S hopanes)
(14) H31/Hopane Index = C31R+S Hopanes/(C31R+S Hopanes + 17a(H)-Hopane)
(15) Tri/Tri+Hopane = Tricyclic terpanes/(Tricyclic terpanes + 17a(H) –Hopane)

Table A5. Calculated gas source $\delta^{13}C$ and percent bacteriogenic methane, according to the method of Chung et al. (1988), assuming $\delta^{13}C$ of –70 permil for pure bacteriogenic methane

Sand	Well	Source $\delta^{13}C$	%Bacteriogenic CH_4
Tiger Shoals			
D		-33.8	9
H		-26.1	4
L		-24.8	0
O		-20.8	0
T		-27.3	11
SMI9			
15600	6	-21.7	41
12200	CA2ST	-21.2	36
10200	CA3/288	-20.5	23
12200	CA3/8	-19.2	14
11300	CA3D	-20.8	39
10300	CA5	-20.3	41
11900	CC1	-20.4	33
SEI330			
GA	C13	-23	20
HB	B18	-25.8	21
HB	C5	-23.2	
JD	B17	-24	11
JD	A1	-24.2	16
JD	A11	-23.1	18
JD	C8	-24.4	20
JD	C8-2	-23.8	14
JD	B7A	-23.8	41
KE	A5	-24.3	24
MG	C8	-24	18
OI	B12(1)	-23.7	10
OI	B12(2)	-23.9	12
OI	C14	-22.8	
Jolliet			
IA7/IB7	A8	-22	26
KS3	A3ST	-21.7	25
JHJ1	A14ST	-21.5	30
HJ1	A13	-22	27
HO/IA1/IB	A3DST	-21.7	29
HO3/IA7/IB7	A19ST	-21.7	29
IF/A12	A18	-21.3	34
GS1/GS2	A14DST	-21.4	32
IF/A12	A2DST	-21.2	32
HO1/IA1	A19ST	-21.4	30
KE1/KE2/KI	A1	-21.8	25
GS1/GS2	A15D	-21.4	31
KP3/KQ3	A7	-21.7	26
GJ A6	A6	-21	27
IF1	A11	-21.7	30
HJ1	A9DST		29

Appendix B. Mass balance calculations for oil-condensate pairs

PVT modeling of liquid-vapor fractionation requires a determination of the original liquid composition. Where the residual liquid and the evaporative fraction (in the form of condensate) are still present, they can be recombined by use of the mass depletion factor to give an estimate of initial fluid composition, much as GOR can be used to recombine liquid and separator gas to arrive at the composition of liquid produced from a reservoir. An additional application of this technique is the determination of the likelihood of finding more oil in a given field based on the amount of condensate present and the liquid-vapor mass balance during fractionation. At Texaco's Tiger Shoals complex, this technique was developed to evaluate the prospectivity for oil below the presently exploited reservoirs. The mass of condensate relative to the mass of gas-washed, n-alkane depleted oil is determined. If the actual amount of condensate in the field exceeds the amount needed to balance the known amount of depleted oil, then more oil is indicated at depth. On the other hand, if the amount of condensate is less than that predicted as having been fractionated from the known depleted oil, then no deeper oil is indicated. As will be shown here, the mass balance method indicates that less condensate is present than would be predicted based on the amount of depleted oil and the extent of its fractionation; thus this method does not predict deeper oil at Tiger Shoals. However, the method would not predict the existence of the 1.8 MMbbl oil known to lie in the '12000 sand', the deepest producing sand in the Tiger Shoals field. In light of this, combined with the ubiquity of oil that was gas-washed at great depth at Tiger Shoals, and which may still lie at great depth, the mass balance method is concluded to not adequately represent gas washing and liquid and vapor phase migration at Tiger Shoals.

Mass balance is here derived for whole-oil reconstruction, given compositional data for the fractionated liquid and for the condensate phases, and the 'fractionation factor' (here called the 'depletion ratio') for one of the pseudo-components. Use of PVT data for determination of oil and vapor composition prior to separation of liquid and gas at the wellhead is also addressed. Any correction needed to convert GC data to 'true' oil compositions would need to be done prior to this analysis

Terminology used in this analysis is as follows:

N= n-alkanes
I = isoalkanes, meaning all branched alkanes, including isoprenoids
NA = naphthenes
AR = aromatics
AS = asphaltenes
V = Vapor (which produces condensate at the wellhead)
L = Fractionated oil (liquid)
O = Original oil prior to gas washing
F= Mass fraction, used in conjunction with other abbreviations. For example, F_{NL} = mass fraction of n-alkanes in fractionated liquid
D_x= depletion ratio, the fraction of component x in the original oil that fractionates into the coexisting vapor phase
T = mass of subscripted substance (L or V)

For the purposes of this analysis, the original oil and gas, prior to washing, are considered to be non-overlapping with respect to composition. The original oil is considered to contain everything heavier than wet gas compounds. The simulations of Meulbroek et al. (1998) involve only methane as the gas, although most washing gases probably are wet gases, containing compounds up to pentane. Since the computation of n-alkane mass depletion begins with nC_{10}, the consideration of the oil and washing gas, prior to fractionation of the oil, as compositionally distinct phases is valid. Thus, the analysis simply tracks the fate of compounds originally in oil as they fractionate between vapor and liquid. Addition of mass from the washing gas itself

is not relevant to the mass balance calculations developed below: the 'vapor phase', as designated here, is a construct used to keep track of oil compounds that have been stripped from the liquid.

The gas condensate produced at the wellhead is considered to represent the subsurface vapor phase in the compositional range of interest in this analysis, C_{10+}. As shown later in the appendix, the gas condensates are a useful proxy for vapor to compounds as light as C_7, and, if recombined with the separator gas at the appropriate gas:liquid ratio, can represent the entire composition of the subsurface vapor.

$T_L + T_V = 1$ (Equation B1)

And, in the original oil,

$N_O + I_O + NA_O + AR_O + AS_O = 1.$ (Equation B2)

For any component, two mass balance equations can be written. Here, the equations are written for the n-alkanes (N), since that is the component for which a depletion ratio is known.

$N_O = N_L + N_V$ (Equation B3)

(the total mass of n-alkanes = n-alkane mass in depleted liquid + n-alkane mass in vapor). Thus,

$N_O = (1-d_N)N_O + d_N N_O$ (Equation B4)

In addition,

$N_O = F_{NL}T_L + F_{NV}T_V.$ (Equation B5)

Substituting $1-T_L$ for T_V,

$N_O = F_{NL}T_L + F_{NV}(1-T_L).$ (Equation B6)

Further, because

$N_L = (1-d_N)N_O$ (Equation B7)

And

$N_L = F_{NL}T_L,$ (Equation B8)

$\mathbf{(1-d_N)N_O = F_{NL}T_L}$ (Equation B9)

Likewise, for the vapor phase, because

$N_V = d_N N_O$ (Equation B10)

And

$Nv = F_{NV}(1-T_L),$ (Equation B11)

$\mathbf{d_N N_O = F_{NV}(1-T_L)}$ (Equation B12)

Equations B9 and B12 are the two independent mass balance equations for each component.

Here, we know F_{NV} and F_{NL} from compositional data, and we know d_N from the molar fraction plot analysis. If we had no independent constraint on the depletion ratio, there would be three unknowns, and there would be no unique solution for the mass balance equations. Because we know d_N, there are only two unknowns, N_O and T_L, for the n-alkanes. From this, we can calculate T_L, the fraction of parent oil that remains in the liquid phase.

For Tiger Shoals oils,

d_N = 0.91, from the molar fraction plot analysis,
F_{NV} = 0.42 (from Texaco data (P. Kelley, pers. comm.), average of four condensates (see also Tables B1 and B3, below)
F_{NL} = 0.21

Accordingly, T_L (which in this case is the mass fraction of fractionated liquid in the L + V system) = 0.165

Thus, T_V = 1 – 0.165, or 0.835. The mass ratio of vapor (condensate being used as a proxy for the C_{10+} fraction) to depleted oil is

thus calculated uniquely as 0.835:0.165, or 5.06. Using API gravities for the oil and condensate at Tiger Shoals, the volume ratio of condensate:oil is computed as 5.42.

Following on this, $N_O = 0.384$. 1 gram of original oil contains 0.384 g n-alkanes.

For each pseudo-component, similar equations can be written. For naphthenes,

$$(1 - d_{NA})NA_O = F_{NAL}T_L \quad \text{(Equation B13)}$$

And

$$D_{NA}NA_O = F_{NAV}(1-T_L) \quad \text{(Equation B14)}$$

Since T_L is now known, each pair of equations now has only two unknowns, d_i and $(NA, AR, I, AS)_O$ (depending on component)

For Tiger Shoals oils,

$F_{NAL} = .50$
$F_{NAV} = .43$

From equations B13 and B14,

$d_{NA} = 0.81$, and $NA_O = 0.441$.

This can be repeated for all the other components to re-create the original oil, and to derive the depletion ratios for computation of PTx conditions of gas washing. Averaged oil and condensate compositions from Tiger Shoals are given in table B1; computed initial oil composition and depletion ratios for the various components are given in table B2.

Table B1.	Analyzed Oil (g compound/g oil)	Condensate (g compound/g liquid)
n-alkane	.21	.42
isoalkanes	.06	.06
naphthenes	.50	.43
aromatics	.18	.10
asphaltenes	.06	0

Table B2.	Initial Oil (g compound/g oil)	Depletion ratio (%)
n-alkanes	.38	91
isoalkanes	.06	82
naphthenes	.44	81
aromatics	.12	74
asphaltenes	.01	0

Condensate compositions and mass depletion ratios both vary over a range of values for Tiger Shoals samples. The sensitivity of the computed condensate:oil mass balance to these variations can be determined by computing the percent liquid using four different condensates, and two different n-alkane mass depletion ratios for each condensate (Table B3).

Table B3.

	Sample				
	T1/250	T1/900	Q1/390	Y/400	Avg
NALK	.33	.60	.39	.34	.21
IALK	.09	.04	.07	.01	.06
NAPH	.53	.32	.50	.37	.50
AROM	.05	.05	.02	.28	.18
ASPH	0	0	.02	0	.06
%L/d_N.91	14	22	16	14	
%L/d_N.85	22	33	24	22	

The most liberal conditions used here (that is, the conditions that would maximize percent liquid and thus be most favorable for exploration for oil) yield a liquid:condensate (oil:vapor) mass ratio of 1:2 (oil is 33% of mixture), or a volume ratio of 1:2.14 (given API gravities of Tiger Shoals oils (35 API) and condensates (50 API)). Actual oil:condensate volume ratio at Tiger Shoals is 17.1:18.9, or 1:0.90. Thus, at most, there is only 42% (0.9/2.14) as much condensate as there should be to balance the amount of oil already found at Tiger Shoals.

The computed liquid-vapor mass balance is not very sensitive to significant compositional variations in the condensate, as shown in Table B3. The calculated mass balance *is* considerably more sensitive to the depletion ratio. The maximum vapor:liquid mass ratio (0.33) was obtained using the minimum observed d_N of 0.85, combined with a 60% n-alkane condensate (sample T1/900).

The effect of variable fractionation conditions and mechanisms on calculated liquid-vapor mass balance

The foregoing analysis considers single-stage (batch) gas washing, and assumes that the present compositions of the oil and condensate represent the compositions of liquid and vapor at the point of phase separation in the subsurface. There are a number of other scenarios, as well as limitations on this method, that must be addressed: 1) the liquid produced as condensate at the separator does not necessarily represent the composition of nC10+ that is in the vapor phase in the reservoir, as some of these compounds may remain in the gas at the separator, 2) gas washing was an incremental process, which is probably more realistic than a batch process from a geologic point of view, and thus the sampled condensate gives but a snapshot of a long, complex process, and 3) the compositions of the oil and vapor phases changed between the point at which separation took place and the reservoir.

1) How representative of the actual vapor phase is the sampled condensate? The n-alkane patterns for Tiger Shoals condensates show depletion of compounds as heavy as nC_{15}. Peter Meulbroek (pers. comm.) has proposed that the reason for this apparent fractionation is that the condensates (vapor phase) separated from oil that was already fractionated, and are thus highly depleted in relatively low-molecular weight n-alkanes to begin with. It is not considered physically possible to fractionate compounds that are already in the vapor phase; i.e., to gas wash a vapor that produces condensate only at the wellhead. Normally, separator-related fractionation only affects compounds up to about C_8 or C_9, depending on separator pressure.

Gas/liquid compositions (Table B4) from a PVT analysis of a condensate from Starfak (Rob L, Vermilion 31 well 10, 101bbl/MMscf, 44.8 API) are here used to evaluate how representative the condensate analyses are of the wellstream fluid. Amounts in the following table are in mole fractions expressed as percents.

Table B4. Mole fractions (Percent)

Compound	Gas	Oil	Recombined
C1	91.27	3.8	85.48
C2	4.27	1.87	4.18
C3	1.7	1.95	1.85
iC4	0.54	1.47	0.67
nC4	0.41	1.47	0.56
iC5	0.18	1.57	0.33
nC5	0.10	1.09	0.21
C6	0.08	1.75	0.24
C7+	0.04	84.92	5.15

Density of the condensate is 0.75 g/cc (computed from API gravity). Assuming that the gas is ideal, having a molar volume of 22.4 liters, one liter of gas contains 4.46 x 10^{-2} moles of gas. The gas is not actually ideal, but such an assumption will not introduce an error of more than 5%. As shown below, the effect of such an error on computing the partitioning of C_{7+} between gas and condensate is not significant.

A liter of wellstream gas, at a volumetric GOR of 1760 (9901 scf/bbl x 1 bbl/5.6 ft^3), will condense 0.57 ml, or 0.43 g, liquid. If the average molecular weight of this liquid is 160 g (by comparison with oil molecular weights that are generally considerably higher), this liquid mass represents 2.69 x 10^{-3} moles

Using these numbers, 1 liter of reservoir gas separates into the following numbers of moles of C_1 through C_{7+} (Table B5). For example, one liter of gas condenses 2.69 x 10^{-3} moles liquid, having a mole fraction of C_{7+} of 0.8492 (table B4), thus containing 2.28 x 10^{-3} moles C_{7+}. One liter of gas, containing 4.46 x 10^{-2} moles total, contains 0.0004 x 4.46 x 10^{-2} moles C_{7+}, or 1.78 x 10^{-5} moles C_{7+}. The ratio of number of moles C7+ in liquid to that in coexisting gas, then, is 128.

Table B5.

	moles in liquid	moles in gas	liquid/gas mole ratio
C1	1.02 x 10^{-4}	4.07 x 10^{-2}	0.0025
C2	5.03 x 10^{-5}	1.90 x 10^{-3}	0.0264
C3	5.24 x 10^{-5}	7.58 x 10^{-4}	0.069
C4s	7.91 x 10^{-5}	4.24 x 10^{-4}	0.19
C5s	7.16 x 10^{-5}	1.25 x 10^{-4}	0.57
C6	4.71 x 10^{-5}	3.57 x 10^{-5}	1.31
C7+	2.28 x 10^{-3}	1.78 x 10^{-5}	128

It can be seen here that, at the given GOR and chemical compositions, over 99% of the mass of C_{7+} in a volume of wellstream gas fractionates into the condensate. C_1-C_4 strongly fractionate into the gas, and C_5 and C_6 show subequal distribution between gas and condensate. Thus, the wellhead condensate gives a good representation of reservoir vapor composition for C_{7+}, thus is useable for the n-alkane analysis, which computes mass balance based on even heavier compounds.

2) Batch vs incremental gas washing. As noted above, the method for computing liquid:vapor mass balance assumed a batch fractionation process: all the vapor separated from the liquid at a single step. However, the compositions employed in the analysis are not functions of fractionation mechanism per se; the averaged condensate composition is simply an integrated endpoint for the

fractionation process. This composition could just as easily represent the cumulative composition of the vapor phase during incremental fractionation as it does the composition of the end product of a batch fractionation process. How the condensate composition varied during fractionation (batch vs incremental) does not matter as far as this mass balance method is concerned.

3) Compositional variations after fractionation but before production. As documented in this report, Tiger Shoals oils probably fractionated at a greater depth, hence higher pressure, than that at which the oils are now found. The question arises: could the composition of the oil and, in particular, the vapor have changed between the point at which gas washing occurred and the reservoir? Could relatively low-fugacity compounds have condensed out of the vapor as it ascended, thus changing the condensate composition significantly? If such a thing happened (as it probably did), it would only mean that the vapor was more 'oil-like' at the point of fractionation from oil than it was in the reservoir. If the vapor that separated from the oil during gas washing was indeed more oil-like than the produced condensate, then it would mean that an even smaller fraction of residual oil would have been left than is calculated. Thus, if the condensate is taken as a proxy for the C_{10+} compounds in the vapor phase (see (1) above), then condensate:oil, hence vapor:liquid, mass ratios computed on the basis of condensate compositions would be minimum values.

Production – related changes in oil and condensate composition are thought to be relatively minor, as the fluids were collected early in the history of the field, before large pressure drops had been experienced (P. Kelley, pers comm.). Furthermore, the liquids were analyzed shortly after collection, minimizing evaporation – related modifications to composition.

Geologic implications of oil – condensate mass balance at Tiger Shoals

The determination that the condensates at the Tiger Shoals study area are products of gas washing, of which the reservoir oils are the residue, leads to the consideration of whether the amount of residual oil in the petroleum system can be estimated on the basis of the amount of condensate that was initially in the reservoirs. That is, does the condensate/oil ratio imply that there is oil yet to be discovered at a particular field? To evaluate this possibility, the average compositions of residual oil and condensate at the Tiger Shoals field were used (table B1, above), with the n-alkane depletion computation described above, to invert a pristine whole-oil composition, along with fractionation ratios for each of the major compound classes. The masses of residual oil and condensate that arise from this computation are compared with amounts that have been produced at Tiger Shoals to determine whether more oil 'ought' to be found there.

For the Tiger Shoals liquids, mass balance computations (above) indicate that 165 g of residual oil is paired with 835 g condensate (from equation B9). Such large fractionation of initial oil components into the vapor phase is compatible with high pressure of gas washing deduced from high break numbers and the presence of highly gas-washed oils well below the top of overpressure. Recombining the condensate (API gravity 50) with residual oil (API gravity 35) indicates the initial oil was of API gravity 47, on the borderline between light oil and condensate in terms of its density. The intense gas washing of this oil produced a residual liquid that, in terms of its API gravity, appears to be a 'normal' oil; however, it is strongly enriched in high-molecular weight compounds relative to its parent.

The condensate:residual oil mass ratio of 4.95 at Tiger Shoals converts to a volume ratio of 5.3 to 1. Accordingly, for the 17.1 MMbbl of gas-washed oil produced from Tiger Shoals, a volume of 90.1 MMbbl condensate is implied to have resulted from

gas washing of that oil. Actual condensate:oil volume ratio at Tiger Shoals is 1.1: only 18.9 MMbbl condensate is ultimately recoverable. The difference, 71.2 MMbbl condensate (or 79% of the condensate total), is presumed to still lie at depth or, more likely, to have been lost from the system along with the gas in which it was in solution. A similar mass balance for the average oil and condensate composition for the entire study area indicates a condensate:oil ratio of 4:1 during washing, on average. As oils from the other fields have experienced gas washing similar to that at Tiger Shoals, and occur with even less gas, with which condensate would be associated, it is likely that those fields have lost even greater percentages of gas and condensate than is the case at Tiger Shoals. Thus, condensate - oil mass balance for the Tiger Shoals area oils does not point to the existence of additional gas-washed oil at depth.

Does the mass balance method work? The utility of mass balance in exploration for deep oil can be tested at Tiger Shoals by determining whether use of this technique would locate oil known to be at depth or, conversely, whether it would accurately predict that deep oil would not be found. At Tiger Shoals, would the prediction that no deeper oil is present be accurate if the holes only penetrated to the Z sand, at a depth of 11,000 feet (Figure 8)? If that were the case, then the known oil volume would be 15.3 MMbbl, which would result in a calculated condensate:oil ratio of 1.23, still much lower than the 5.31 volume ratio that would be required by the mass balance method to indicate favorable conditions for the existence of deep oil. If this method were used to guide a deep drilling program, then the holes would not have been deepened into the '12000 sand', *and 1.8 MMbbl oil would not have been discovered*. Clearly, the mass balance method of determining or precluding the existence of deep oil does not work at Tiger Shoals.

The discrepancy between the predictions made on the basis of mass balance and the actual distribution of oil and gas may be attributable to the impossibility of knowing how 'open' the system was to the escape of gas relative to oil. If 79% of the total vapor that was involved in gas washing escaped from the reservoir system, the known amount of condensate would then be consistent with the known amount of oil. Clearly, if a greater percentage escaped, or migrated into another field, then still more oil could lie at depth. The mass balance method developed herein does not provide a unique solution in an open system.

What is important with regard to exploration is that the oils throughout the Tiger Shoals area were all gas washed at similar PTx conditions, with pressures probably on the order of 10,000 psi. As noted in the main text regarding the Tiger Shoals field, these high pressures are presently found at depths on the order of 14,000 feet. In the past, fluids at this pressure would have been found only at greater depths. Thus, it is likely that the oils throughout the Tiger Shoals area were gas washed at depths of at least 14,000 feet, and that, if the migration pathways and traps exist at Tiger Shoals and the other fields as is likely, the possibility of deeper, undiscovered oils in those fields, in particular in the Rob L sand, is high.

The observation that the mass balance method fails to predict the occurrence of deeper oil at Tiger Shoals raises a question as to its general utility. If a negative prediction of the method can be explained as the result of causes that are unquantifiable, such as escape of gas from the system, then the method has little if any actual predictive capability. However, the ability to reconstruct a pristine oil from available fractionated oil and condensate data represents progress in the successful modeling of gas washing.